Nonperturbative effects in the semileptonic decays of pseudoscalar mesons

James Gill

Doctor of Philosophy

The University of Edinburgh
2002

To my family

0.1 Abstract

This thesis describes the calculation of the form factors for four semileptonic decays. The decays considered are those where a pseudoscalar meson composed of a heavy and a light valence quark decays to a vector meson containing only light valence quarks. The form factors were calculated in nonperturbatively $\mathcal{O}(a)$ improved quenched lattice QCD. To estimate discretisation effects the calculation was done at $\beta = 6.0$ and $\beta = 6.2$, with lattice sizes $16^3 \times 48$ and $24^3 \times 48$ respectively.

Results are presented for the following semileptonic decays of charmed mesons: $D_s \to \phi$, $D \to K^*$ and $D \to \rho$. The $\beta = 6.2$ and $\beta = 6.0$ results agree within errors. The $\beta = 6.2$ results were used to calculate integrated decay rates and form factor ratios at $q^2 = 0$. The lattice predictions for integrated decay rates are in reasonable agreement with experiment. In some cases the lattice form factor ratios differ significantly from experiment.

The simulation results were extrapolated in heavy quark mass to obtain $B \to \rho$ form factors at high q^2. These were used to determine $|V_{ub}|$ from the CLEO collaboration's measurement of the partial decay rate $B \to \rho$ in the range $14\ \mathrm{GeV}^2 < q^2 < 21$. This gave $|V_{ub}| = 3.4^{+0.4}_{-0.2} \pm 0.7 \pm 0.6 \times 10^{-3}$ where the errors are statistical, systematic and experimental. This is in agreement with the determination of $|V_{ub}|$ by the Particle Data Group.

Declaration

This thesis, written entirely by me, is a presentation of the research work I did as a member of the UKQCD collaboration. My calculations used gauge configurations and correlation functions generated by other members of UKQCD. The statistical analysis was done by me using code I wrote. Some of the routines used in the analysis were adapted from existing UKQCD codes.

Preliminary results from these calculations were presented at the conference Lattice 2001 and in

> Semileptonic decay of a heavy-light pseudoscalar to a light vector meson, J. Gill, UKQCD Collaboration, hep-lat/0109035.

James Gill

Acknowledgments

Thanks to all the people who have helped me get to grips with particle physics and lattice gauge theory. I have had assistance, illuminating discussions and illuminating arguments with many people. I would like to offer particular thanks to Victor Lesk who I collaborated with, to Chris Maynard, Jonathan Flynn and Tony Kennedy for their expert advice, and to my supervisors Ken Bowler and Richard Kenway.

I also thank my friends and family for their many kindnesses.

Contents

Chapter 1

Introduction

Particle physics is the study of the most fundamental constituents of matter. The aim is to identify the building blocks of matter and understand their interactions. The Standard Model (SM) of particle physics describes the observed particles and their interactions in terms of a quantum field theory. The SM is a spectacularly successful theory; it gives a unified description of a vast range of different phenomena and agrees with all experimental results to date[1]. This introduction describes aspects of the SM relevant to this thesis, and reviews recent work to confront the theory of flavour changing interactions with experiment.

1.1 Charged currents

The electroweak sector of the standard model is an elegant and intricate theory. It gives a unified description of electromagnetism and the weak force in terms of a spontaneously broken gauge theory. Without the symmetry breaking all the particles in the theory are massless. The symmetry breaking generates an effective mass for the fermions and three of the gauge bosons. The residual signature of the symmetry breaking mechanism is a particle, the Higgs boson. Despite much effort, the Higgs boson has not yet been observed. It is the only SM particle that

[1]The recent strong evidence that neutrinos have mass is the only exception to this [1]. However, the SM can be generalised to accommodate neutrino mass [2].

has not been observed.

The weak interactions relevant to this work are the interactions of the W bosons with fermions. After symmetry breaking the interaction between the W, leptons, and neutrinos is given by the effective Lagrangian density [3],

$$\mathcal{L}_{W\ell} = \frac{-g}{\sqrt{2}}(W_\mu^+ J_\ell^\mu + W_\mu^- J_\ell^{\mu\dagger}) \ . \tag{1.1}$$

The current J_ℓ^μ is given by

$$J_\ell^\mu = \bar{\nu_e}\gamma^\mu P_L e + \bar{\nu_\mu}\gamma^\mu P_L \mu + \bar{\nu_\tau}\gamma^\mu P_L \tau \ , \tag{1.2}$$

where the neutrino and lepton fields in this expression are four-component Dirac fields. P_L projects out the left-handed component of a spinor,

$$P_L = \frac{1}{2}(1-\gamma^5) \ . \tag{1.3}$$

The leptons only interact with neutrinos from the same generation.

The interaction between the W and quarks is given by the effective-Lagrangian density [3],

$$\mathcal{L}_{Wq} = \frac{-g}{\sqrt{2}}(W_\mu^+ J_q^\mu + W_\mu^- J_q^{\mu\dagger}) \ , \tag{1.4}$$

where the current J_q^μ is

$$J_q^\mu = (\bar{u} \quad \bar{c} \quad \bar{t})\gamma^\mu P_L \begin{pmatrix} V_{ud} & V_{us} & V_{ub} \\ V_{cd} & V_{cs} & V_{cb} \\ V_{td} & V_{ts} & V_{tb} \end{pmatrix} \begin{pmatrix} d \\ s \\ b \end{pmatrix} \ . \tag{1.5}$$

The matrix in the above expression is the Cabibbo-Kobayashi-Maskawa (CKM) matrix. It is not diagonal, so quarks from different generations do interact.

The coupling constant g, in (1.1) and (1.4), measures the strength of the interaction between the W boson and fermions. It turns out that g is much smaller than unity [4]. This is very fortunate for theoretical calculations, because perturbation theory can be accurately applied. The decays of interest in this work involve the exchange of a highly virtual W boson; the four-momentum of the boson (q^μ) satisfies $q^2 << M_W^2$. For these decays the W boson field can be integrated out of the Lagrangian. The resulting effective Lagrangian has interactions between four fermions, with coupling $G_F = g^2/(8M_W^2)$.

1.2 Quantum chromodynamics

Quantum chromodynamics (QCD) is the theory that describes the interaction between quarks and gluons. From a theoretical point of view QCD is the most complicated part of the standard model. In many interesting processes perturbation theory cannot be applied to QCD.

Quantum field theories have UV divergences and need to be renormalised to give finite results. Renormalisation causes the parameters of a quantum field theory to depend on the energy scale at which they are measured. In the case of QCD the coupling between quarks and gluons is [5]

$$\alpha_s(\mu^2) = \frac{12\pi}{(33 - 2N_F)\ \log(\mu^2/\Lambda_{QCD}^2)}\ , \tag{1.6}$$

where Λ_{QCD} is approximately 0.2 GeV, N_F is the number of quark flavours, and μ is the energy scale. This result is calculated in perturbation theory, and is only valid if α_s is small. In modern collider experiments quarks interact at high enough energies for α_s to be fairly small. Perturbative QCD calculations agree very well with the results of collider experiments. This is the main reason that QCD has become established as the correct theory of strong interactions.

The quarks bound in a hadron interact at low energies, at which α_s is large. Perturbation theory cannot be applied to the quarks in a hadron. A nonperturbative approach is required. This thesis is about a calculation of nonperturbative QCD effects using the lattice QCD approach.

1.3 Weak decays of mesons

The weak decays of mesons are of interest because they can be used to determine elements of the CKM matrix. The theoretical description of these decays requires electroweak theory and QCD. The electroweak part of the decay can be accurately calculated in perturbation theory, but the QCD part is inherently nonperturbative. Weak decays which take place by single W exchange have an amplitude of $\mathcal{O}(G_F)$. The contribution from loops to these decays is insignificant because G_F is so small. The decays mediated by single W exchange can be divided into three classes: leptonic, semileptonic and nonleptonic. In a nonleptonic decay one meson decays to two mesons, for example $K \to \pi\pi$. These are difficult to describe theoretically because the final state mesons interact by the strong force. In the case of semileptonic and leptonic decays there is one or no mesons in the final state, and the QCD effects can be separated from the weak effects.

An example leptonic decay is shown in figure 1.1. The diagram shows a specific leptonic decay, but can easily be generalised. Figure 1.1 is the tree-level Feynman diagram for the decay in a world without QCD. In the real world low energy QCD interactions strongly bind the quarks in the initial state. This binding cannot be visualised with a Feynman diagram or calculated in perturbation theory. The amplitude for the decay in figure 1.1 is [6],

$$\mathcal{M}(B^- \to \ell^- \nu) = i\frac{G_F}{\sqrt{2}} V_{ub} f_B L^\nu q_\mu \tag{1.7}$$

were q^μ is the four-momentum of the B^-, the leptonic current is

$$L^\mu = \bar{\ell}\gamma^\mu(1-\gamma_5)\nu \tag{1.8}$$

and f_B describes the nonperturbative QCD effects.

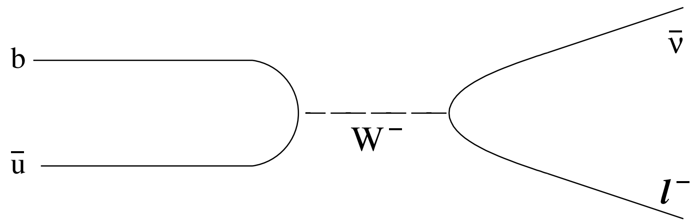

Figure 1.1: The tree-level Feynman diagram for $B^- \to \ell^- \bar{\nu}$, in the absence of QCD. This is a leptonic decay.

An example semileptonic decay is shown in figure 1.2. The amplitude for this decay is [6],

$$\mathcal{M}(\bar{B}^0 \to \rho^+ \ell^- \bar{\nu}) = i\frac{G_F}{\sqrt{2}} V_{ub} L^\mu H_\mu \ , \tag{1.9}$$

where

$$H_\mu = \langle \rho^+ | \bar{u}\gamma_\mu(1-\gamma_5) b | \bar{B}^0 \rangle \ . \tag{1.10}$$

The current H_μ is called a weak matrix element. It describes the QCD effects in the semileptonic decay. Symmetry arguments show that H_μ can be expressed in terms of a few functions of q^2, called form factors. This is shown explicitly in section 5.1.

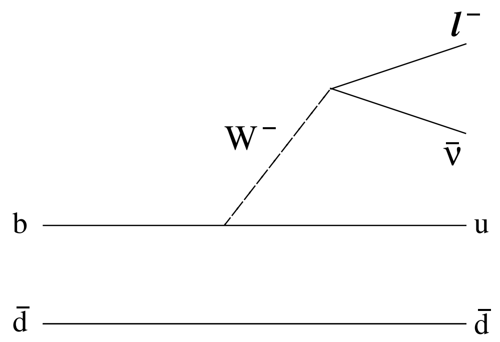

Figure 1.2: The tree-level Feynman diagram for the decay $\bar{B}^0 \to \rho^+ \ell^- \bar{\nu}$, in the absence of QCD. This is a semileptonic decay.

1.4 The CKM matrix

The CKM matrix is a unitary matrix. A general 3×3 unitary matrix is defined by 3^2 free parameters. In the case of the CKM matrix five of these free parameters are unphysical. Five arbitrary phases can be absorbed into the definition of the quark fields.

A convenient parametrisation of the CKM matrix was introduced by Wolfenstein [7]. The parametrisation uses four real parameters A, η, ρ, and λ. The parameters A, η, ρ are of the order of unity, but λ is small; experiment gives $\lambda = 0.223 \pm 0.004$ [4]. The Wolfenstein parametrisation neatly summarises the hierarchy in the magnitudes of CKM matrix elements. This hierarchy is an experimental observation and is not derived from the SM. The parametrisation is

$$V_{CKM} = \begin{pmatrix} 1-\lambda^2/2 & \lambda & A\lambda^3(\rho - i\eta) \\ -\lambda & 1-\lambda^2/2 & A\lambda^2 \\ A\lambda^3(1-\rho-i\eta) & -A\lambda^2 & 1 \end{pmatrix} + \mathcal{O}(\lambda^4)\ , \qquad (1.11)$$

where the suppressed $\mathcal{O}(\lambda^4)$ terms have been omitted.

There is one phase in V_{CKM} which cannot be absorbed into the quark fields. The physical significance of this is that the interaction between the W boson and quarks (1.4) is not invariant under a combined charge parity (CP) transformation. This is the only interaction in the standard model which violates CP symmetry.

Several of the alternatives to the SM predict new mechanisms for flavour changing interactions, and for CP violation. In these alternative models the effective Lagrangian for flavour changing interactions would have a nonunitary CKM matrix. Therefore it is important to test experimentally the unitarity of V_{CKM}. The unitarity condition,

$$V_{CKM}V^{\dagger}_{CKM} = 1 \ , \tag{1.12}$$

gives six independent relations for the elements of V_{CKM}. The most interesting relation is

$$V_{ud}V^{*}_{ub} + V_{cd}V^{*}_{cb} + V_{td}V^{*}_{tb} = 0 \ . \tag{1.13}$$

Each of the terms on the left hand side are $\mathcal{O}(\lambda^4)$ in the Wolfenstein parametrisation. Each term is similar in magnitude and two of them are expected to have a large phase. This equation can be elegantly presented as a unitarity triangle. The three terms in the equation are represented as vectors in the complex plane, and these vectors form a closed triangle if the terms sum to zero. The unitarity triangle for (1.13) is shown in figure 1.3. Note that many authors rescale the sides of the triangle in some way.

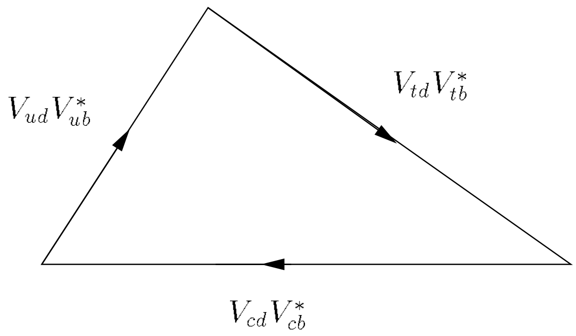

Figure 1.3: The unitarity triangle for relation (1.13).

The unitarity triangle gives a beautiful way of visualising the experimental tests of unitarity. Each test is interpreted as restricting the apex of the triangle to a region of the complex plane. For example the measurement of $|V_{ud}V_{ub}^*|$ restricts the apex of the triangle to an annular region. The width of the annulus is the error on $|V_{ud}V_{ub}^*|$. The different experimental results for the apex of the triangle are combined by superimposing the different allowed regions of the complex plane. At present there is a region of the complex plane where all the allowed regions overlap and so experiment is consistent with the Standard Model.

1.5 $|V_{ub}|$ from B decays

The CKM matrix element $|V_{ub}|$ gives an important constraint on the apex of the unitarity triangle. Its current value from the Particle Data Group is $|V_{ub}| = 0.0035 \pm 0.0015$ [4]. Knowledge of the unitarity triangle (figure 1.3) would be greatly increased if $|V_{ub}|$ could be determined more accurately.

The inclusive semileptonic decay $B \to X_u \ell \bar{\nu}$ can be used to determine $|V_{ub}|$. The measured branching ratio $\mathcal{B}$ is used to compute

$$|V_{ub}| = \sqrt{\frac{\mathcal{B}(\bar{B} \to X_u \ell \bar{\nu})}{\tilde{\Gamma}_{thy} \tau_{\bar{B}}}}\,, \qquad (1.14)$$

where $\tau_{\bar{B}}$ is the B life time, and $\tilde{\Gamma}_{thy}$ is calculated from theory. A semileptonic decay is described by three kinematic variables. These are E_ℓ, the lepton energy, $E_{\bar{\nu}}$ the neutrino energy (in the B rest frame) and q^2, where $q = p_\ell - p_{\bar{\nu}}$. The formula (1.14) is correct for a branching ratio integrated over part or all of phase space, although of course the value of $\tilde{\Gamma}_{thy}$ changes. If the branching ratio is integrated over all of phase space then $\tilde{\Gamma}_{thy}$ can be calculated as a series in $\alpha_s(m_b)$ and Λ_{QCD}/m_b, using an operator product expansion (OPE). The error on $\tilde{\Gamma}_{thy}$ is estimated to be about 8% [8]. If the experimental measurement could be made, this would allow a determination of $|V_{ub}|$ with a 4% theoretical error. In practice however, the decay $B \to X_u \ell \bar{\nu}$ has a huge background of $B \to X_c \ell \bar{\nu}$ events. To distinguish the two decays, cuts are placed on the kinematic variables. There are two widely used cuts, $m_B/2 > E_\ell > (m_B^2 - m_D^2)/2m_B$ and $(m_B - m_D)^2 < q^2 < m_B^2$. Unfortunately, imposing these cuts makes the OPE calculation unreliable [8, 9] and results in a large theoretical error on $|V_{ub}|$. Recently two solutions for this problem have been proposed. One strategy is to apply an unconventional cut that uses both E_ℓ and q^2 [10]. It should be possible to use the cut for the experimental measurement and the OPE is well behaved. Another strategy uses the data for $\mathcal{B}(B \to X_s\gamma)$ with the conventional cut $m_B/2 > E_\ell > (m_B^2 - m_D^2)/2m_B$. The uncontrolled terms in the OPE are determined from experimental measurement of the inclusive decay $B \to X_s\gamma$ [11]. These methods are expected to allow a determination of $|V_{ub}|$ with 10% theoretical errors. However, neither method has yet been implemented.

An alternative way to determine $|V_{ub}|$ is to use exclusive decays of B mesons. Currently the best exclusive and inclusive determinations of $|V_{ub}|$ have similar errors [9]. The simplest exclusive decay is the leptonic decay $B^- \to \ell^-\bar{\nu}$ where the nonperturbative effects are described entirely by the decay constant f_B. However the branching ratio for leptonic B decay is predicted to be very small and is unlikely to be observed experimentally for some time. The semileptonic decays $B \to \rho\ell\nu$ and $B \to \pi\ell\nu$ offer a good opportunity to determine $|V_{ub}|$. Both these decays have now been observed by the CLEO collaboration [12, 13]. To determine $|V_{ub}|$ the weak matrix elements (1.10) for these decay needs to be calculated. With the weak matrix element as the theoretical input $|V_{ub}|$ is obtained by a formula similar to (1.14). At the moment the best measured inclusive decay is $B \to \rho\ell\nu$. The CLEO collaboration use five different theoretical calculations of the weak matrix element to determine $|V_{ub}|$ and estimate a theoretical error from the spread of results. They obtain [13]

$$|V_{ub}| = 3.25 \pm 0.14^{+0.21}_{-0.29} \pm 0.55 \times 10^{-3} \ , \tag{1.15}$$

where the errors are statistical, systematic and theoretical. The dominant error is the theoretical uncertainty.

This thesis describes a lattice QCD calculation of the matrix element for the decay $B \to \rho\ell\nu$. In principle this is the best method for calculating the necessary weak matrix element. The lattice is the only fundamental approach to nonperturbative QCD. However the current systematic errors on lattice calculations are large, and comparable to the systematic errors claimed for light cone sum rules [14] and quark models [15].

There are two major experiments currently gathering data, which are devoted to B physics. These are Barbar in California, and Belle in Japan. These experiments are expected to greatly improve knowledge of B decays over the coming years.

Chapter 2

Lattice QCD

This chapter gives an overview of some theoretical aspects of lattice QCD. More detailed accounts can be found in [16, 17].

2.1 The path integral

In QCD all important information is contained in the Green functions. These can be formally expressed in terms of a path integral.

$$\langle 0|\, T\mathcal{O}[\psi,\bar{\psi},A]\, |0\rangle = \frac{1}{Z}\int \mathcal{D}\psi\mathcal{D}\bar{\psi}\mathcal{D}A\ \mathcal{O}[\psi,\bar{\psi},A]e^{iS[A,\psi,\bar{\psi}]}$$

$$Z = \int \mathcal{D}\psi\mathcal{D}\bar{\psi}\mathcal{D}Ae^{iS[A,\psi,\bar{\psi}]} \tag{2.1}$$

where $\mathcal{O}$ is a function of fields, and T is the time ordering operator. The functional integral $\mathcal{D}$ means an integral over all possible values of the field at every point in spacetime. Equivalently the functional integral can be thought of as an integral over all possible field configurations.

Lattice QCD is a way of defining what (2.1) means. The first step is to formulate the theory in Euclidean space time. Let (x^0, x^1, x^2, x^3) be the coordinates of Minkowski spacetime. If instead of x^0 the imaginary time coordinate

$$x^4 = ix^0 \tag{2.2}$$

is used, then the set of coordinates (x^1, x^2, x^3, x^4) have a Euclidean metric. The change from real to imaginary time can be thought of as a rotation in the complex time plane and is known as a Wick rotation. It has been proved that Euclidean correlation functions can be analytically continued to Minkowski space.

In Euclidean space (2.1) is modified to

$$\begin{aligned} \langle 0|\, T\mathcal{O}[\psi,\bar{\psi},A]\,|0\rangle &= \frac{1}{Z}\int \mathcal{D}\psi\mathcal{D}\bar{\psi}\mathcal{D}A\ \mathcal{O}[\psi,\bar{\psi},A]e^{-S_E[A,\psi,\bar{\psi}]} \\ Z &= \int \mathcal{D}\psi\mathcal{D}\bar{\psi}\mathcal{D}Ae^{-S_E[A,\psi,\bar{\psi}]}\ , \end{aligned} \tag{2.3}$$

where S_E is the Euclidean action and is, in general, different from S. S_E is a positive real quantity. The key benefit of (2.3) is that each field configuration receives a weighting as opposed to a phase in (2.1). This is an essential feature for Monte Carlo calculations and is also much better defined mathematically.

2.2 Discrete spacetime

In lattice QCD spacetime is reduced to a finite number of points. As a consequence fields have a finite number of degrees of freedom, and the path integral can be given a precise definition. A hypercubic lattice is used with coordinates (x^1, x^2, x^3, x^4). The lattice consists of all points whose coordinates satisfy

$$\begin{aligned} x^\mu = an^\mu\ ,\ n^\mu \in \mathbb{Z} \qquad & 0 \le n^\mu < L \text{ for } \mu = 1,2,3 \\ & 0 \le n^4 < T\ , \end{aligned} \tag{2.4}$$

where a is the lattice spacing and has dimensions of length, L is dimensionless. To define an action boundary conditions are required. For fermion fields the boundary conditions are periodic in the space dimensions and antiperiodic in the time dimension. The boundary conditions for scalar and gauge fields are periodic in all dimensions. It follows that momentum space is discretised. In the case of fermion fields momentum space is discretised on the lattice

$$\begin{aligned} p^\mu &= \frac{2\pi}{aL}n^\mu \qquad 0 \le n^\mu < L \ \text{ for } \mu = 1,2,3 \\ p^4 &= \frac{2\pi}{aT}(n^4 + \frac{1}{2}) \qquad 0 \le n^0 < T\ \ . \end{aligned} \tag{2.5}$$

Note that there is a maximum allowable momentum so there are no UV divergences in lattice quantum field theory.

Other discretisation schemes are possible, but are not considered here.

2.3 Lattice gauge fields

In this section fields with an $SU(N)$ symmetry are considered, as specialising to $SU(3)$ does not simplify the discussion. For a more thorough discussion see [18].

The simplest discretisation of the gauge fields would be to have the gauge field at each lattice point and replace the derivatives in the continuum action with finite differences. Classically gauge invariance is broken for finite a and is restored in the limit $a \to 0$. However, in the quantum theory renormalisation interferes and gauge invariance may not be restored as $a \to 0$.

A discretisation is required which retains gauge invariance for all a. To do this the theory is formulated in terms of variables living on the links between nearest neighbour lattice sites. The link variables are $SU(N)$ matrices. Let $U_{x,\mu}$ be the link variable from lattice site x to site $x + \hat{\mu}$. The link variable in the opposite direction is not an extra degree of freedom and is defined to be

$$U_{x+\hat{\mu},-\mu} = U^{\dagger}_{x,\mu} \ . \tag{2.6}$$

The gauge transformation of a link variable is given by

$$U'_{x,\mu} = \Lambda_x \ U_{x,\mu} \ \Lambda^{\dagger}_{x+\hat{\mu}} \ , \tag{2.7}$$

where the Λ are $SU(N)$ matrices.

The trace of the product of link variables around a closed path is gauge invariant. The simplest, nontrivial closed path is around a unit square of the lattice. This gives the plaquette variable,

$$P_{x,\mu\nu} = \ U_{x,\mu} U_{x+\hat{\mu},\nu} U^{\dagger}_{x+\hat{\nu},\mu} U^{\dagger}_{x,\nu} \ . \tag{2.8}$$

The plaquette variable is shown diagramatically in figure 2.1.

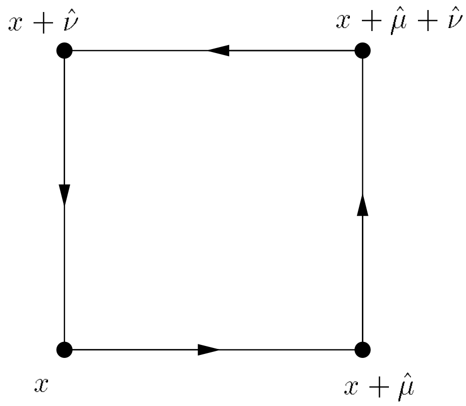

Figure 2.1: Graphical representation of the closed path of link variables which gives the plaquette variable (2.8).

The Wilson action for pure gauge theory is a sum over plaquettes

$$S_g[U] = \beta \sum_P (1 - \frac{1}{N}\text{Re Tr } P) \ , \tag{2.9}$$

where the sum over plaquettes means all distinct plaquettes.

The integration measure for gauge fields is an integral over the group manifold for each link,

$$\mathcal{D}U \ \equiv \ \prod_{x,\mu} dU_{x,\mu} \ . \tag{2.10}$$

The integral over the group manifold is defined in a gauge-invariant way and is known as the Haar measure.

In the limit $a \to 0$ the lattice gauge theory in terms of link variables tends to continuum Yang-Mills gauge theory. The starting point for showing this is

$$\lim_{a\to 0} \frac{U_{x,\mu} - 1}{a} = T_i \ A^i_\mu(x) \ , \tag{2.11}$$

where $\{T_i\}$ are $SU(N)$ generators and $\{A^i_\mu(x)\}$ are continuum gauge fields. The β parameter in (2.9) is related to the continuum bare coupling by

$$\beta = \frac{2N}{g_0^2} \ . \tag{2.12}$$

2.4 Free lattice fermion fields

Fermion fields have to be discretised carefully to avoid what is known as the doubling problem. In this section the problem and its resolution are discussed for the case of a single Dirac spinor. The fields and mass parameter are chosen to be dimensionless. To relate them to their continuum counterparts they need to be multiplied by the appropriate power of a.

The naive approach to lattice fermions is to define the field at each site and replace the derivatives in the Lagrangian with finite differences. The naive action using a convenient notation is

$$S_{naive} = \bar{\psi}_{\tilde{x}} K_{\tilde{x}\tilde{y}} \psi_{\tilde{y}} \ , \tag{2.13}$$

where the index $\tilde{x}$ is spacetime and spin, and the summation convention is used for the repeated indices. The quark matrix is

$$K_{xy} = \frac{1}{2} \sum_{\mu} \gamma_\mu (\delta_{x,y-\hat{\mu}} - \delta_{x,y+\hat{\mu}}) + m\delta_{xy} \ , \tag{2.14}$$

where spinor indices have been suppressed. Note that the quark matrix is modified at the boundary to satisfy the antiperiodic boundary condition [16]. The integration measure for the fermion field is given by

$$\mathcal{D}\bar{\psi}\mathcal{D}\psi \ \equiv \ \prod_{\tilde{x}} d\bar{\psi}_{\tilde{x}} d\psi_{\tilde{x}} \ . \tag{2.15}$$

The lattice free-quark propagator is a countable number of Gaussian integrals. Evaluating the integrals by the standard generating functional technique gives

$$\langle \bar{\psi}_{\tilde{x}} \ \psi_{\tilde{y}} \rangle = K^{-1}_{\tilde{x}\tilde{y}} \ . \tag{2.16}$$

The matrix inverse in (2.16) can be done explicitly. In the limit $a \to 0$ this quark propagator describes 16 propagating fermions. For the interacting theory this is a disaster. This is known as the fermion doubling problem.

The solution used in this work was first proposed by Wilson [18]. An extra term is added to S_{naive}, which is suppressed by a positive power of a in the classical continuum limit. The extra term gives a large mass to 15 of the fermions, leaving a theory with 1 propagating fermion as desired. The Wilson action is

$$S_{Wilson} = S_{naive} + \bar{\psi}_{x,\alpha}\Big[\frac{r}{2}\sum_{\hat{\mu}}(-\delta_{x,y+\hat{\mu}} + 2\delta_{xy} - \delta_{x,y-\hat{\mu}})\Big]\psi_{y,\alpha} \ , \tag{2.17}$$

where the index α is spin and r is a free parameter known as the Wilson parameter. The penalty for the extra term in the action is that chiral symmetry is explicitly broken.

2.5 Lattice QCD action

The lattice QCD Lagrangian consists of link variables and fermion fields. The fermion fields are triplets of Dirac spinors. There is a triplet of spinors for each flavour of quark. The components of the triplet correspond to the three colours of QCD, referred to as red, green and blue. The lattice QCD Lagrangian is constructed to be invariant under an $SU(3)$ gauge transform. The gauge transform for the link variables is given in (2.7), the gauge transform for the fermion fields is

$$\psi'_x = \Lambda_x \psi_x \quad , \quad \bar{\psi}'_x = \bar{\psi}_x \Lambda_x^\dagger \ , \tag{2.18}$$

where Λ_x is an $SU(3)$ matrix. The Wilson action is

$$S_{QCD} = S_q[U, \psi, \bar{\psi}] + S_g[U] \ , \tag{2.19}$$

where S_g is the gauge action given in (2.9) and S_q is

$$S_q[U, \psi, \bar{\psi}] = \bar{\psi}_{\tilde{x}} K_{\tilde{x}\tilde{y}} \psi_{\tilde{y}} \ , \tag{2.20}$$

where the index $\tilde{x}$ is spacetime, spin, colour and flavour. The quark matrix is

$$K_{xy}[U] = \delta_{xy} - \kappa \sum_{\mu} \left[\delta_{x,y-\hat{\mu}}(r - \gamma_\mu)U_{x,\mu} + \delta_{x-\hat{\mu},y}(r + \gamma_\mu)U^\dagger_{y,\mu}\right] . \tag{2.21}$$

The spinor indices are carried by the gamma matrices, the colour indices by the link variables and there is a Kronecker delta in flavour space. All these indices are suppressed. The hopping parameter, κ, is related to the free quark mass by

$$\kappa = \frac{1}{2m + 8} \ , \tag{2.22}$$

and the quark fields have been rescaled from those in (2.17) for convenience.

2.6 The continuum limit

The formulation of Lattice QCD presented in this chapter is dimensionless, so any lattice observable $\mathcal{O}_{Latt}$, such as a hadron mass, is dimensionless. For simplicity $\mathcal{O}_{Latt}$ is assumed to be independent of quark mass for the following discussion. The continuum value of the observable is given by

$$\mathcal{O}_{cont} = \lim_{a \to 0} \frac{\mathcal{O}_{Latt}(a)}{a^N} , \tag{2.23}$$

where N is the dimension of $\mathcal{O}_{cont}$ in energy units. However the lattice spacing, a, does not appear explicitly in the lattice QCD action. The free parameter of the action is $\beta(g_0)$, which is a function of a. The relation between a and β can be calculated in perturbation theory using the renormalisation group . To leading order this gives [17]

$$a = \frac{1}{\Lambda_{latt}} e^{-\frac{\beta}{12\beta_0}} \tag{2.24}$$

where Λ_{latt} is the free parameter of massless QCD and β_0 is the first coefficient in the power series expansion of the β-function.

$$\beta_0 = \frac{1}{16\pi^2}(11 - \frac{2}{3}n_f) \tag{2.25}$$

where n_f is the number of flavours. In the Standard Model $n_f = 6$, so β_0 is positive and continuum limit $a \to 0$ is equivalent to $\beta \to \infty$.

Massless lattice QCD contains one free parameter, so one observable is used to determine the lattice spacing before predictions can be made. In the theory with quark masses additional observables are needed to determine these. The lattice spacing is given by

$$a = (\mathcal{O}_{Latt}/\mathcal{O}_{cont})^{1/N} . \tag{2.26}$$

The value of lattice spacing obtained will depend on the observable used, because different observables have different discretisation errors. If the lattice spacing is fine enough and there are no other sources of error, then the variation in a will be small.

Chapter 3

Numerical techniques of Lattice QCD

In general lattice QCD path integrals cannot be solved analytically. However, given certain bounds on the number of lattice points and on the free parameters of the Lagrangian, integrals can be done numerically to an acceptable accuracy. They are done most efficiently by algorithms based on the Monte Carlo principle. This chapter describes some of the techniques and theory used in Monte Carlo calculations.

3.1 The quark propagator

The QCD path integral is over gauge and fermion fields. The fermion field is composed of Grassmann variables. These are rather formal mathematical objects and very difficult to handle on a computer. Fortunately the action is quadratic in the fermion fields and the fermion path integral can be performed analytically. This leaves a path integral over gauge fields which can be expressed in terms of integrals over real numbers. The simplest case of integrating out the fermions is the quark propagator. The quark propagator is the expectation value of the product of a ψ and $\bar{\psi}$ field,

$$\begin{aligned} \langle \psi_{\tilde{x}} \bar{\psi}_{\tilde{y}} \rangle &= \frac{1}{Z} \int \mathcal{D}\psi \mathcal{D}\bar{\psi} \mathcal{D}U \; e^{-S_g - S_q} \psi_{\tilde{x}} \bar{\psi}_{\tilde{y}} \\ Z &= \int \mathcal{D}\psi \mathcal{D}\bar{\psi} \mathcal{D}U \; e^{-S_g - S_q} \; , \end{aligned} \tag{3.1}$$

where the index $\tilde{x}$ is space, spin, colour and flavour. The gluonic part of the action, S_g, is given in (2.9) and the fermionic part of the action, S_q, is given in (2.20). The quark propagator is not gauge invariant because independent gauge transformations can be applied to the fields at x and y. After doing the fermion integral

$$\begin{aligned} \langle \psi_{\tilde{x}} \bar{\psi}_{\tilde{y}} \rangle &= \frac{1}{Z} \int \mathcal{D}U \; e^{-S_g} (\det K) K^{-1}_{\tilde{x}\tilde{y}} = \frac{1}{Z} \int \mathcal{D}U \; e^{-S_{eff}} K^{-1}_{\tilde{x}\tilde{y}} \\ Z &= \int \mathcal{D}U \; e^{-S_{eff}} \; , \end{aligned} \tag{3.2}$$

with the effective action given by

$$S_{eff} = S_g - \log \, \det K \; . \tag{3.3}$$

It is useful to introduce the quark propagator, $G = K^{-1}$, for gauge configuration U,

$$G^{\alpha\beta}_{ab}(x, y; U) K_{(\beta,b,y),(\gamma,c,z)}[U] = \delta_{\alpha\gamma} \delta_{ac} \delta_{xz} \tag{3.4}$$

where α, β, γ are spin, a, b, c are colour and x, y, z are space time indices, and repeated indices are summed over. The flavour dependence of G is just a Kronecker delta so it is suppressed. For a given gauge configuration it is possible to solve the matrix equation (3.4) using an iterative algorithm. An efficient algorithm exploits the fact that K is a sparse matrix.

3.2 Monte Carlo integration

It is convenient to approximate the path integral as

$$\langle \mathcal{O} \rangle = \sum_{\{U\}} \mathcal{O}[U] P[U] \quad , \tag{3.5}$$

where

$$P[U] = \frac{e^{-S_{eff}[U]}}{Z} \mathcal{D}U \tag{3.6}$$

is the probability associated with gauge configuration U. The sum corresponds to some unbiased discretisation of the space of gauge configurations, and $\mathcal{D}U$ is the volume of gauge configuration space associated with U. Note that computers store floating point numbers with a finite number of bits so the space of gauge configurations on a computer is finite. The algorithms used to evaluate (3.5) randomly samples N gauge configurations. This is done in such a way that the probability of sampling gauge configuration U_i is $P[U_i]$. Then

$$\langle \mathcal{O} \rangle = \lim_{N\to\infty} \frac{1}{N} \sum_{i=1}^{N} \mathcal{O}_i \tag{3.7}$$

where $\mathcal{O}_i$ is the value of $\mathcal{O}$ for the i'th gauge configuration. In a simulation $\mathcal{O}_i$ is calculated for N configurations and averaged. This gives an unbiased estimate of $\langle \mathcal{O} \rangle$, i.e. the result of the simulation is from a distribution with mean $\langle \mathcal{O} \rangle$. This determination of $\langle \mathcal{O} \rangle$ has an error which can be estimated using the bootstrap method. The error decreases with increasing N. More precisely, the result of the simulation is from a distribution with standard deviation

$$[\text{standard deviation}]^2 = \left\langle \ \left(\langle \mathcal{O} \rangle - \frac{1}{N} \sum_{i=1}^{N} \mathcal{O}_i \right)^2 \ \right\rangle \ \propto \ \frac{1}{N} \tag{3.8}$$

where the outer expectation value is over different sets of N configurations.

Gauge configurations are generated from the correct distribution by a Markov chain. A sequence of gauge configurations is generated one after the other, starting with a typical gauge configuration. Whenever a new configuration is added to the chain it is selected from a distribution depending on the current configuration. Configurations which are close on the chain will be correlated and, for instance, (3.8) will not be true. A subset of configurations with negligible correlations is used for the final analysis.

3.3 The quenched approximation

The correct action for lattice QCD is S_{eff}. This is nonlocal because of the second term in (3.3). Unfortunately, generating a Markov chain for a system with a nonlocal action is much slower than generating a Markov chain for a similar system with a local action. This study uses the quenched approximation, which is a modification of lattice QCD with a local action. The determinant in (3.2) is replaced by a gauge field independent constant. In perturbation theory the quenched approximation corresponds to omitting closed fermion loops. Although the quenching is an uncontrolled approximation, the theory still retains the essential features of QCD. Calculations of the light hadron spectrum in quenched QCD are within about 10 % of the experimental results [19, 20]. It is hoped that the error on other hadronic quantities is similarly small.

3.4 Symanzik improvement programme

The purpose of the improvement programme is to eliminate the $\mathcal{O}(a)$ errors of lattice QCD expectation values. The hope is that results will be closer to the continuum limit values without the expense of going to a finer lattice spacing. For a detailed discussion see [21, 22].

An expectation value calculated exactly in lattice QCD has a discretisation error. This error can be written as

$$\langle \mathcal{O} \rangle_{lattice} = \langle \mathcal{O} \rangle_{continuum} + a \langle \mathcal{O}' \rangle_{continuum} + \mathcal{O}(a^2) \tag{3.9}$$

where the subscript on the expectation value indicates whether an expectation value is taken with respect to lattice QCD or continuum QCD. The lattice theory at non-zero a can be thought of as an effective continuum field theory with action

$$S_{eff} = S_0 + aS_1 + \mathcal{O}(a^2) \tag{3.10}$$

where S_0 is the QCD action and S_1... are unwanted additional operators with the correct symmetries and dimension. Local composite, gauge invariant renormalised fields on the lattice (e.g. $\bar{\psi}\psi$, referred to simply as fields for the rest of this section) are also expanded as a power series in the effective continuum theory. The lattice field ϕ is expanded as

$$\phi_{eff} = \phi_0 + a\phi_1 + \mathcal{O}(a^2) \tag{3.11}$$

where ϕ_0 is the continuum analogue of ϕ and ϕ_1... are unwanted operators with the correct symmetries and dimension. In the fully $\mathcal{O}(a)$ improved theory the operator $\mathcal{O}'$ in (3.9) is 0. This is achieved if S_1 and ϕ_1 in (3.10, 3.11) are cancelled by adding $\mathcal{O}(a)$ terms to the lattice action and fields.

There are five operators with the appropriate dimension and symmetries that can be added to the action. Only one of these has a non-trivial effect on the physics, the clover term.

$$c_{SW} \sum_x \bar{\psi}_x \frac{i}{4} \sigma_{\mu\nu} F_{x,\mu\nu} \psi_x \ , \tag{3.12}$$

where $F_{x,\mu\nu}$ is the lattice analogue of the continuum field strength tensor [21],

$$F_{x,\mu\nu} = \frac{1}{8}(\mathcal{P}_{x,\mu\nu} - \mathcal{P}_{x,\nu\mu}) \ , \tag{3.13}$$

with

$$\begin{aligned} \mathcal{P}_{x,\mu\nu} = & \ U_{x,\mu}\, U_{x+\hat{\mu},\nu}\, U^\dagger_{x+\hat{\nu},\mu}\, U^\dagger_{x,\nu} \\ & + U_{x,\nu}\, U^\dagger_{x-\hat{\mu}+\hat{\nu},\mu}\, U^\dagger_{x-\hat{\mu},\nu}\, U_{x-\hat{\mu},\mu} \\ & + U^\dagger_{x-\hat{\mu},\mu}\, U^\dagger_{x-\hat{\mu}-\hat{\nu},\nu}\, U_{x-\hat{\nu},\mu}\, U_{x-\hat{\nu},\nu} \\ & + U^\dagger_{x-\hat{\nu},\nu}\, U_{x-\hat{\nu},\mu} U_{x+\hat{\mu}-\hat{\nu},\nu}\, U^\dagger_{x,\mu} \quad . \end{aligned} \tag{3.14}$$

The ψ_x in (3.12) are dimensionless as in chapter 2. The clover term gets its name because the four plaquettes of $F_{x,\mu\nu}$ look like a four leaf clover.

To discuss the counter terms added to lattice fields the following bilinears are defined:

$$\begin{aligned} V^a_\mu(x) &= \bar{\psi}(x)\gamma_\mu \frac{1}{2}\tau^a \psi(x) \\ A^a_\mu(x) &= \bar{\psi}(x)\gamma_\mu\gamma_5 \frac{1}{2}\tau^a \psi(x) \\ T^a_{\mu\nu}(x) &= \bar{\psi}(x)\sigma_{\mu\nu} \frac{i}{2}\tau^a \psi(x) \\ P^a &= \bar{\psi}(x)\gamma_5 \frac{1}{2}\tau^a \psi(x) \end{aligned} \tag{3.15}$$

where τ^a are the Pauli matrices, ψ is a doublet of quark fields. The continuum notation $\psi(x)$ is used for dimensionful lattice spinors. The counter terms for these fields are constrained by dimension counting and symmetry giving $\mathcal{O}(a)$ improved fields

$$\begin{aligned} V^I_\mu &= V_\mu + c_V a \partial_\nu T_{\mu\nu} \\ A^I_\mu &= A_\mu + c_A a \partial_\mu P \end{aligned} \tag{3.16}$$

where ∂_ν is the symmetrical lattice derivative.

The final step of improvement is to renormalise the fields by multiplication with a mass dependent renormalisation factor. The improved renormalised operator is

$$\phi^I_{Ren} = Z_\phi(1 + b_\phi a m_q)\phi^I_{bare} \tag{3.17}$$

where ϕ^I_{bare} are the improved bare fields V^I, A^I, etc.

To implement improvement the dimensionless factors weighting the counter terms, c_{x}, and the renormalisation parameters Z_ϕ and b_ϕ need to be determined. These parameters are functions of β. A great deal of effort has been put into calculating these parameters. They can be calculated using perturbation theory, but this is unsatisfactory because there are still discretisation errors of $\mathcal{O}(\alpha_s^n a)$. More recently many of the parameters have been determined nonperturbatively [23, 24]. The coefficients used in this work are discussed in later chapters.

3.5 Meson operators

Meson operators, Ω_M are used to create and annihilate mesons on the lattice. A meson operator must have non-zero overlap with the state it is intended to relate to and no overlap with lighter states. The operator for the state $|M\rangle$ must satisfy

$$\begin{aligned} \langle 0|\Omega_M|M\rangle &\neq 0 \ , \\ \langle 0|\Omega_M|M'\rangle &= 0 \ , \end{aligned} \tag{3.18}$$

where $|M'\rangle$ is any state lighter than $|M\rangle$. The states considered here are eigenstates of the angular momentum (J), parity (P) and charge conjugation operators (C). The pseudoscalar meson has eigenvalues $0, -1, +1$ and the vector meson has eigenvalues $1, -1, -1$.

The simplest meson operator is a local bilinear of the quark fields, generically

$$\Omega_M(x) = \bar{\psi}_1(x)\Gamma_M\psi_2(x) \tag{3.19}$$

where Γ_M is a gamma matrix or some combination of gamma matrices chosen so that the operator satisfies (3.18). The index on $\bar{\psi}$ and ψ is flavour. A local meson operator has overlap with the meson ground state as desired but also unwanted overlap with higher energy states with the same quantum numbers. A good meson operator maximises the overlap with the groundstate relative to the excited states, especially the first excited state. This is achieved by using a non-local gauge invariant operator. In its most general form this is

$$\Omega_M(\vec{x},t) = \sum_{\vec{y}} \bar{\psi}_1(\vec{y},t)\mathcal{F}(\vec{y},\vec{x},t)\Gamma_M\psi_2(\vec{x},t) \tag{3.20}$$

where $\mathcal{F}(\vec{y},\vec{x},t)$ is a weighted sum of path ordered products of link variables. An efficient procedure for implementing an operator of this type, used here, is known as fuzzing [25]. Another method used here is Boyling [26].

3.6 Two-point correlation functions

The two-point correlation function of meson operators has simple time dependence in the limit of large time. It is used to determine the mass and the overlap of the meson operator with the state.

The two-point correlator is defied as

$$C(t,\vec{p}) = \sum_{\vec{x}} e^{-i\vec{p}.\vec{x}} \langle 0|\, T\{\Omega_M(\vec{x},t)\Omega_M^\dagger(0)\}\,|0\rangle \ . \tag{3.21}$$

Specialising to the time ordering $t > 0$ and inserting a complete set of energy eigenstates gives

$$C(t,\vec{p}) = \sum_{\vec{x},S,\vec{k}} \frac{e^{-i\vec{p}.\vec{x}}}{2L^3E_S(\vec{k})} \langle 0|\, \Omega_M(x)|S,\vec{k}\rangle\langle S,\vec{k}|\Omega_M^\dagger(0)\,|0\rangle \ , \tag{3.22}$$

where the states have norm

$$\langle S,\vec{k}|S,\vec{k}\rangle = 2E_S(\vec{k})L^3 \ . \tag{3.23}$$

The complete set of states in (3.22) is discrete for a finite lattice. Multiparticle states have a discrete spectrum because they are restricted to discrete momenta.

A quantum operator $\mathcal{O}$ obeys the Heisenberg equations of motion

$$\mathcal{O}(x) = e^{Ht-i\vec{p}.\vec{x}}\mathcal{O}(0)e^{-Ht+i\vec{p}.\vec{x}} \ , \tag{3.24}$$

where H is the Hamiltonian and $\vec{p}$ is the three-momentum operator. There is no factor of i in front of the Hamiltonian in Euclidean space. Using this to rearrange (3.22) gives

$$C(t,\vec{p}) = \sum_{\vec{x},S,\vec{k}} e^{-i\vec{p}.\vec{x}} \frac{e^{i\vec{k}.\vec{x}}}{2L^3 E_S(\vec{k})} e^{-E_S(\vec{k})t} \langle 0|\, \Omega_M(0)|S,\vec{k}\rangle\langle S,\vec{k}|\Omega_M^\dagger(0)\,|0\rangle \ . \quad (3.25)$$

The time dependence in this expression is all in the exponential; the matrix element is time independent. It is simplified further by noting that it contains a Kronecker delta in the form

$$\delta_{\vec{k},\vec{p}} = \frac{1}{L^3}\sum_{\vec{x}} e^{i(\vec{k}-\vec{p}).\vec{x}} \ . \quad (3.26)$$

This result is trivial for $\vec{k} = \vec{p}$ and is proved for $\vec{k} \neq \vec{p}$ by noting that it is the sum of a finite geometric series. Performing the sum over $\vec{k}$ and $\vec{x}$ in (3.25) gives

$$C(t,\vec{p}) = \sum_{S} \frac{e^{-E_S(\vec{p})t}}{2E_S(\vec{p})} |\, \langle 0|\, \Omega_M(0)|S,\vec{p}\rangle|^2 \ . \quad (3.27)$$

This formula is correct for an infinite lattice. On the finite lattices used in this work it is modified to

$$C(t,\vec{p}) = \sum_{S} \frac{e^{-E_S(\vec{p})t} + e^{-E_S(\vec{p})(T-t)}}{2E_S(\vec{p})} |\, \langle 0|\, \Omega_M(0)|S,\vec{p}\rangle|^2 \ . \quad (3.28)$$

If $T-t$ and t are large then the ground state meson dominates the sum and

$$C(t,\vec{p}) \approx \frac{e^{-E_{S_0}t} + e^{-E_{S_0}(T-t)}}{2E_{S_0}} |\, \langle 0|\, \Omega_M(0)|S_0,\vec{p}\rangle|^2 \ , \quad (3.29)$$

where S_0 is the ground state meson.

3.7 Pseudoscalar mesons

The operator used to put a pseudoscalar meson onto the lattice is of the form (3.19) or (3.20) with $\Gamma_M = \gamma_5$. For example the local operator is

$$\Omega_{\mathrm{P}}(x) = \bar{\psi}_1(x)\gamma_5\psi_2(x) \quad (3.30)$$

It is conventional to define

$$Z_{\mathrm{P}}(\vec{p}) = \langle 0|\, \Omega_{\mathrm{P}}(0)\,|S_0,\vec{p}\rangle \ . \quad (3.31)$$

Lorentz invariance implies that Z_{P} is independent of $\vec{p}$ if Ω_{P} is local.

3.8 Vector mesons

The local operator used to put the vector meson onto the lattice is

$$\Omega^{\mu}_{\mathrm{V}}(x) = \bar{\psi}_1(x)\gamma^{\mu}\psi_2(x) \ , \tag{3.32}$$

and the fuzzed operator has the same γ matrix structure. The operator has a Lorentz index so the two-point vector correlator has two indices,

$$C^{\mu\nu}_{V,2PT}(t,\vec{p}) = \sum_{\vec{x}} e^{-i\vec{p}.\vec{x}} \langle 0|\, \Omega^{\mu}_{\mathrm{V}}(x)\Omega^{\nu\dagger}_{\mathrm{V}}(0)\,|0\rangle \ . \tag{3.33}$$

There is a slight complication to analysing the time dependence of this function. When the complete set of states is inserted in (3.22), these states come in degenerate triplets. The states in a triplet are distinguished by the three possible independent polarisations of a vector meson. Rewriting (3.25) for a vector meson with an explicit sum over polarisation gives

$$C^{\mu\nu}_{V,2PT}(t,\vec{p}) = \sum_{S,r} \frac{e^{-E_S(\vec{p})t}}{2E_S(\vec{p})} \langle 0|\, \Omega^{\mu}_{\mathrm{V}}(0)|S,\vec{p},\eta_r\rangle \ \langle S,\vec{p},\eta_r|\Omega^{\nu}_{\mathrm{V}}(0)\,|0\rangle \, , \tag{3.34}$$

where r labels the three polarisation axial vectors η_r.

The matrix element in (3.34) is an axial vector. The only axial vector that the matrix element can depend on is η_r so

$$Z_{\mathrm{V}}(\vec{p})\eta^{\mu}_r = \langle 0|\, \Omega^{\mu}_{\mathrm{V}}(0)|S_0,\vec{p},\eta_r\rangle \tag{3.35}$$

which defines Z_{V}. Lorentz invariance implies that Z_{V} is independent of $\vec{p}$ if Ω_M is local. Rewriting (3.34) in terms of Z_{V} gives

$$C^{\mu\nu}_{V,2PT}(t,\vec{p}) \approx \frac{|Z_V|^2}{2E_{\mathrm{V}}} e^{-E_{\mathrm{V}}t} \sum_{r=1}^{3} \eta^{\mu}_r \eta^{\nu\ *}_r \ , \tag{3.36}$$

where higher excited states have been omitted. It can be shown that for massive vector mesons

$$\sum_r \eta^{\mu}_r \eta^{\nu\ *}_r = -g^{\mu\nu} + \frac{p^{\mu}p^{\nu}}{m^2} \ . \tag{3.37}$$

3.9 Evaluating two-point correlation functions

To obtain the two-point correlator (3.21) the required matrix element is evaluated by Monte Carlo. The approach is shown here for the case of the local meson operator (3.19). The expectation value needed is

$$\mathcal{M}_2 = \langle \Omega_M(x)\Omega_M^\dagger(0)\rangle = \langle \bar{\psi}_1\Gamma_M\psi_2(x) \quad \bar{\psi}_2\tilde{\Gamma}_M\psi_1(0)\rangle \ , \tag{3.38}$$

where $1, 2$ are flavour indices and

$$\tilde{\Gamma}_M = \gamma_4\Gamma_M^\dagger\gamma_4 \ . \tag{3.39}$$

After analytically evaluating the fermion integrals

$$\mathcal{M}_2 = -\Big\langle \ \mathrm{Tr}\Big(\Gamma_M G^2(x,0;U)\tilde{\Gamma}_M G^1(0,x;U)\Big) \ \Big\rangle_{S_{eff}} \tag{3.40}$$

where the trace is over spin and colour and G is the quark propagator. Note that if flavour 1 and 2 are the same then there is an additional term. It saves computer time to calculate G only for the case $G(0,x)$. The quark propagators have the following γ_5 symmetry,

$$G(x,y;U) = \gamma_5 G^\dagger(y,x;U)\gamma_5 \tag{3.41}$$

where † is the adjoint with respect to spin and colour. Then

$$\mathcal{M}_2 = -\Big\langle \ \mathrm{Tr}\Big(\Gamma_M\gamma_5 G^{2\dagger}(0,x;U)\gamma_5\tilde{\Gamma}_M G^1(0,x;U)\Big) \ \Big\rangle_{S_{eff}} \ . \tag{3.42}$$

3.10 Three-point correlation functions

Three-point correlation functions are used to calculate weak matrix elements. The three-point correlation functions used in this work are of the form

$$C_{3PT}^{\mu\nu}(\vec{p},t_x,\vec{q},t_y) = \sum_{\vec{x},\vec{y}} e^{-i(\vec{p}.\vec{x}+\vec{q}.\vec{y})} \ \langle 0|\, T\{\Omega_{\rm P}(\vec{x},t_x)J^\mu(\vec{y},t_y)\Omega_{\rm V}^{\dagger\nu}(0)\}\,|0\rangle \tag{3.43}$$

where J is the local, flavour changing axial or vector current. To analyse the time dependence specialise to the case $t_x > t_y > 0$. The procedure is similar to analysing the time dependence of the two-point correlator. First insert two complete sets of states

$$C^{\mu\nu}_{3PT} = \sum_{\vec{x},\vec{y},\vec{k}_1,\vec{k}_2,B,A,r} e^{-i(\vec{p}.\vec{x}+\vec{q}.\vec{y})} \frac{1}{2L^3 E_B(\vec{k}_1)} \frac{1}{2L^3 E_A(\vec{k}_2)} \times$$
$$\langle 0|\, \Omega_{\rm P}(x)|B,\vec{k}_1\rangle\langle B,\vec{k}_1|J^\mu(y)|A,\vec{k}_2,\eta_r\rangle\langle A,\vec{k}_2,\eta_r|\Omega^{\dagger\nu}_{\rm V}(0)\,|0\rangle \ . \quad (3.44)$$

Shifting the current and pseudoscalar operators to the origin using the Heisenberg equations of motion and summing over $\vec{x},\vec{y},\vec{k}_1,\vec{k}_2$ using the Kronecker delta identity (3.26) gives

$$C^{\mu\nu}_{3PT} = \sum_{B,A,r} \frac{e^{-E_B(\vec{p})(t_x-t_y)}}{2E_B(\vec{p})} \frac{e^{-E_A(\vec{k})t_y}}{2E_A(\vec{k})} \times$$
$$\langle 0|\, \Omega_{\rm P}(0)|B,\vec{p}\rangle\langle B,\vec{p}|J^\mu(0)|A,\vec{k},\eta_r\rangle\langle A,\vec{k},\eta_r|\Omega^{\dagger\nu}_{\rm V}(0)\,|0\rangle \quad (3.45)$$

where $\vec{k}=\vec{p}-\vec{q}$. For large t_y and t_x-t_y only the slowest-decaying exponentials in (3.45) are significant and

$$C^{\mu\nu}_{3PT} \approx \frac{e^{-E_{\rm P}(t_x-t_y)}}{2E_{\rm P}} Z_{\rm P} \frac{e^{-E_{\rm V}t_y}}{2E_{\rm V}} Z^*_{\rm V} \sum_r \eta^{*\nu}_r \ \langle {\rm P},\vec{p}|J^\mu|{\rm V},\vec{k},\eta_r\rangle \ , \quad (3.46)$$

where P is the ground state pseudoscalar meson and V is the ground state vector meson. The above expression contains a polarisation-averaged matrix element which is the object of interest for calculating form factors.

An important alternative time ordering is $t_y > t_x$. In this case the asymptotic form of the three-point correlation function is

$$C^{\mu\nu}_{3PT} = \frac{Z^*_{\rm P} Z_{\rm V}}{2E_{\rm P}2E_{\rm V}} e^{-E_{\rm V}T} e^{E_{\rm P}t_x} e^{-t_y(E_{\rm P}-E_{\rm V})} \sum_r \eta^\nu_r \langle {\rm V},-\vec{k},\eta_r|J^{\mu\ \dagger}(0)|{\rm P},-\vec{p}\rangle \ . \quad (3.47)$$

The † on the flavour-changing current is not made explicit elsewhere in this work, but is implied by context. A Hermitian definition of the γ matrices was used so the † does not change the sign of the correlation function.

3.11 Evaluating three-point correlation functions

To numerically evaluate a three-point function we need the matrix element in (3.43). For local meson operators this is

$$\mathcal{M}_3 = \langle \bar\psi_1\gamma^5\psi_2(x) \ \ \bar\psi_2\Gamma^\mu\psi_3(y) \ \ \bar\psi_3\tilde\gamma^\nu\psi_1(0)\rangle \ , \quad (3.48)$$

where $1, 2, 3$ are flavour indices, $\tilde{\gamma}^\mu = \gamma^4\gamma^\mu\gamma^4$ and $\Gamma^\mu = \gamma^\mu$ or $\gamma^\mu\gamma^5$. Analytically integrating out the fermions in the path integral expression for (3.48) gives

$$\mathcal{M}_3 = -\left\langle \mathrm{Tr}\left(G^1(0,x;U)\gamma^5 G^2(x,y;U)\Gamma^\mu G^3(y,0;U)\tilde{\gamma}^\nu\right)\right\rangle_{S_{eff}} , \qquad (3.49)$$

with the same notation as (3.40). Calculating (3.49) in terms of quark propagators is computationally expensive because it contains an all-to-all propagator, $G^2(x,y;U)$. Recall that the two-point function only requires origin to all propagators. A more efficient approach is to calculate (3.49) in terms of a quark propagator and an extended propagator. The extended propagator is

$$E(0,y;U) = G^1(0,x;U)\gamma^5 G^2(x,y;U) , \qquad (3.50)$$

so

$$E(0,y;U)K^2_{yz}[U] = G^1(0,x;U)\gamma^5\delta_{xy} . \qquad (3.51)$$

The extended propagator is given by a matrix equation similar to the equation for the quark propagator (3.4) and can be calculated using an iterative algorithm. The matrix element can now be rewritten as

$$\mathcal{M}_3 = -\left\langle \ \mathrm{Tr}\left(E(0,y;U)\Gamma^\mu\gamma^5 G^3(0,y;U)\gamma^5\tilde{\gamma}^\nu\right) \ \right\rangle_{S_{eff}} , \qquad (3.52)$$

which contains no all-to-all propagator.

3.12 Discrete symmetries

The action used to generate the gauge configurations is invariant under the discrete symmetries parity (P), charge conjugation (C) and time reversal (T) [27, 28]. If gauge configurations U and U' are related by one of these discrete symmetries then the quark propagators calculated on U and U' are related. The relations are [29]

- Parity

$$G(x,y;U) = \gamma^4 G(x^P, y^P; U^P)\gamma^4 \qquad (3.53)$$

- Hermiticity

$$G(x,y;U) = \gamma^5 G^\dagger(y,x;U)\gamma^5 \qquad (3.54)$$

- Time reversal

$$G(x,y;U) = \gamma^4\gamma^5 G(y^T,x^T;U^T)\gamma^5\gamma^4 \tag{3.55}$$

- Charge conjugation

$$G(x,y;U) = \gamma^4\gamma^2 G(y,x;U^C)\gamma^2\gamma^4 \tag{3.56}$$

Note that the gamma matrices appearing on the right hand side of these relations are particular to the gamma matrix convention used in this work. The discrete symmetries show that the three-point correlators, averaged over all gauge configurations are pure real or pure imaginary. However, a three-point correlator calculated on a particular gauge configuration has nonzero real and nonzero imaginary parts. One of these parts is a stochastic estimator of zero and can be discarded.

3.13 Fits

In a generic lattice calculation a set of observables $\{d_i\}$ is calculated on N gauge configurations. This set of numbers is referred to as data. Typically the d_i are values of a correlation function at a particular time slice. To extract physical quantities the data are fitted to a model by minimizing chi-square with respect to the model parameters [30].

For correlated data chi-square is defined as

$$\chi^2(\vec{x}) \equiv \sum_{i,j} (\bar{d}_i - m_i(\vec{x}))C^{-1}_{ij}(\bar{d}_j - m_j(\vec{x})) \ , \tag{3.57}$$

where $\bar{d}_i$ is the average value of quantity i, $\vec{x}$ are the free parameters of the model, $m_i(\vec{x})$ is the model prediction for quantity d_i and C is the covariance matrix.

The elements of the covariance matrix are estimated from the data according to

$$C_{ij} = \frac{1}{N(N-1)}\sum_{\alpha=1}^{N}(\bar{d}_i - d_i^\alpha)(\bar{d}_j - d_j^\alpha) \ , \tag{3.58}$$

where d_i^α is the value of d_i measured on configuration α. In the limit of an infinite number of configurations (3.58) tends to the true covariance matrix.

The minimum of chi-square is the point at which

$$\frac{\partial \chi^2}{\partial x_i} = 0 \ , \tag{3.59}$$

for each model parameter. If the model function is linear then (3.59) is a set of linear equations which can be solved analytically. For a nonlinear model function χ^2 is minimised numerically. The algorithm used in this work is the Marquardt-Levenberg algorithm [30].

If there are enough configurations then, to a good approximation, the data averages ($\bar{d}_i$) are from Gaussian distributions and the covariance matrix is accurately estimated. In this case chi-square can be used to rigorously test if a fit is acceptable at a particular confidence level. This is done by $Q(\chi^2, \nu)$, where the number of degrees of freedom is

$$\nu = [\text{Fit parameters}] - [\text{Data points}] \ . \tag{3.60}$$

Q is the probability that chi-square exceeds χ^2 assuming that the model function is exactly right. In a typical lattice fit it isn't possible to apply a stringent test to Q, but it can still be used as a guide to whether a fit is acceptable. Another useful guide is reduced chi-square $= \chi^2/\nu$. This should be about 1 for an acceptable fit.

3.14 Statistical errors

The fitted parameters $\vec{x}$ have an error, called the statistical error, due to the finite number of gauge configurations. It is important to estimate this error. In general a lattice calculation has a small data sample (N of the order of a few hundred) and a non-Gaussian distribution of the data. The method that has been chosen to cope with this is the bootstrap. N gauge configurations are picked at random (with repetition) from the sample, to create a bootstrap sub-ensemble. The fitting procedure is then repeated with the sub-ensemble exactly as for the true sample. This gives a new estimate of the fit parameters. This procedure is repeated N_{boot}

times to generate a bootstrap distribution for each of the fit parameters. The upper and lower bounds on parameter x_i at confidence level $X\%$ is given by the following procedure. Put the N_{boot} values for x_i in ascending order, then the $XN_{boot}/200$'th value is the lower bound and the $(100-X)N_{boot}/200$'th is the upper bound.

3.15 Remarks on the covariance matrix

To gain an intuitive understanding of correlated chi-square (3.57) diagonalise the covariance matrix

$$C' = RCR^T \ , \tag{3.61}$$

where C is the covariance matrix and R is an orthogonal matrix chosen so that C' is diagonal. Chi-square can then be written in the more familiar uncorrelated form

$$\chi^2(\vec{x}) \equiv \sum_i \frac{1}{C'_{ii}}(\bar{d}'_i - m'_i(\vec{x}))^2 \ , \tag{3.62}$$

where $\vec{d}' = R\vec{d}$ and $\vec{m}' = R\vec{m}$ using vector notation instead of the index i. Note that C'_{ii} are the eigenvalues of C. The correlated observables can be considered as a linear combination of uncorrelated observables.

If two observables i and j have very different systematic errors, or are known to be uncorrelated then the covariance matrix elements C_{ij} and C_{ji} should be set to 0 by hand. The covariance matrix can have very small eigenvalues due to statistical fluctuations in the data. In extreme circumstances the matrix cannot be inverted. The approach taken in this work is to use the singular value decomposition (SVD) inverse. Very small eigenvalues are set to infinity for calculating the inverse. A more sophisticated approach proposed in [31] is eigenvalue smoothing. The N lowest eigenvalues of the covariance matrix are replaced with their average. However fits using this method gave the same results as fits using SVD where tested in this work.

The correlation matrix is given by

$$Corr_{ij} = \frac{C_{ij}}{\sqrt{C_{ii}C_{jj}}} \ . \tag{3.63}$$

The correlation matrix is a normalised version of the covariance matrix. If an element is 1 the observables are completely correlated (so the diagonal elements are 1), if 0 not correlated and if -1 completely anticorrelated. As the number of gauge configurations increases the correlation matrix tend to a constant matrix.

Chapter 4

Analysis of two-point correlators

4.1 Details of the simulation

Two ensembles of gauge configurations were used in this work, generated using the Wilson plaquette action and the quenched approximation. There are 302 $\beta = 6.0$ configurations and 216 $\beta = 6.2$ configurations. The propagators were calculated using the clover improved Wilson action. The improvement coefficient c_{SW} used is the nonperturbative value calculated by the Alpha collaboration [23]. This information and hopping parameters (κ) used are summarised in table 4.1.

	$\beta = 6.0$	$\beta = 6.2$
C_{SW}	1.769	1.614
$L^3 \times T$	$16^3 \times 48$	24×48
#config.	302	216
Light κ	0.13344, 0.13417, 0.13455	0.13460, 0.13510, 0.13530
Heavy κ	0.11230, 0.1730, 0.12230, 0.12730	0.12000, 0.12330, 0.12660, 0.12990

Table 4.1: Parameters of the simulation.

The two-point correlators were calculated with momentum $\vec{p}$ for the cases $|\vec{p}| = 0, 1, \sqrt{2}, \sqrt{3}, \sqrt{4}$ in units of $2\pi/aL$ (these units are used for momentum throughout this chapter). In the $|\vec{p}| \neq 0$ cases several $\vec{p}$ were used to increase statistics. The momenta used for the three lowest values of $|\vec{p}|$ are listed in table 4.2. Only one of the pair $\vec{p}, -\vec{p}$ was used because the corresponding correlators are trivially related.

$\lvert\vec{p}\rvert$	$\vec{p}$
0	(0,0,0)
1	(0,0,-1), (0,-1,0), (-1,0,0)
$\sqrt{2}$	(-1,-1,0), (-1,0,-1), (0,-1,-1), (-1,1,0), (-1,0,1), (0,-1,1)

Table 4.2: Momenta used to calculate the meson correlators, in units of $2\pi/aL$.

4.2 Operator smearing

The meson correlators were calculated with smeared operators to increase overlap with the groundstate. The situation for the heavy-light mesons is simpler as only one smearing combination is of interest here. The heavy quark propagator is Boyled at source and sink and the light propagator is local at source and sink. This is visualised in figure 4.1.

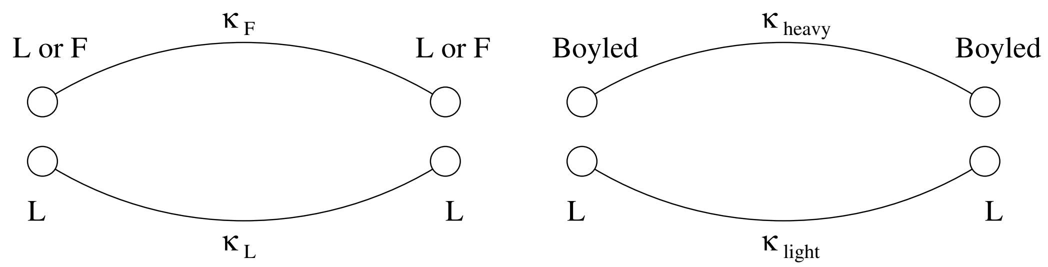

Figure 4.1: Schematic of the light-light smearing (left) and heavy-light smearing (right). 'F' is fuzzed, 'L' is local.

The light-light meson correlators were calculated with one propagator local at source and sink. The other propagator was local or fuzzed at source and local or fuzzed at sink, giving four possibilities. This is visualised in figure 4.1. The following notation is used to specify a light-light correlator

$$XY\kappa_F, LL\kappa_L \ , \tag{4.1}$$

where quark propagator with hopping parameter κ_F has smearing X at source and Y at sink, quark propagator with κ_L is local at source and sink. In total there are four correlators for a degenerate meson and seven correlators for a nondegenerate meson. In fact not all correlators were calculated. It turns out that correlators of the form $LF\kappa_F, LL\kappa_L$ are very noisy in comparison with the other three possibilities and are not useful.

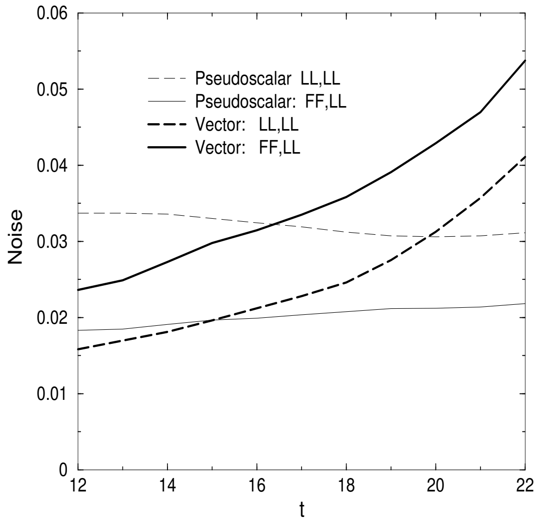

Figure 4.2: The noise on four light-light meson correlators, as a function of time. Noise is defined to be [standard deviation]/[mean] for each time slice. The correlator shown is $\beta = 6.2,\ \kappa = 0.13460, 0.13460$.

Figure 4.2 shows the noise for four light-light correlators. The noise on the pseudoscalar correlator is approximately constant with time whereas the noise on the vector correlator increases approximately exponentially. This agrees with the simple analytic prediction [32]. The fuzzing reduces the noise on the pseudoscalar correlator, but unfortunately it increases the noise on the vector correlator.

4.3 Overview of the fits

Fitting lattice correlation functions requires intuition and experience. There is no recipe that gives the best procedure. There are several useful ways of visualising whether a fit is good or not. These are described here using the $\beta = 6.2$, $\kappa = 0.12000, 0.13460$, $|\vec{p}| = 0$ correlator as an example. In the graphs shown circles are the average of the correlator over configurations, errors are calculated by bootstrap. 1000 sub-ensembles are used in the bootstrap analysis. In a few cases increasing the number of bootstrap sub-ensembles to 2000 was investigated. This was found to have a negligible effect on the error suggesting that 1000 sub-ensembles is enough.

A meson two-point correlator is predicted to be a sum of exponentials (3.28). The simplest fit ansatz assumes that the groundstate dominates the sum. The fit function is

$$f(t) = x_1(e^{-x_2 t} + e^{-x_2(T-t)}) \ , \tag{4.2}$$

where the x_i are free parameters; x_1 is the overlap of the meson operator with the state and x_2 is the meson mass in lattice units. This is referred to as the single exponential ansatz because there is only one free parameter in an exponential. The single exponential is only good when t and $T - t$ are sufficiently large. A fit range must be chosen for which the groundstate approximation is good.

The two-point correlator is shown on a log plot in figure 4.3. In practice a log plot is not very useful for choosing fit ranges. A much more useful quantity to plot is effective mass

$$m_{eff}(t) = \cosh^{-1}\frac{\mathrm{C_{2PT}(t-1) + C_{2PT}(t+1)}}{\mathrm{2C_{2PT}(t)}} \ . \tag{4.3}$$

An effective mass plot is shown in figure 4.4. The correlator at time t has been averaged with time slice $T - t$. If the groundstate approximation is correct, the effective mass is constant and equal to the groundstate mass in lattice units.

A sliding window analysis can be used to investigate different fit ranges. Ansatz (4.2) is fitted to the correlator in the range t to t_{max} for many different t. The fit parameters x_1, x_2 and the goodness of fit criterion Q are plotted as

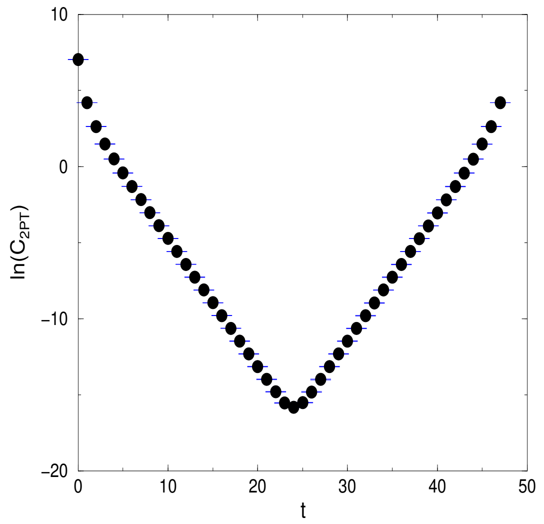

Figure 4.3: Logarithmic plot of the $\beta = 6.2,\ \kappa = 0.1200, 0.13460,\ |\vec{p}| = 0$ Boyled pseudoscalar correlator. The error bars are smaller than the points.

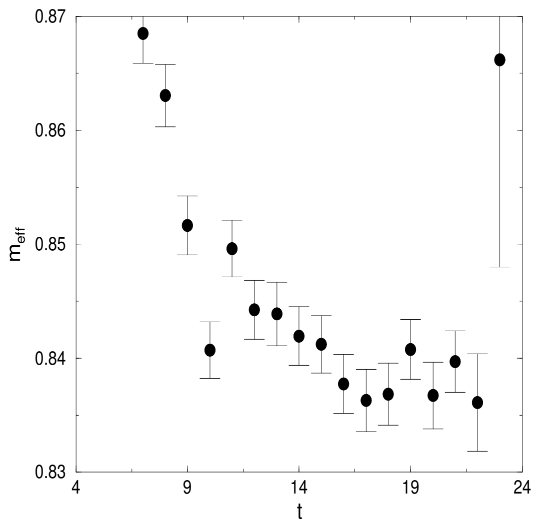

Figure 4.4: Effective mass plot. The same correlator as in figure 4.3 is shown.

a function of t. This is shown in figure 4.5. The fits used correlated chi-square and $t_{max} = 22$. Time slice 23 is too noisy to be useful. Nearby time slices are extremely correlated. For example time slices 12 to 15 of the correlator have

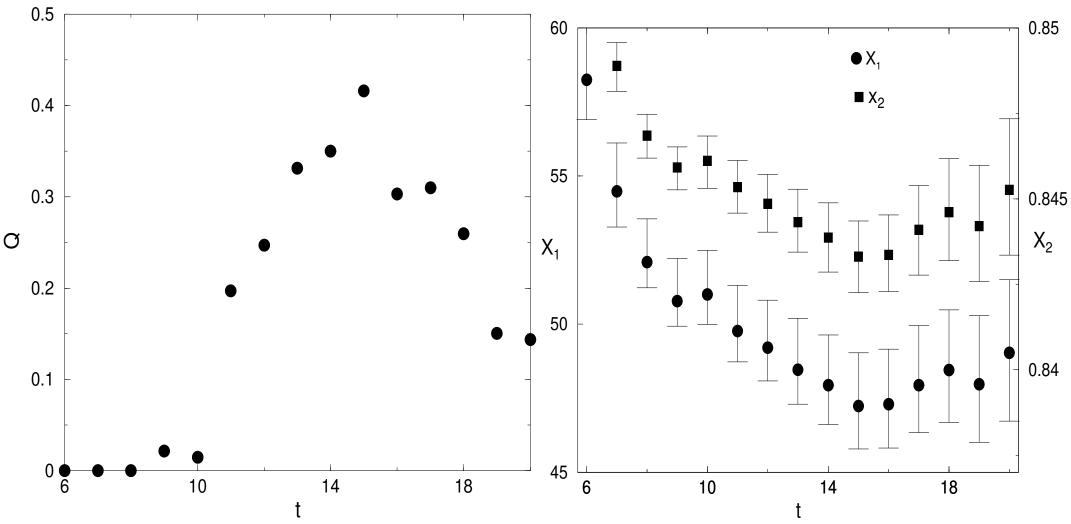

Figure 4.5: Sliding window plots for a single exponential fit. The fit range used is from t to 22. The left plot shows how the goodness of fit criterion Q, the right plot shows the free parameters of the fit, described in (4.2). The same correlator as in figure 4.3 was used in the fits.

correlation matrix,

$$\begin{pmatrix} 1 & 0.983 & 0.962 & 0.939 \\ 0.983 & 1 & 0.987 & 0.969 \\ 0.962 & 0.987 & 1 & 0.988 \\ 0.939 & 0.969 & 0.988 & 1 \end{pmatrix} . \tag{4.4}$$

The low value of Q for $t < 11$ relative to $t \geq 11$ in figure 4.5 indicates a bad fit when $t < 11$.

4.4 The heavy-light pseudoscalar

As a general principle, estimates of the same quantity are averaged before fitting. Time slices t and $T - t$ and all momenta with the same $|\vec{p}|$ are averaged. From looking at sliding window and effective mass plots (e.g. figure 4.4) it was decided to use single exponential fits for the pseudoscalar meson. Figure 4.4 shows that the Boyle type smearing does a good job of reducing overlap with excited states without making the correlators noisy. All 4 heavy $\times$ 3 light $|\vec{p}| = 0, 1, \sqrt{2}$ correlators were fitted to a single exponential (4.2) with x_1 and x_2 as free parameters. The fit range was chosen to be times 12 to 22 for both $\beta = 6.2$ and $\beta = 6.0$. Correlated chi-square fits were used. The $\beta = 6.2$ results are in tables A.1, A.2 and A.3, the $\beta = 6.0$ results are in tables A.7, A.8 and A.9.

In the continuum, energies at different momenta are related by the dispersion relation

$$E^2 = |\vec{p}|^2 + m^2 \ . \tag{4.5}$$

On the lattice Lorentz symmetry is broken to hypercubic symmetry and the dispersion relation does not hold exactly. The fitted energies are compared to the dispersion relation in figure 4.6.

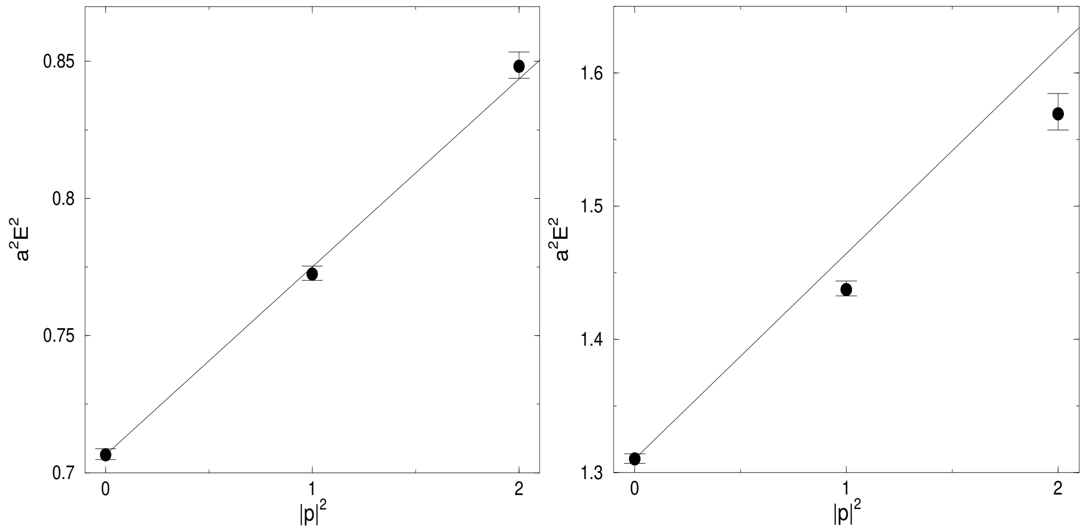

Figure 4.6: Testing the dispersion relation. The data points are fitted energies, the line is the dispersion relation calculated using the fitted mass. Momentum is in units of $2\pi/aL$. The left-hand graph is $\beta = 6.2$, the right-hand graph is $\beta = 6.0$. The kappa combinations are 0.13460, 0.12000 and 0.13344, 0.1230 respectively.

Figure 4.6 shows no detectable deviation from the dispersion relation for $\beta = 6.2$, but very clear deviation for $\beta = 6.0$. It would be interesting to continue the $\beta = 6.2$ graph to higher $|\vec{p}|^2$ and try and find at what point the energy noticeably deviates from the dispersion relation. However, the sliding window analysis for the $\beta = 6.2$, $|\vec{p}|^2 = 3$ correlator indicates an unreliable fit if time slices less than 15 are included. Fitting times 15 to 23 gives a value for the energy but its errors are too large for it to be useful.

To reduce the error on the parameter x_1 for the $\beta = 6.2$ case the fits were repeated with the energy held fixed at its dispersion relation value. These results are in tables A.2 and A.3.

4.5 The light-light vector, $|\vec{p}|^2 = 0$

There is an extra complication to the vector not present for the pseudoscalar; there are two Lorentz indices on the correlator (3.33). In the $|\vec{p}|^2 = 0$ case

$$C^{11}_{V,2PT} = C^{22}_{V,2PT} = C^{33}_{V,2PT} = \tilde{C}_V \quad \text{otherwise} \quad C^{\mu\nu}_{V,2PT} = 0 \tag{4.6}$$

where, in the groundstate dominance approximation,

$$\tilde{C}_V(t, |\vec{p}|) = \frac{|Z_V|^2}{2E_{\rm V}}(e^{-E_{\rm V}t} + e^{-E_{\rm V}(T-t)}) \ . \tag{4.7}$$

The situation is not much different than for the pseudoscalar. The three non-zero correlators are averaged for the fit and the other correlators, which are stochastic estimators of zero, are discarded. Fit ranges were chosen using the sliding window analysis and effective mass plots. The fit parameters are in tables A.4 and A.10.

In general the fit parameters for the vector have larger errors than the fit parameters for the pseudoscalar. These error bars reflect the noise on the FF, LL correlator. Figure 4.2 shows that the LL, LL correlator is considerably less noisy than the FF, LL. The noise level of the FL, LL correlator is in between. Including all three correlators in the fit might reduce the errors on the fitted parameters, although it requires introducing additional free parameters. Unfortunately the groundstate approximation is not good for the LL, LL correlator. To include it in the fit a double exponential fit is used which takes account of the groundstate and the first excited state. The double exponential ansatz is

$$f(t) = x_1(e^{-x_2 t} + e^{-x_2(T-t)}) + x_3(e^{-x_4 t} + e^{-x_4(T-t)}) \ , \tag{4.8}$$

where x_2 is the energy of the groundstate and x_4 is the energy of the first excited state. The three correlators are simultaneously fitted with a double exponential. The masses $x_2,\ x_4$ are the same for each correlator, x_1, x_3 are different for the different correlators but not completely independent. To show this the following notation is introduced,

$$Z^i_X \eta^\mu_r = \langle 0 |\, \Omega^\mu_{\mathrm{V},\ X}(0) | S_i, \vec{p}, \eta_r \rangle \ , \tag{4.9}$$

where X is F or L and i is 0 or 1; S_0 is the groundstate, S_1 is the first excited state. Here L means that the source (or sink) of both quark propagators is local, F means that the source (or sink) of one of the quark propagators is fuzzed the other is local. The parameters x_1, x_3 have the following values for the three different correlators

$$x_1 = \frac{|Z^0_L|^2}{2x_2}, \quad x_3 = \frac{|Z^1_L|^2}{2x_4} \quad \text{for} \quad \mathrm{LL, LL}$$

$$x_1 = \frac{Z^0_L Z^0_F}{2x_2}, \quad x_3 = \frac{Z^1_L Z^1_F}{2x_4} \quad \text{for} \quad \mathrm{FL, LL}$$

$$x_1 = \frac{|Z^0_F|^2}{2x_2}, \quad x_3 = \frac{|Z^1_F|^2}{2x_4} \quad \text{for} \quad \mathrm{FF, LL}$$

In total there are 6 free parameters in the fit.

In general double exponential fits are unstable. To find the minimum of chi-square the algorithm needs to be started from a point already close to the minimum. This was achieved by first doing a single exponential fit to obtain x_2, Z^0_F, Z^0_L. Secondly the double exponential fit was done, but with the parameters x_2, Z^0_F, Z^0_L held fixed at their values from the first fit. This gave the starting point for the full double exponential fit.

Choosing fit ranges for double exponential fits is difficult. Effective mass plots are no use, and there are many more parameters to consider in the sliding window analysis. There are three correlators and in the full sliding window analysis the three fit ranges can be varied independently. Figure 4.7 shows an example sliding window plot. The strong dependence of am_1 on fit range makes the fits difficult to trust. The final fit range used for $\beta = 6.2$ was 9 to 23 for all three correlators as this was the largest range which gives an acceptable Q. The fitted parameters

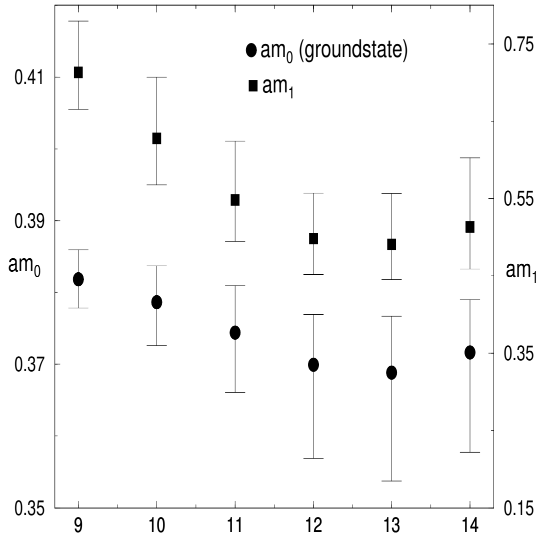

Figure 4.7: A sliding window plot for the double exponential fits described. The fit ranges are 9 to 23 $\beta = 6.2$ for the FF, LL and FL, LL correlators and t to 23 for the LL, LL. All the fits shown have a good Q. $\kappa = 0.13460, 0.13460$, $\beta = 6.2$, $|\vec{p}|^2 = 0$ correlators were used in the fit.

are in table A.12 and a comparison with the single exponential fit is made in table A.4.

The parameters from the double exponential fits agree with those from the single exponential fit. This suggests that both methods are reliable. It also suggests that the right strategy was used to chose the fit range for the double exponential fit. The fuzzing enhances the ground state relative to the first excited state. Using the 0.13460, 0.13460 case as an example

$$\frac{Z_F^1}{Z_F^0} = 0.75$$

$$\frac{Z_L^1}{Z_L^0} = 2.6 \ .$$

The enhancement of the groundstate is important for the analysis of the three-point correlators.

4.6 The light-light vector, $|\vec{p}|^2 \neq 0$

At momentum $|\vec{p}|^2 = 1, 2$ the diagonal correlators (i.e. of the form $C^{\mu\mu}_{V,2PT}$) have three different values. Ignoring possible lattice artefacts these are

$$\begin{array}{rlllll} C^{ii}_{V,2PT} = & \tilde{C}_V & i = 1,2,3 & p^i = 0 & \text{(case 1)} \\ C^{ii}_{V,2PT} = & (1 + (\frac{2\pi}{amL})^2)\ \tilde{C}_V & i = 1,2,3 & p^i \neq 0 & \text{(case 2)} \\ C^{44}_{V,2PT} = & -|\vec{p}|^2 (\frac{2\pi}{amL})^2\ \tilde{C}_V & & & \text{(case 3).} \end{array} \tag{4.10}$$

The factor multiplying $\tilde{C}_V$ is the polarisation sum given in (3.37). In the $|\vec{p}|^2 = 1$ case all the off-diagonal correlators are zero. In the $|\vec{p}|^2 = 2$ case the off-diagonal correlators

$$C^{ij}_{V,2PT} \quad \text{for} \quad i \neq j \quad \text{and} \quad |p^i| = |p^j| = 1 \tag{4.11}$$

are non-zero. Unfortunately the off-diagonal correlators were not saved and so have not been used in the fits.

Two approaches were considered for fitting the vector correlator at $|\vec{p}| \neq 0$, which are described in the following subsections.

4.6.1 Method 1

The form factor calculation in chapter 5 requires the factor Z_{V} (4.7). The mass-dependent factors multiplying $\tilde{C}_V$ in cases 2 and 3 of (4.10) need to be dealt with. A simple approach is to sum the diagonal correlators giving

$$\sum_{\mu} C^{\mu\mu}_{V,2PT}(t, \vec{p}) = 3\tilde{C}_V(t, |\vec{p}|)\ . \tag{4.12}$$

The mass dependent factors in the sum cancel. The fit procedure is now the same as in the pseudoscalar case.

This method is unsatisfactory because it involves averaging correlators which are estimates of different quantities. The three different cases of correlator may have different statistical errors. Summing over all the correlators hides this fact and could lead to an unnecessarily large error on the fitted parameters.

4.6.2 Method 2

The motivation for this method is to avoid averaging correlators which are not equal. Correlators which are equal according to (4.10) are averaged. This gives 3 average correlators, one for each case. These are simultaneously fitted with the ansatz

$$f(t) = K_{(\text{case i})}(\vec{p}, m) x_1 (e^{-x_2 t} + e^{-x_2 (T-t)}) \;, \tag{4.13}$$

where K is the factor multiplying $\tilde{C}_V$ in (4.10) and x_1, x_2 are the free parameters. The fitted mass is used to calculate K. Sliding window plots for this method are shown in figure 4.8. The fits use correlated chi-square, with a block diagonal correlation matrix, that is correlations between the different cases are set to 0. The Q values are good for fits starting at $t \geq 10$.

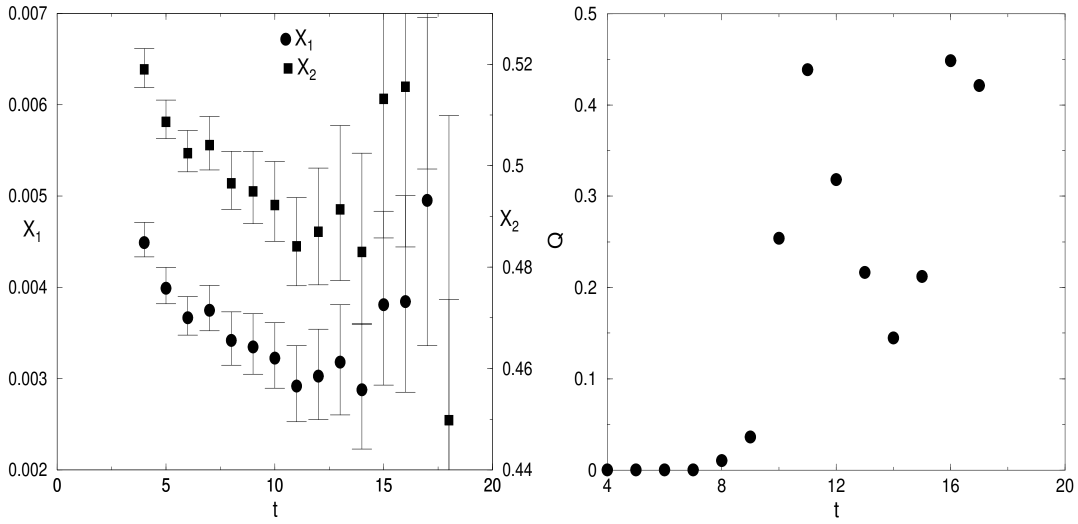

Figure 4.8: Sliding window plots for fits to the light-light vector meson using method 2. The fit range is from t to 23. The FF 0.1346, LL 0.013460 $\beta = 6.2$ $|\vec{p}|^2 = 1$ correlator was used in the fit.

4.6.3 Comparison of the methods

Four possibilities were considered for fitting the vector two-point function at $|\vec{p}|^2 \neq 0$. The options were: method 1 or 2, with the energy a free parameter or fixed at its dispersion relation value. The results from the four possible fits to the heaviest vector are compared in table 4.3.

	method 1		method 2	
Parameter	E fixed	E free	E fixed	E free
$Z_{\rm V}(\lvert\vec{p}\rvert^2=1)$	0.0695^{+19}_{-17}	0.071^{+5}_{-4}	0.0670^{+17}_{-18}	0.070^{+3}_{-2}
$aE(\lvert\vec{p}\rvert^2=1)$	0.461^{+3}_{-3}	0.464^{+9}_{-7}	0.461^{+3}_{-3}	0.465^{+5}_{-5}
$Z_{\rm V}(\lvert\vec{p}\rvert^2=2)$	0.0592^{+17}_{-21}	0.065^{+10}_{-8}	0.0561^{+16}_{-15}	0.055^{+5}_{-4}
$aE(\lvert\vec{p}\rvert^2=2)$	0.530^{+3}_{-2}	0.544^{+21}_{-17}	0.530^{+3}_{-2}	0.527^{+13}_{-11}

Table 4.3: Comparison of the parameters $Z_{\rm V}$, aE obtained by different types of fit. The correlator FF 3460, LL 3460, $\beta = 6.2$ was used.

The fitted energies in table 4.3 satisfy the dispersion relation within errors. This is shown graphically for $\beta = 6.2$ and $\beta = 6.0$ in figure 4.9. It was decided to use a one-parameter fit as these give much smaller errors on $Z_{\rm V}$.

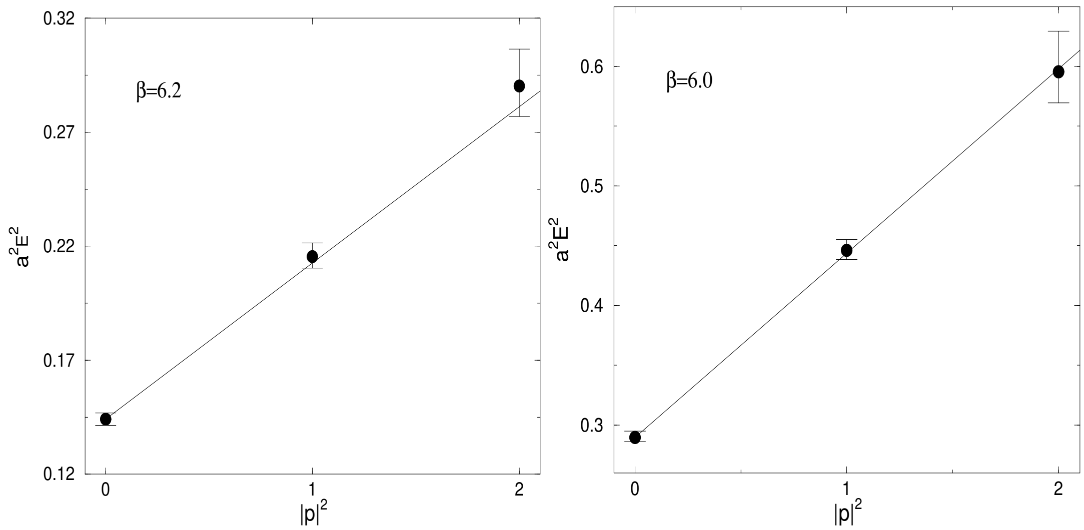

Figure 4.9: Testing the dispersion relation for the light-light vector. The data points are fitted energies, using method 2, the line is the dispersion relation calculated using the fitted mass. Momenta are in units of $2\pi/aL$. The kappa combinations are 0.13460, 0.13460 and 0.13344, 0.13344.

The value for $Z_{\rm V}$ depends significantly on whether method 1 or method 2 is used. The reason is that the vector two-point correlator does not satisfy the continuum prediction for the three possible values multiplying $\tilde{C}_{\rm V}$ given in (4.10). This was found by repeating the method 2 fit with the full correlation matrix, i.e. correlations between the different cases *not* set to zero. The value of Q obtained indicated a bad fit. This is nicely illustrated by dividing the averaged case 2 correlator by the averaged case 1 correlator. This ratio is referred to as ζ. The numerator and denominator of ζ are highly correlated, so there is a dramatic cancellation of statistical errors. In the continuum, and with groundstate dominance this ratio is $1 + (\frac{2\pi}{amL})^2$. The method 2 fit relies on this result. The continuum and lattice ratios are compared in figure 4.10.

4.6.4 Fuzzing and rotational symmetry

Figure 4.10 shows that the $LL,\ LL$ correlator agrees with the continuum prediction for the ratio ζ, but the $LL,\ FF$ correlator disagrees. At time slices 12 and 13 the disagreement is at more than the 6σ level. The $LL,\ LF$ and $LL,\ FL$ are in slight disagreement with the continuum prediction, at between the 1 and 2 σ level. These results suggest that the local vector operator is more continuum-like than the fuzzed vector operator.

The continuum value of ζ was derived in section 3.8 by using the sum over polarisations for a massive vector particle. An equivalent derivation relies on rotational symmetry. The vector two-point function ($C^{\mu\nu}_{V,2PT}$) is a tensor with two indices. The only tensors with the same transformations under rotations are $p^\mu p^\nu$ and $g^{\mu\nu}$. Therefore

$$C^{\mu\nu}_{V,2PT}(t,\vec{p}) = \frac{|Z_{\rm V}|^2}{2E_{\rm V}}(-g^{\mu\nu} + \alpha p^\mu p^\nu)e^{-E_{\rm V}t} \ , \tag{4.14}$$

where the variable α is not determined by rotational symmetry. The continuum Ward-Takahashi identity for a flavour-changing vector current [16] gives

$$p_\mu C^{\mu\nu}_{V,2PT} = 0 \ , \tag{4.15}$$

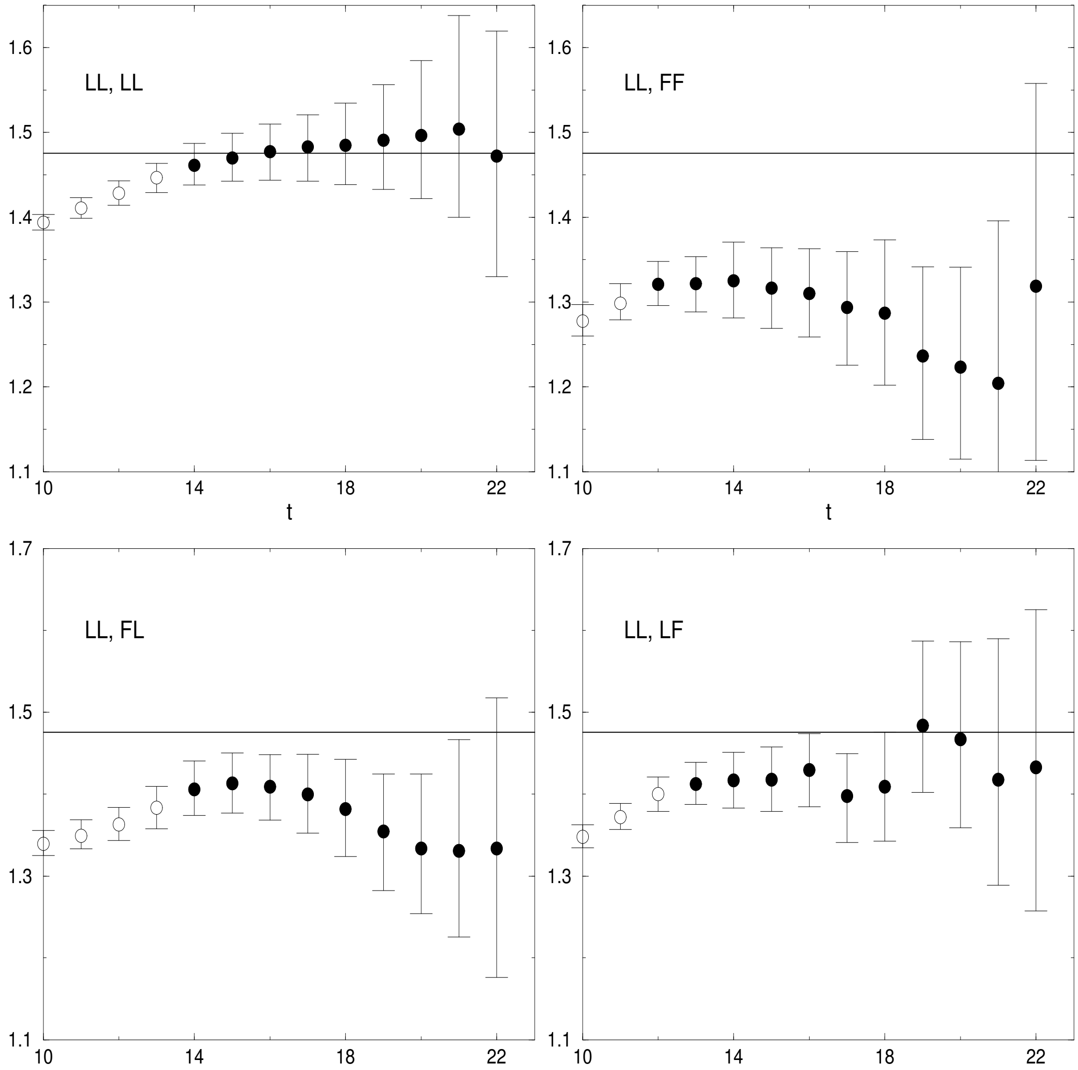

Figure 4.10: The ratio ζ. The data points are the lattice value of the ratio, the line is the continuum prediction. The filled circles are time slices where the groundstate-dominance approximation is reliable. Each graph is for a two point function with different smearing (the smearing is noted on each graph). The correlator used is $\kappa = 0.13460, 0.13460,\ \ \beta = 6.2,\ \ |\vec{p}|^2 = 1$.

so $\alpha = 1/m_{\rm V}^2$. Therefore

$$C^{\mu\nu}_{V,2PT}(t,\vec{p}) = \frac{|Z_{\rm V}|^2}{2E_{\rm V}}(-g^{\mu\nu} + \frac{p^\mu p^\nu}{m^2})e^{-E_{\rm V}t} \tag{4.16}$$

as was derived earlier. Results (4.14) and (4.15) are exact in the continuum, but not exact on the lattice. However, if the lattice spacing is fine enough these conditions will be approximately true. Fuzzing the vector operator makes either (4.14), (4.15) or both a less good approximation.

A reasonable conjecture is that rotational symmetry is violated more strongly for the $LL,\ FF$ correlator than for the $LL,\ LL$ correlator. To justify this consider the fuzzed vector meson operator [25]

$$\Omega^{\mu}_{Fuzz}(\vec{x},t) = \frac{1}{6}\sum_{i=1}^{6} \bar{\psi}_1(\vec{x}+\vec{r}_i,t)\mathcal{F}(\vec{x},t;\vec{r}_i,)\gamma^{\mu}\psi_2(\vec{x},t)\ . \tag{4.17}$$

Here the $\vec{r}_i$ are in the direction of the lattice axes and $\mathcal{F}(\vec{x},t;\vec{r}_i,)$ is the product of fuzzed links between $\vec{x}$ and $\vec{x}+\vec{r}_i$ at time slice t. The fuzzing treats the three spatial lattice axes differently from other directions. It is easy to imagine a more rotationally symmetric smearing procedure than (4.17), which includes additional terms with $\vec{r}_i$ not in the direction of the lattice axes. This study uses $|\vec{r}_i| = 6a$ at $\beta = 6.0$, $|\vec{r}_i| = 8a$ at $\beta = 6.2$. At momentum 1 in lattice units the wavelength associated with the momentum is aL. The fuzzing length is smaller than the wavelength of the momentum, but not insignificant. If rotational symmetry is being spoiled by the fuzzing then (4.14) is modified by terms forbidden by rotational symmetry, but permitted by hypercubic symmetry. The additional term which is lowest order in the lattice spacing is

$$(p^{\mu})^3 p^{\nu} + p^{\mu}(p^{\nu})^3\ . \tag{4.18}$$

with no summation convention. The fuzzed vector operator at $|\vec{p}| \neq 0$ needs to be investigated further.

The results for fitting the $|\vec{p}| \neq 0$ $LL,\ FF$ correlator are listed in tables A.5 A.6 and A.11. The results for method 1 and 2 are both listed. For the form factor calculation the method 1 calculation of Z_{V} was used. The difference between the two results was treated as a systematic error.

4.7 Quark mass

The free parameter which determines quark mass in a simulation is the hopping parameter, κ. For free fermions the quark mass is

$$am_q = \frac{1}{2\kappa} - 4 \ , \tag{4.19}$$

which is a rearrangement of (2.22). However in the interacting theory this expression is modified by renormalisation. For the Wilson action the quark mass is modified by an additive renormalisation. The quark mass is given by

$$am_q^W = \frac{1}{2\kappa} - \frac{1}{2\kappa_c} \ . \tag{4.20}$$

where κ_c is the critical value of the hopping parameter, at which the quark mass vanishes. This work uses the $\mathcal{O}(a)$ improved Wilson action which causes an additional mass dependent multiplicative renormalisation of quark mass. In this case the quark mass is given by

$$m_q = m_q^W(1 + b_m am_q^W) \ . \tag{4.21}$$

The value used here for b_m is the one-loop tadpole improved perturbation theory result [33]

$$b_m = -\frac{1}{2} - 0.0962 g_0^2 \ . \tag{4.22}$$

b_m has also been calculated nonperturbatively for $\beta = 6.2$ [34]. There is a fairly large error on this result and it is in good agreement with perturbation theory so it has not been used.

Chiral symmetry arguments suggest that the mass of a pseudoscalar meson composed of light quarks satisfies

$$m_{\mathrm{P}}^2 = B(m_{q,1} + m_{q,2}) \quad , \tag{4.23}$$

where $m_{q,i}$ are the quark masses given by (4.21) and B is a mass independent parameter of QCD. This relation (4.23) is used to determine the critical value of the hopping parameter and the light quark masses. Substituting (4.21) in to (4.23) yields

$$m_{\mathrm{P}}^2 = \frac{B}{\kappa_c}\Big(-1 + \frac{b_m}{2\kappa_c}\Big) + \frac{B}{2}\Big(1 - \frac{b_m}{\kappa_c}\Big)\Big(\frac{1}{\kappa_1} + \frac{1}{\kappa_2}\Big) + \frac{Bb_m}{4}\Big(\frac{1}{\kappa_1^2} + \frac{1}{\kappa_2^2}\Big) \ . \tag{4.24}$$

This relation was used to determine κ_c. The lattice results for $am_{\rm P}$ were fitted to 3×3 κ_1, κ_2 combinations with aB and κ_c as unknown parameters. This was done in [19], giving

$$\begin{aligned} \kappa_c &= 0.135252^{+16}_{-9} \qquad (\beta = 6.0) \\ \kappa_c &= 0.135815^{+17}_{-14} \qquad (\beta = 6.2)\ . \end{aligned} \tag{4.25}$$

Table 4.4 contains the quark mass for each of the κ values used in the simulation, calculated using 4.21.

$\beta = 6.2$		$\beta = 6.0$	
κ	am	κ	am
0.13530	0.014	0.13455	0.019
0.13510	0.019	0.13417	0.029
0.13460	0.033	0.13344	0.049
0.12990	0.15	0.12730	0.20
0.12660	0.23	0.12230	0.30
0.12330	0.29	0.11730	0.37
0.1200	0.35	0.11230	0.42

Table 4.4: The quark mass for each of the κ values used in the simulation.

4.8 Matching quark masses to experiment

The masses of the light pseudoscalar mesons are used to determine light quark masses. Applying (4.23) to the observed light pseudoscalar mesons gives

$$\begin{aligned} m^2_{\pi^\pm} &= B(m_u + m_d) \\ m^2_{K^\pm} &= B(m_u + m_s) \\ m^2_{K^0} &= B(m_d + m_s)\ . \end{aligned} \tag{4.26}$$

In this study isospin symmetry is assumed, i. e. $m_u = m_d$, and the kaon masses are averaged according to

$$m_K^2 = \frac{1}{2}(m_{K^\pm}^2 + m_{K^0}^2)\ . \tag{4.27}$$

The lattice light quark masses are given by

$$am_d = (a\mathcal{O})^2 \frac{(m_\pi/\mathcal{O})^2_{exp}}{2aB} \tag{4.28}$$

$$a(m_s + m_d) = (a\mathcal{O})^2 \frac{(m_K/\mathcal{O})^2_{exp}}{aB}\ , \tag{4.29}$$

where $\mathcal{O}$ is the quantity used to set the scale (lattice spacing) and the ratios with subscript exp are the experimental values. aB and $a\mathcal{O}$ are calculated on the lattice.

The values am_s, am_d calculated by the above procedure depend on which physical quantity is used to set the scale. This is not a surprise because the theoretical pseudoscalar masses are not calculated in the right theory; they are calculated in quenched QCD at nonzero lattice spacing. This problem always occurs when comparing quenched calculations with experiment. The standard approach is to use several different physical quantities to set the scale, and treat the variation in the result as a systematic error. In this work r_0 is used to set the scale unless otherwise stated. Phenomenological results are also calculated using m_ρ to test the scale dependence of the result and estimate the systematic error.

4.9 Quark mass dependence of the pseudoscalar

The pseudoscalar masses are extrapolated in light quark mass for the form factor calculation. This is done separately for each heavy quark mass. The meson masses are linear in light quark mass to a very good approximation, as shown in figure 4.11.

Given the size of the error bars on the data in figure 4.11, it is surprising that the central values are so close to the fitted line. This is because the three data

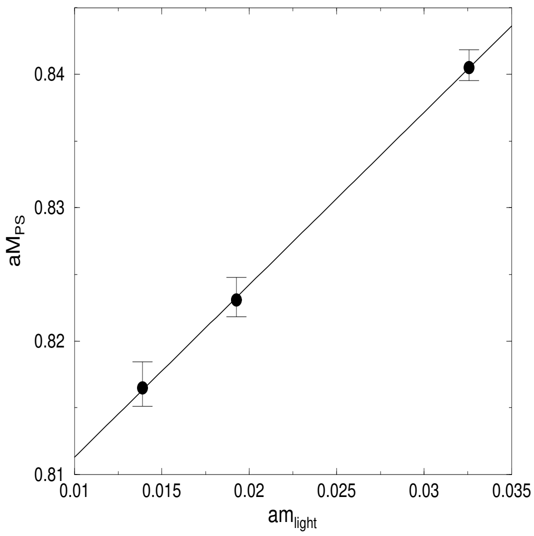

Figure 4.11: The dependence of the heavy-light pseudoscalar mass on the light quark mass. The data are fitted masses, the line is a linear fit. $\kappa_{heavy} = 0.12000$.

points are highly correlated. The correlation matrix for the data in figure 4.11 is

$$\begin{pmatrix} 1 & 0.979 & 0.876 \\ 0.979 & 1 & 0.950 \\ 0.876 & 0.950 & 1 \end{pmatrix} \tag{4.30}$$

with κ_{light} in the order 0.13530, 0.13510, 0.13460. The parameters from correlated and uncorrelated fits are virtually the same in this case. However, for the fit shown in figure 4.11, a correlated fit gives $Q = 0.116$ and an uncorrelated fit gives $Q = 0.892$. Clearly the uncorrelated fit overestimates Q. Correlated fits were used.

In this situation correlated data is an advantage. Errors on the fit parameters are calculated by using the bootstrap method. The fit is repeated for each bootstrap sub-ensemble. To correctly handle the correlations, the three data points fitted always come from the same bootstrap sub-ensemble. To find out what the errors would be if the data were uncorrelated the fits are repeated using different bootstrap sub-ensembles for the three-points. Comparing the resulting fit parameters:

$$\begin{array}{lllll} \text{Slope :} & 1.25^{+10}_{-10} & \text{(uncorrelated)} & 1.25^{+2}_{-3} & \text{(correlated)} \\ \text{Intercept :} & 0.798^{+3}_{-2} & \text{(uncorrelated)} & 0.798^{+2}_{-2} & \text{(correlated)} \ . \end{array}$$

The correlations in the data allow a much more accurate determination of slope than would be possible with uncorrelated data.

4.10 Quark mass dependence of the vector

Figure 4.12 shows the dependence of vector meson mass on average quark mass. As before the data are highly correlated. A linear ansatz fits the data well.

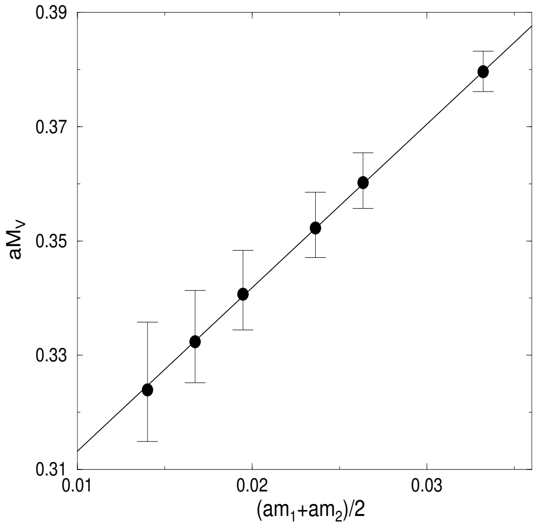

Figure 4.12: The dependence of the light-light vector mass on averaged quark mass. The data are the fitted masses, the line is a linear fit.

Chapter 5

Analysis of the three-point correlators

5.1 Form factors

The three-point correlators depend on the matrix element

$$\langle \mathrm{V}, k, \eta | J_\mu | \mathrm{P}, p \rangle \ , \tag{5.1}$$

where J^μ is either A^μ or V^μ, η is the polarisation vector of the V and p, k are four-momenta. This matrix element describes the nonperturbative part of a semileptonic decay. The matrix element can be decomposed in terms of form factors, that is, the matrix element can be expressed in terms of a few functions of q^2 (where $q = p - k$). This is proved by using the Lorentz, parity and charge conjugation symmetries of the current and states.

The matrix element (5.1) with a vector current depends on one form factor. The conventional parametrisation, used here, is

$$\langle \mathrm{V}, k, \eta | V_\mu | \mathrm{P}, p \rangle = \frac{2V(q^2)}{m_\mathrm{P} + m_V} \varepsilon_{\mu\rho\sigma\delta} p^\rho k^\sigma \eta^{\star\delta} \ . \tag{5.2}$$

For the case of an axial current the matrix element depends on three form factors. A parametrisation convenient for phenomenology is

$$\langle \mathrm{V}, k, \eta_r | A_\mu | \mathrm{P}, p \rangle \quad = i(m_\mathrm{P} + m_\mathrm{V}) A_1(q^2) g_{\mu\sigma} \eta_r^{\star\sigma}$$

$$
\begin{aligned}
&-\frac{iA_2(q^2)}{m_\mathrm{P}+m_\mathrm{V}}(p+k)_\mu q_\sigma \eta_r^{\star\sigma} \\
&+\frac{2im_\mathrm{V}A(q^2)}{q^2}(p-k)_\mu (p+k)_\sigma \eta_r^{\star\sigma} \quad .
\end{aligned} \tag{5.3}
$$

Any three form factors related to $A_1,\ A_2,\ A$ by an invertible linear transformation can be used for the form factor decomposition. The following form factors are sometimes useful

$$
A_3(q^2) = \frac{m_\mathrm{P}+m_\mathrm{V}}{2m_\mathrm{V}} A_1(q^2) - \frac{m_\mathrm{P}-m_\mathrm{V}}{2m_\mathrm{V}} A_2(q^2) \tag{5.4}
$$

$$
A_0(q^2) = A(q^2) + A_3(q^2) \quad . \tag{5.5}
$$

At $q^2 = 0$ there are only two independent axial form factors. This is expressed by the constraint

$$
A_0(0) = A_3(0) \ . \tag{5.6}
$$

The three-point correlators depend on the polarisation-averaged matrix elements. In terms of form factors these are

$$
\sum_r \eta_\nu^r \langle \mathrm{V}, k, \eta_r | V_\mu | \mathrm{P}, p\rangle = \frac{2V(q^2)}{m_\mathrm{P}+m_V}\varepsilon_{\mu\rho\sigma\nu} p^\rho k^\sigma \tag{5.7}
$$

$$
\begin{aligned}
\sum_r \eta_\nu^r \langle \mathrm{V}, k, \eta_r | A_\mu | \mathrm{P}, p\rangle = {} & i(m_\mathrm{P}+m_\mathrm{V})A_1(q^2)(g_{\mu\nu} - \frac{k_\mu k_\nu}{m_\mathrm{V}^2}) \\
&+\frac{iA_2(q^2)}{m_\mathrm{P}+m_\mathrm{V}}(p+k)_\mu (\frac{p\cdot k}{m_\mathrm{V}^2}k_\nu - p_\nu) \\
&-\frac{2im_\mathrm{V}A(q^2)}{q^2}(p-k)_\mu (\frac{p\cdot k}{m_\mathrm{V}^2}k_\nu - p_\nu) \ ,
\end{aligned} \tag{5.8}
$$

where r labels the three possible polarisations of the vector.

The form factor decomposition presented here is for continuum Minkowski space. The Euclidean space decomposition is obtained by the substitution

$$
\begin{aligned}
J^4 &= iJ^0 \\
\eta^4 &= i\eta^0 \ .
\end{aligned} \tag{5.9}
$$

In principle the form factor decomposition is different on the lattice, because Lorentz symmetry is modified to hypercubic symmetry. The lattice form factor decomposition will tend towards the continuum one as the lattice spacing is reduced and is not considered here.

5.2 Lattice details

The same gauge configurations described in chapter 4 were used in the calculation. The three-point functions calculated are of the generic form

$$C^{\mu\nu}_{3PT}(\vec{p},\vec{q},t) = \sum_{\vec{x},\vec{y}} e^{-i(\vec{p}.\vec{x}-\vec{q}.\vec{y})} \ \langle 0|\, T\{\Omega_{\rm P}(\vec{x},t_E=28)J^{\mu}(\vec{y},t)\Omega^{\dagger\nu}_{\rm V}(0)\}\,|0\rangle \ , \quad (5.10)$$

described in section 3.10. The flavour-changing current J^μ is either A^μ or V^μ. For the improvement counter terms the correlator is also calculated with the flavour-changing tensor and pseudoscalar. The pseudoscalar operator, $\Omega_{\rm P}$, is always at time $t_E = 28$. Moving this would require recalculating the extended propagator. The three-point function is calculated with all possible values of t. The situation $t > 28$ is referred to as the back of the lattice and $t < 28$ is referred to as the front of the lattice. p is the momentum of the pseudoscalar, q is the momentum transfer of the decay. The momentum of the vector is k, where

$$k = p - q \ . \quad (5.11)$$

The three-point correlator and most of the notation conventions are shown in figure 5.1. The quarks are refered to as active, passive and heavy with hopping parameters κ_A, κ_P and κ_H respectively.

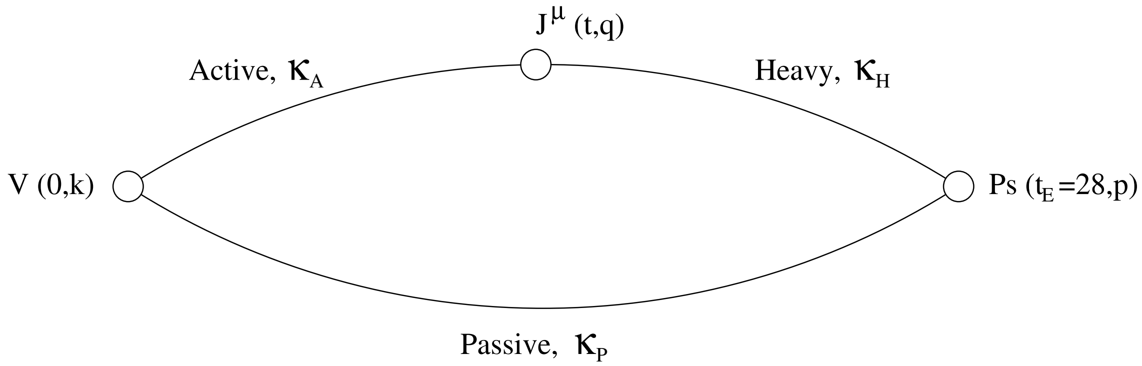

Figure 5.1: Schematic of the three-point correlator.

The combinations of the momenta $\vec{p}$ and $\vec{k}$ used in the simulation are listed in table 5.1. The $\vec{p}$, $\vec{k}$ combinations have been grouped into 9 momentum chan-

Channel name	$\vec{p}$	$\vec{k}$
$0 \to 0$	(0,0,0)	(0,0,0)
$0 \to 1$	(0,0,0)	(0,0,-1), (0,-1,0), (-1,0,0)
$0 \to 2$	(0,0,0)	(-1,-1,0), (-1,0,-1), (0,-1,-1), (-1,1,0), (1,0,-1), (0,-1,1)
$1 \to 0$	(0,0,1)	(0,0,0)
$1 \to 1 \parallel$	(1,0,0)	(1,0,0)
$1 \to 1 \perp$	(1,0,0)	(0,-1,0)
$1 \to 1_{\downharpoonleft\upharpoonright}$	(1,0,0)	(-1,0,0)
$1 \to 2 \parallel$	(1,0,0)	(1,1,0), (1,0,1), (1,-1,0) (1,-1,0)
$1 \to 2 \perp$	(1,0,0)	(0,1,1), (0,1,-1), (0,-1,1) (0,-1,-1)

Table 5.1: $\vec{p}$, $\vec{k}$ combinations used in the simulation, grouped into momentum channels. The momentum channels are referred to by a name of the form $|\vec{p}|^2 \to |\vec{k}|^2$. Where necessary the name includes the orientation of $\vec{p}$ and $\vec{k}$. For example $\perp$ indicates that $\vec{p}$ and $\vec{k}$ are perpendicular.

nels. All the $\vec{p}$, $\vec{k}$ combinations in a particular channel are related by hypercubic symmetry and have the same q^2. Each channel has a name so that it can be referred to in the tables and text. The name is of the form $|\vec{p}|^2 \to |\vec{k}|^2$. If $|\vec{p}|^2$ and $|\vec{k}|^2$ are both nonzero, then the channel name includes the relative orientation of $\vec{p}$ and $\vec{k}$. For channel $1 \to 1$ there are three possible orientations of $\vec{p}$ and $\vec{k}$; parallel, perpendicular, and antiparallel. These orientations are included in the channel name using the symbols $\perp$, $\downharpoonleft\upharpoonright$, and $\parallel$ respectively. For channel $1 \to 2$ two orientations were considered. These were referred to as $1 \to 2 \perp$ and $1 \to 2 \parallel$, although $\vec{p}$ and $\vec{k}$ are not parallel in the latter channel.

The three-point correlators are calulated with 4 κ_H values, 3 κ_A and 2 κ_P, giving 24 κ combinations in total. The active quark propagator is fuzzed at Ω_{V}, the heavy quark is Boyled at Ω_{P}. The flavour-changing current is local and both ends of the passive propagator are local.

5.3 Improvement and renormalisation

The action used in the simulation is the $\mathcal{O}(a)$ improved SW action. The axial and vector currents need to be improved by adding counter terms, given in (3.16). This can be simply implemented by improving the three-point correlator. In the case of the axial correlator,

$$C^{\mu\nu\ I}_{A,3PT} = \begin{cases} C^{\mu\nu}_{A,3PT} + ic_A \sin(\mathrm{q}^\mu)\ \mathrm{C}^{\nu}_{\mathrm{P,3PT}} & \text{for } \mu = 1,2,3 \\ C^{\mu\nu}_{A,3PT} \pm c_A \sinh(\mathrm{q}^\mu)\ \mathrm{C}^{\nu}_{\mathrm{P,3PT}} & \text{for } \mu = 4,\ + \text{for t} < 28,\ - \text{for t} > 28 \end{cases} \tag{5.12}$$

where $C^{(I)}_{A,3PT}$ is the (improved) axial correlator, $C_{P,3PT}$ is the three-point correlator with a flavour-changing pseudoscalar and q^μ is in lattice units. q^4 is defined to be positive. This result is from applying the discretised partial derivative to $C_{P,3PT}$. The case $\mu = 4$ assumes that the correlator is decaying exponentially and is different for back ($t > 28$) and front of the lattice. The constants used for improvement and renormalisation are listed in table 5.2.

coefficient	$\beta = 6.0$	$\beta = 6.2$	reference
Z_V	0.770	0.7874	LANL [24]
b_V	1.53	1.42	LANL [24]
Z_A	0.807	0.818	LANL [24]
b_A	1.28	1.32	LANL [24]
c_V	-0.107	-0.09	LANL [24]
c_A	-0.037	-0.032	LANL [24]
c_{SW}	1.769	1.614	Alpha [23]
b_m	-0.5962	-0.5931	Alpha [33]

Table 5.2: Constants needed to implement improvement in this work. All except for b_m are calculated nonperturbatively. Note that the Z_V in this table is the renoramlisation coefficient, not the overlap of a meson operator with the vector state.

In practice it was convenient to fit the improved three-point correlator and then renormalise the form factors. The renormalisation prescription is

$$F^{(renorm)} = Z_J \left(1 + b_J \frac{am_a + am_h}{2}\right) F^{(bare)} , \tag{5.13}$$

where m_a is the active quark mass, m_h is the heavy quark mass, and F is the form factor. The subscript J is A for the axial form factors or V for the vector form factor.

Apart from b_m, the constants in table 5.2 were all determined nonperturbatively. Also they are consistent with each other. The LANL constants were calculated with gauge configurations generated using the Alpha value for c_{SW}. b_m is calculated in boosted perturbation theory. This constant is only needed to calculate improved quark mass. It does not appear in the form factor calculation and is the least important coefficient for this work.

A nonperturbative calculation of an improvement coefficient has a discretisation error. Comparing different calculations of the same improvement coefficient gives some indication of the discretisation error. Most of the coefficients are found to vary slightly between calculations. However c_V depends rather strongly on the method used to calculate it, especially for $\beta = 6.0$.

5.4 Overview of the fits

The approximate time dependence of the three-point correlator for the back of the lattice is

$$C^{\mu\nu}_{3PT} = \frac{Z^*_{\mathrm{P}} Z_{\mathrm{V}}}{2E_{\mathrm{P}} 2E_{\mathrm{V}}} e^{-E_{\mathrm{V}} T} e^{E_{\mathrm{P}}\ t_E} e^{-t(E_{\mathrm{P}} - E_{\mathrm{V}})} \sum_r \eta^\nu_r \langle \mathrm{V}, -\vec{k}, \eta_r | J^\mu(0) | \mathrm{P}, -\vec{p}\rangle \ . \tag{5.14}$$

This was derived in section 3.10 and is the starting point for the fit. Consider $C^{\mu\nu}_{3PT}$ with a specific $\vec{p}$, $\vec{k}$ and J. The correlator is calculated for all 16 possible combinations of Lorentz indices. The form factor decomposition is applied to (5.14) for these 16 cases. In some cases the correlator is zero and is discarded from the fit. The remaining correlators may include symmetry-related correlators, which have equal magnitude. The symmetry-related correlators are averaged, some multiplied by -1 if necessary. This leaves N_{ave} averaged correlators which all have different form factor decompositions. The other $\vec{p}$, $\vec{k}$ combinations from the channel have the same N_{ave} distinct correlators. All correlators from a channel that can be averaged, are averaged. These are then fitted with the form factors as free parameters.

The value of N_{ave} for the different channels and currents is in table 5.3. For the vector current and channel $0 \to 0$, $N_{ave} = 0$ so the form factor V cannot be determined. For the axial current and channel $0 \to 0$, $N_{ave} = 1$, so only one linear combination of form factors can be determined. It turns out that only A_1 can be determined for this channel. For all the other channels used all the form factors can be obtained.

Channel	$N_{ave}(A)$	$N_{ave}(V)$
$0 \to 0$	1	0
$0 \to 1$	5	1
$0 \to 2$	6	2
$1 \to 0$	3	2
$1 \to 1 \parallel$	4	2
$1 \to 1 \perp$	10	3
$1 \to 1_{\rfloor\lceil}$	5	1
$1 \to 2 \perp$	10	3
$1 \to 2 \parallel$	10	not used

Table 5.3: The number of correlators to fit after averaging and throwing away stochastic estimators of zero.

To fit the three-point function the time-dependent factor multiplying the matrix element in (5.14) is needed. Two ways were considered for estimating this factor. One method uses the values for $E_{\rm P}$, $E_{\rm V}$, $Z_{\rm V}$, $Z_{\rm P}$ obtained in chapter 4 to construct the time-dependent factor. The alternative method uses the result

$$\frac{C_{3PT}(\vec{p}, t_E, \vec{k}, t)}{C_{{\rm P},2PT}(|t - t_E|, \vec{k}) \;\; \tilde{C}_{{\rm V},2PT}(t, \vec{p})} = \begin{cases} Z_{\rm V}^* Z_{\rm P} \sum_r \eta_r^{*\nu} \langle {\rm P}, \vec{p} | J^\mu(0) | {\rm V}, \vec{k}, \eta_r \rangle & t < 28 \\ Z_{\rm V} Z_{\rm P}^* \sum_r \eta_r^{\nu} \langle {\rm V}, -\vec{k}, \eta_r | J^\mu(0) | {\rm P}, -\vec{p} \rangle & t > 28 \end{cases} \tag{5.15}$$

which assumes that the ground state dominates the two-point functions.

The two methods can be compared by plotting the three-point correlator with the time dependence divided off. These plots are referred to as plateau plots because there should be a plateau where the approximations are valid. A plateau plot for each method is shown in figure 5.2. The plateau plot using fitted energies has a plateau for $33 \leq t \leq 47$ and possibly a very noisy plateau for $12 \leq t \leq 20$. The plateau plot using meson correlators has a much shorter plateau $34 \leq t \leq 40$ because outside this region the groundstate dominance approximation is not valid for the two-point correlators. Even at time slice 38 there is a difference of about 10% between the two types of plots because the groundstate dominance approximation is violated. It was decided that using fitted energies is the better method.

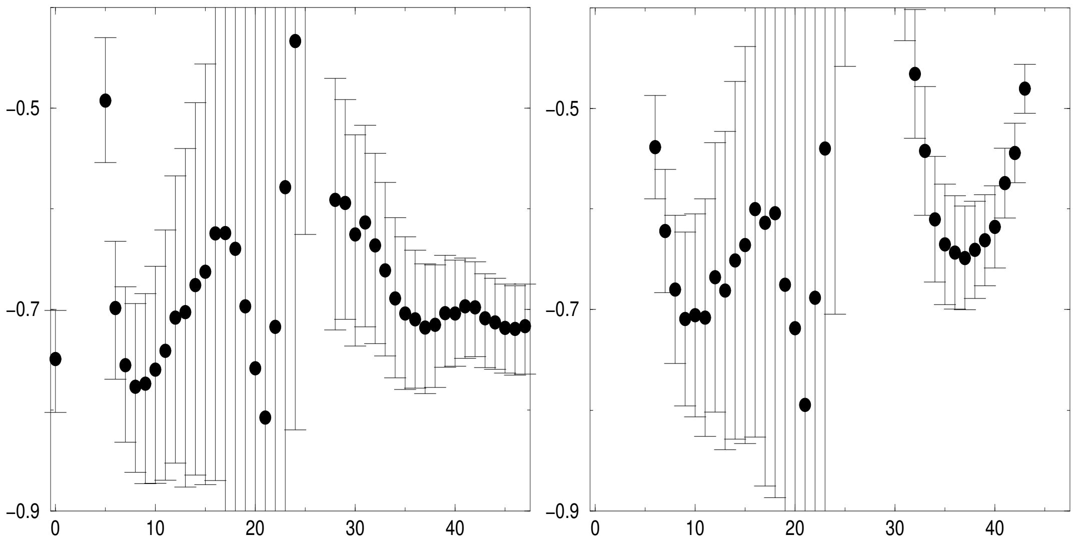

Figure 5.2: Example plateau plots for the two different methods. The same three-point correlator is used in both plots. Time dependence is removed in the left plot using fitted energies, in the right plot using meson correlators. The plot is for single correlator (no averaging) from the $0 \to 1$ case, $\beta = 6.2$.

The coefficients appearing in the form factor decomposition were needed for the fit. These were calculated using the momenta and the fitted masses. Correlated chi-square fits were used, but with correlations between different averaged correlators set to zero. This is thought to be the best procedure because different correlators have different systematic errors not taken account of by the correlation matrix. The error analysis used the bootstrap method and includes the errors on the fitted two-point parameters. Exactly the same bootstrap subensembles were used for the two-point fits and three-point fits. This may reduce the errors on the fitted form factors because of correlations between two-point and three-point correlators.

5.5 Choosing fit ranges

There are a large number of correlators to fit. For each β there are 9 channels in the axial case and 7 channels in the vector case. Each channel has N_{ave} averaged, improved correlators and 24 κ combinations. Fit ranges were chosen separately for each channel, current, β, and averaged correlator. The same fit ranges were used for the 24 κ combinations. The fit ranges were chosen by studying plateau plots. All the plateau plots were looked at for two different κ combinations. The sliding window analysis, which is very useful for choosing fit ranges for the two-point functions, is too complicated to apply to the three-point functions. A lot of correlators are being fitted and both the start and end of the fit needs to be varied. For example, in the axial $1 \rightarrow 1 \perp$ case, $N_{ave} = 10$ so the full sliding window analysis is in a 20 dimensional space.

Some example plateau plots are shown in figure 5.3. The correlators in figure 5.3 are much noisier at the front than at the back of the lattice. This was found to always be the case, so all fit ranges were chosen at the back of the lattice. The $0 \rightarrow 1$ correlator shown in figure 5.3 has a very long, definite plateau for $33 \leq t \leq 47$. There is no definite plateau at the front, but time slices $8 \leq t \leq 10$ are possibly a noisy plateau and agree with the plateau at the back of the lattice. The $1 \rightarrow 0$ correlator shown does not have such a good plateau at the back of the lattice. It was decided to fit time slices $36 \leq t \leq 39$ as these are midway between the pseudoscalar and vector meson operators and are consistent with the noisy plateau on the front of the lattice. The $\beta = 6.2$ plateau plots typically have a plateau which is more definite than the $1 \rightarrow 0$ case, but less definite than the $0 \rightarrow 1$ case shown in figure 5.3

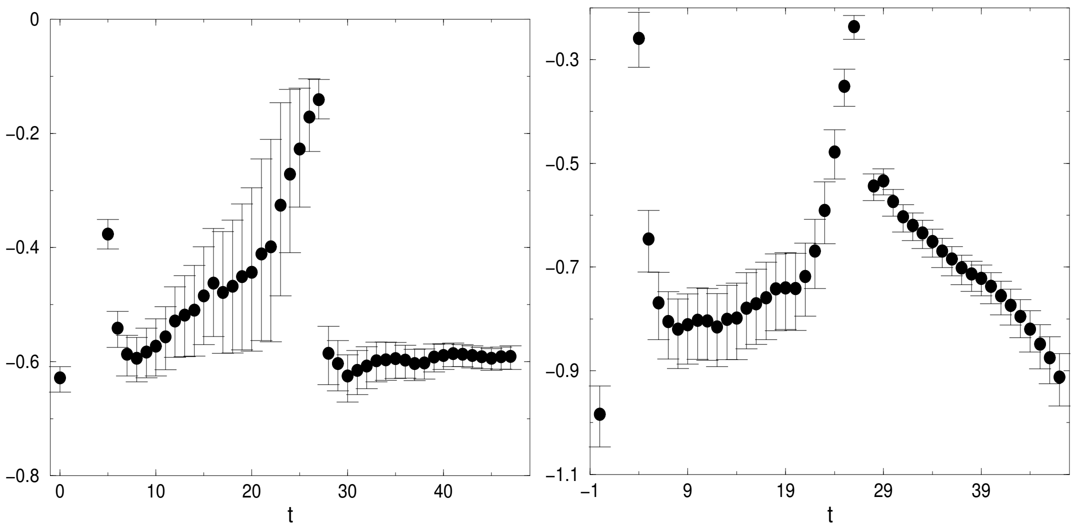

Figure 5.3: Two plateau plots used for picking fit ranges. The left graph is the same correlator as figure 5.2 ($0 \to 1$, $\beta = 6.2$), averaged with the other symmetry related correlators and improved. The right hand graph is from channel $1 \to 0$, $\beta = 6.2$.

In the $\beta = 6.2$ case all the channels listed in table 5.3 were used. In the $\beta = 6.0$ case plateau plots for some of the channels did not have a well-defined plateau. An example of this is figure 5.4. Many of the $\beta = 6.0$ channels were not fitted because the plateau plots suggest that the form factors would be unreliable. Channels $0 \to 0$, $0 \to 1$ and $1 \to 0$ were fitted in the axial case, channels $0 \to 1$, $1 \to 0$ and $1 \to 1 \perp$ were fitted in the vector case.

The form factors are eventually extrapolated in light quark mass. It is important to check that the extrapolation is not strongly affected by the fit ranges used. To do this the plateau plots for the 6 light κ combinations with a particular κ_H were superimposed. An example is shown in figure 5.5. The six plateaus are approximately a constant distance apart for the entire fit range. In this case the light-quark extrapolation would give similar results irrespective of the fit range used. The plateaus in figure 5.5 are highly correlated.

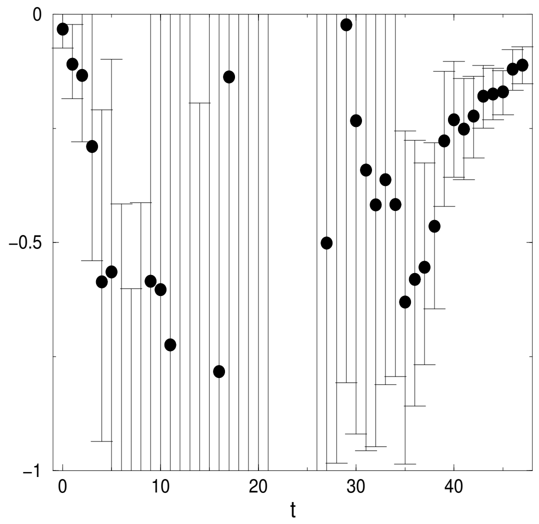

Figure 5.4: An example of a plateau plot from a rejected $\beta = 6.0$ channel. The plot is for channel $1 \to 1 \perp$, $\kappa_P = 0.13417$, $\kappa_A = 0.13417$, $\kappa_H = 0.12230$.

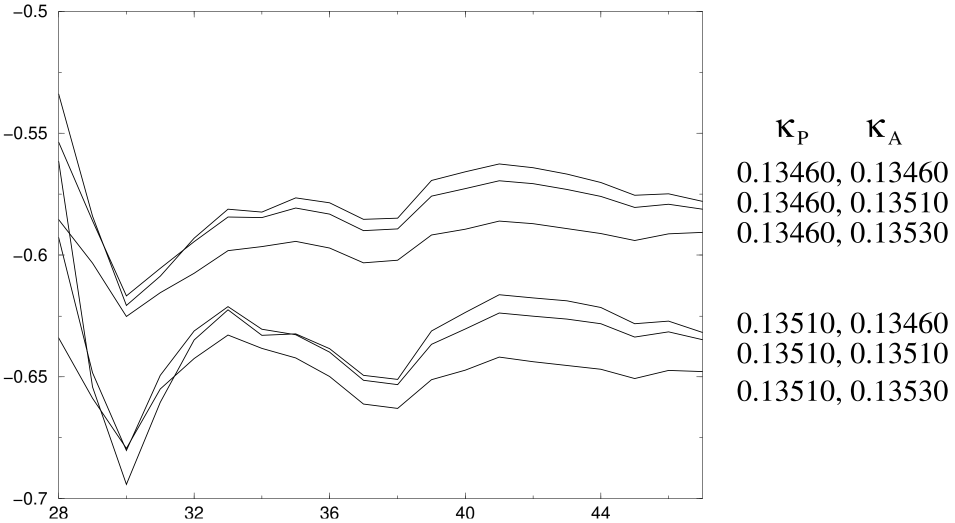

Figure 5.5: Comparison of plateau plots with different light quark mass. The plateau plots all have $\beta = 6.2$, $\kappa_H = 0.12000$, but different κ_A, κ_P. For clarity error bars are not shown. The correlator is the same as the left side of figure 5.3.

5.6 Results

The fitted form factors A, A_1, A_2 and V for all channels and κ combinations are in tables in appendix B. In all cases the fits gave an acceptable Q. Fits were checked visually by comparing the fit with plateau plots. An example visual comparison is shown in figure 5.6.

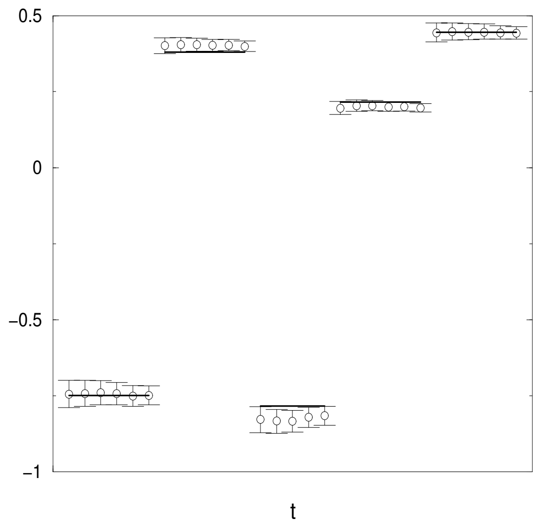

Figure 5.6: A comparison of the channel $0 \to 1$ correlators, with time dependence divided off, and the fit. The sections of plateau used in the fit are shown with error bars and the best fit is superimposed. The plateaus have been shifted in time so that they do not lie on top of each other. The correlator is $\kappa_P = 0.13460$, $\kappa_A = 0.13460$, $\kappa_H = 0.12000$, $\beta = 6.2$.

The four $\beta = 6.2$ form factors are plotted as a function of q^2 in figure 5.7, for a particular κ combination. The form factors are expected to be smooth functions of q^2, but the results in figure 5.7 are definitely not smooth functions of q^2. However the $\beta = 6.2$ form factor results are smooth functions of q^2 if the channels with $|\vec{k}| = \sqrt{2}$ and channel $1 \to 1_{\parallel}$ are excluded. The excluded channels are referred to as unreliable.

The strange results for the $|\vec{k}| = \sqrt{2}$ form factors were very surprising. The same gauge configurations, fuzzing radius and techniques were used to obtain the form factors for the transition heavy-light pseudoscalar to light-light pseudoscalar in [35]. For these decay channels where the light pseudoscalar has momentum $\sqrt{2}$ agree with lower momentum channels. A possible explanation why the $|\vec{k}| = \sqrt{2}$ results are unreliable for P $\to$ V is given below. The argument is heuristic and

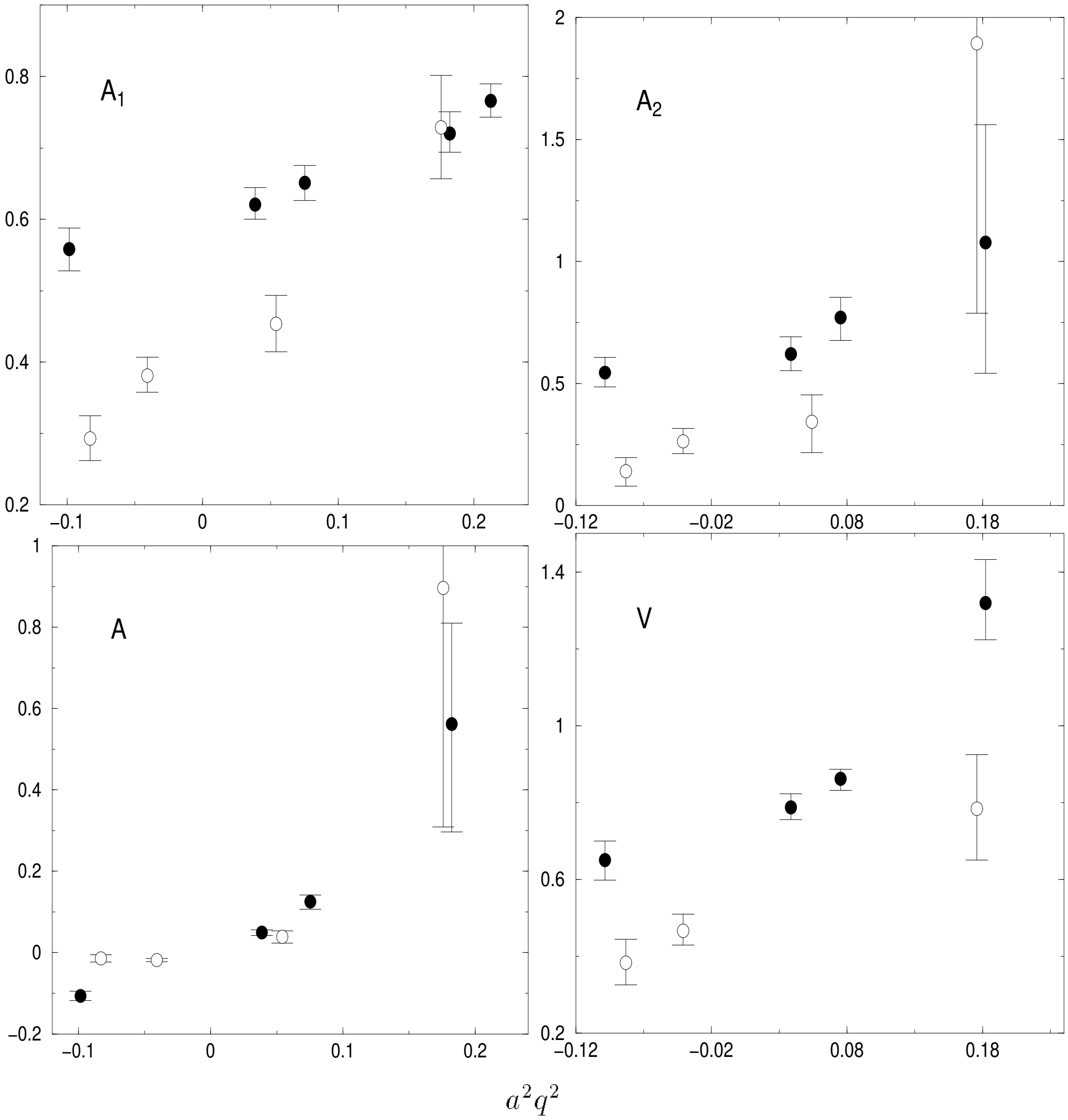

Figure 5.7: The four form factors, for all channels and $\kappa_P = 0.13460$, $\kappa_A = 0.13460$, $\kappa_H = 0.12000$, $\beta = 6.2$. The unreliable channels are open circles.

needs to be investigated further.

There is evidence from the two-point correlation functions that the fuzzed vector meson operator suffers from large violations of rotational symmetry. This was discussed in section 4.6.4. The form factor decomposition of the three point correlator used the result (3.35)

$$Z_{\mathrm{V}}\eta_r^{\mu} = \langle 0|\, \Omega_{\mathrm{V}}^{\mu}(0)|\mathrm{V}, \vec{k}, \eta_r\rangle, \tag{5.16}$$

which relies on rotational symmetry. On the lattice, additional terms such as $(\eta_r^\mu)^3$ need to be included, although these terms are suppressed by powers of the lattice spacing. If the operator Ω_{V}^μ is fuzzed using a distance similar to the wavelength of $\vec{k}$, then maybe the additional terms forbidden by rotational symmetry are important. The form factor decomposition of the three-point correlator for pseudoscalar to pseudoscalar transitions can be derived in a very similar way. This uses the result

$$Z_{\mathrm{P}} = \langle 0|\, \Omega_{\mathrm{P}}(0)|\mathrm{P}, \vec{k}\rangle\ , \tag{5.17}$$

which does not rely on rotational symmetry. Therefore the large fuzzing length is not a problem for pseudoscalar to pseudoscalar transitions.

The plateau plot for the vector current, channel $1 \rightarrow 1_{\;\mathrm{II}}$ is shown in figure 5.8. There is a well defined plateau on the back of the lattice, but with a completely different value from the indistinct plateau at the front of the lattice. This is evidence that the result for V from channel $1 \rightarrow 1_{\;\mathrm{II}}$ is unreliable. Channel $1 \rightarrow 1_{\;\mathrm{II}}$ was rejected in the axial case because the correlators do not behave well as a function of light quark mass. This was determined by looking at a plot of the same type as figure 5.5. The unreliable form factors are not used in the phenomenological calculations of the next two chapters.

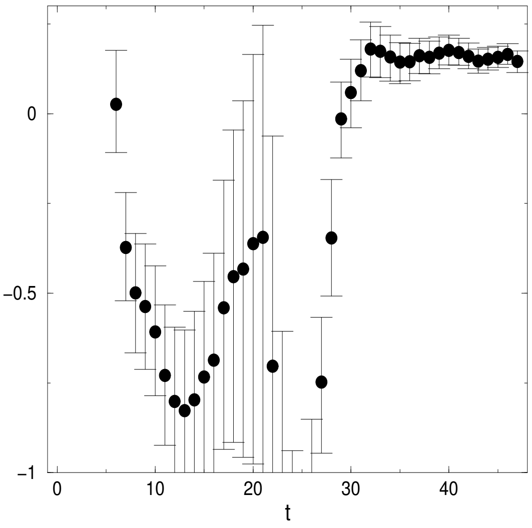

Figure 5.8: The plateau plot for channel $1 \rightarrow 1_{\;\mathrm{II}}$, with the vector current and $\kappa_P = 0.13460,\ \kappa_A = 0.13460,\ \kappa_H = 0.12000,\ \beta = 6.2$.

In section 4.6.3 it was shown that there is a systematic error on the overlap factor for a vector meson, $Z_{\rm V}$. The two different fit methods used to obtain $Z_{\rm V}$ give results which differ slightly more than the statistical error. The method 1 determination of $Z_{\rm V}$ was used to determine the form factors presented in appendix B. The method 2 determination of $Z_{\rm V}$ is typically 4% lower (see tables 4.3 and A.5). Fortunately the quark mass dependence of $Z_{\rm V}$ is almost the same for both methods; extrapolating the form factors in quark mass does not increase this 4% difference. Using the method 2 determination of $Z_{\rm V}$ gives form factors which are 4% higher. In most cases this systematic error is small compared to the statistical error and can be ignored. The exceptions are A_1, V for channel $0 \rightarrow 1$ and A_1, V for channel $1 \rightarrow 1 \perp$. In these cases the statistical errors are about 4%.

5.7 Issues for a future study

This section gives some suggestions for how a future study could improve the determination of the form factors. The three-point functions are fitted to an ansatz which assumes that the three operators are well separated in time. For some channels the fit range is only a few time slices. With such a small range it is difficult to be sure that the operators really are well separated in time and, for example, there is no contamination from excited states. This could be solved by using lattices with a slightly longer time dimension. This has already been successfully implemented in [36], which used 24×62, $\beta = 6.2$ lattices to study the semileptonic decay of a heavy-light pseudoscalar meson to a light-light pseudoscalar meson.

The calculation could be improved by using more gauge configurations. This would make it easier to distinguish systematic and statistical fluctuations in the plateau plots. A very high statistics study would reveal the systematic deviation of the three-point functions from the continuum form factor decomposition. However it turns out in the next two chapters that the statistical error is not the dominant source of error for comparison between lattice and experiment.

In this study the pseudoscalar meson operator was fixed at time slice 28. If this operator is put at the midpoint of the lattice then the three-point correlator at the front and back of the lattice can be averaged. This would reduce the statistical error.

In chapter 4 some surprising results for the two-point correlator of fuzzed vector-meson operators were presented. A possible explanation of these results is that fuzzing enhances violations of rotational symmetry. This effect should be investigated further and its implication for the three-point functions assessed.

Chapter 6

Semileptonic decays of charmed mesons

Chapter 5 described how form factors were obtained from the lattice simulation. The form factors were calculated for many quark mass combinations and values of q^2. To make contact with experimental results the form factors need to be extrapolated and interpolated to physical quark masses. This chapter describes how the lattice results were applied to semileptonic decays where the heavy quark is the charm quark. Three decays were considered; $D_s^+ \to \phi \ell^+ \nu$, $D^+ \to \bar{K}^{*0} \ell^+ \nu$, $D^+ \to \rho^0 \ell^+ \nu$. The decay to a ϕ meson was treated in the same way as the other two decays, although in reality it is more complicated. The ϕ was assumed to be pure $s\bar{s}$, and the OZI rule suppressed disconnected diagrams were ignored.

6.1 Extrapolation in light quark mass

The form factors are functions of q^2 and three quark masses. That is

$$F \equiv F(m_h, m_a, m_p, q^2) \ , \tag{6.1}$$

where F is a generic form factor, and m_h, m_a, m_p are the heavy, active and passive quark masses respectively. The quark masses have a lower case subscript to avoid confusion with meson masses. The quark masses are the improved masses calculated from κ as described in section 4.7.

The form factors were first extrapolated to physical values of the light quark masses m_a, m_p. This was done separately for each heavy quark mass and momentum channel. The heavy quark mass is not changed by the extrapolation. However q^2 is a function of meson mass and implicitly a function of light quark mass, so it is changed by the extrapolation.

The function used to extrapolate the form factors in light quark mass is motivated by the following discussion. The q^2 dependence of the form factors can be modelled by a simple pole,

$$F(q^2) = \frac{F(0)}{1 - q^2/M_{pole}^2} , \tag{6.2}$$

or the sum of a few simple poles. This is discussed further and shown to give a good fit to the data in section 6.5. M_{pole} is the mass of a heavy-light meson composed of the heavy and active quarks. Therefore the variation in M_{pole} during the light-quark extrapolation is approximately

$$M_{pole} \approx a_1 + a_2 m_a . \tag{6.3}$$

It is reasonable to assume that the quark mass dependence of $F(0)$ can be Taylor expanded. To first order

$$F(0) \approx b_1 + b_2 m_a + b_3 m_p . \tag{6.4}$$

The form factors are extrapolated at constant channel, i.e. constant $|\vec{p}|^2$, $|\vec{k}|^2$, $|\vec{q}|^2$. The exact dependence of q^2 on meson mass is known, and the meson masses are implicitly functions of light quark mass. Substituting (6.3), (6.4) and the exact dependence of q^2 on the meson masses into (6.2) and Taylor expanding to first-order gives

$$F \mid_{constant\ channel} = c_1 + c_2 m_p + c_3 m_a + c_4 m_{\mathrm{P}} + c_5 m_{\mathrm{V}} . \tag{6.5}$$

The c_i have different values for different channels. The m_a dependence of $F(q^2)$ due to variation in M_{pole} and $F(0)$ has been combined. This expansion is a good approximation provided that the change in both meson masses is small compared to $(M_{pole}^2 - q^2)^{1/2}$. In chapter 4 it was shown that $m_{\rm V}$ and $m_{\rm P}$ are linear in light quark mass. Therefore the expansion (6.5) is equivalent to the ansatz

$$F = x_1 + x_2 m_p + x_3 m_a \ , \tag{6.6}$$

which was used to extrapolate the form factors. Note that x_1 is the value of F with chiral light quarks. All the form factors were fitted with (6.6) and in all cases Q indicated a good fit. The lattice values of the strange quark mass and up/down quark mass was determined by the method described in section 4.8.

The form factors for the semileptonic decay heavy-light pseudoscalar $\rightarrow$ light-light pseudoscalar have been calculated in several lattice studies. These can be extrapolated in light quark mass using the expansion (6.5), with $m_{\rm V}$ exchanged for the mass of the light pseudoscalar. The mass of a light pseudoscalar is not linear in quark mass, so an extra term needs to be included in (6.6).

An example light-quark extrapolation is shown in figure 6.1. The example extrapolation was done using both a correlated fit and an uncorrelated fit. The uncorrelated fit gives $Q = 0.998$, the correlated fit gives $Q = 0.402$. To test goodness of fit the correlated fit must be used. However the uncorrelated fit was used for the extrapolation. The fit function is only an estimate of the mass dependence of the form factors. In fact the form factors are expected to deviate systematically from the function due to higher-order terms in the Taylor expansion. Correlated and uncorrelated fits both assume that there are no systematic errors. However the uncorrelated fit is thought to be more robust to small systematic errors. In the example shown in figure 6.1 the uncorrelated fit looks the more reasonable.

6.2 Interpolation in heavy quark mass

The four heavy quark masses used in the simulation are around the charm quark mass. After the light-quark extrapolation the form factors were interpolated in heavy quark mass to the charm quark mass. The interpolation was done in terms of the heavy-meson mass, which is implicitly a function of heavy quark mass.

The value of the interpolated form factor depends very weakly on the inter-

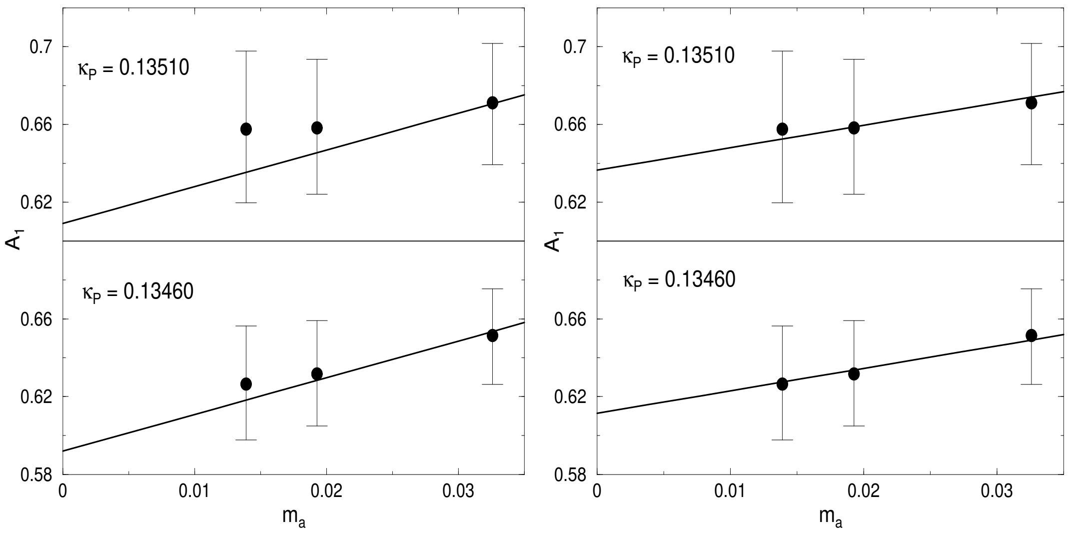

Figure 6.1: An example light quark mass extrapolation. The left graph used a correlated fit, the right graph used an uncorrelated fit. In each of these cases the form factor is plotted against m_a on two separate graphs, one for each κ_P. The form factor shown is A_1, $\beta = 6.2$, $0 \to 1$, $\kappa_H = 0.1200$.

polation function used if the function is reasonably smooth and fits the data well. The ansatz used was

$$F\ m_{\mathrm{P}}^{N} = (x_0 + \frac{x_1}{m_{\mathrm{P}}} + \frac{x_2}{m_{\mathrm{P}}^2})\ , \tag{6.7}$$

where the x_i are free parameters and $N = \frac{1}{2}$ if F is A_1, $N = -\frac{1}{2}$ if F is A_0, A_2 or V. Heavy quark effective theory suggests that this is a good interpolation function (this is discussed in more detail in section 7.1). In all cases this interpolation function gives a good fit to the data and is smooth. Two example fits are shown in figure 6.2. The graphs have horizontal axis $1/(am_{\mathrm{P}})$ and vertical axis $F\ (am_{\mathrm{P}})^N$, so that the fitted curves are quadratic.

The point in the interpolation which corresponds to the charm quark was determined using experimental meson masses. The results were interpolated to the D meson mass if the passive quark is the up/down quark, and interpolated to the D_s meson mass if the passive quark is the strange quark. Converting the experimental meson mass to lattice units requires a determination of the lattice spacing, and introduces a slight scale dependence. The q^2 of a momentum channel was calculated using the dispersion relation, experimental meson masses and a

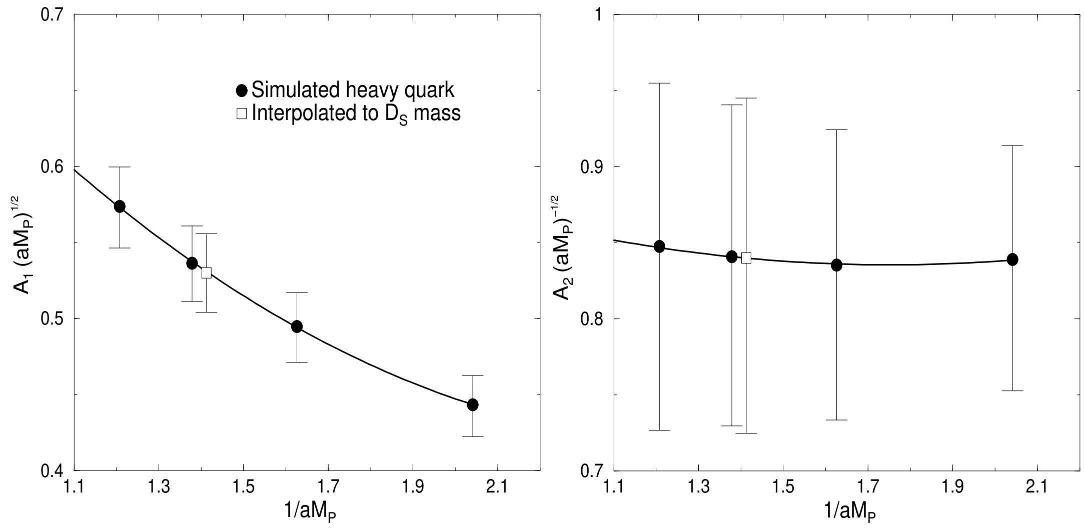

Figure 6.2: Two examples of interpolating to the D_s mass. Both graphs are for channel $0 \to 1$, $\beta = 6.2$, m_a and m_p interpolated to the strange quark mass.

determination of the lattice spacing. q^2 is also a scale dependent quantity. The form factors obtained are in tables in appendix C.

6.3 Comparison of $\beta = 6.0$ and $\beta = 6.2$

After the extrapolation to a physical decay the $\beta = 6.2$ and $\beta = 6.0$ form factors are obtained at the same quark masses. The results for the two lattice spacings can be directly compared to test for discretisation effects. The comparison is most stringent for the decay $D_s^+ \to \phi \ell^+ \nu$ where the data have the smallest errors. To put form factors at both β on the same graph the ratio of the lattice spacings is required. The ratio of the $\beta = 6.2$ and $\beta = 6.0$ lattice spacings is almost independent of the physical quantity used to set the scale. The $D \to \phi$ $\beta = 6.0$ and 6.2 form factors are compared in figure 6.3. The $\beta = 6.2$ and $\beta = 6.0$ results in figure 6.3 all agree within errors. The same conclusion is reached for the $D \to K^*$ and $D \to \rho$ decays, although in these cases the data have larger errors.

In many modern lattice calculations results are extrapolated to the continuum

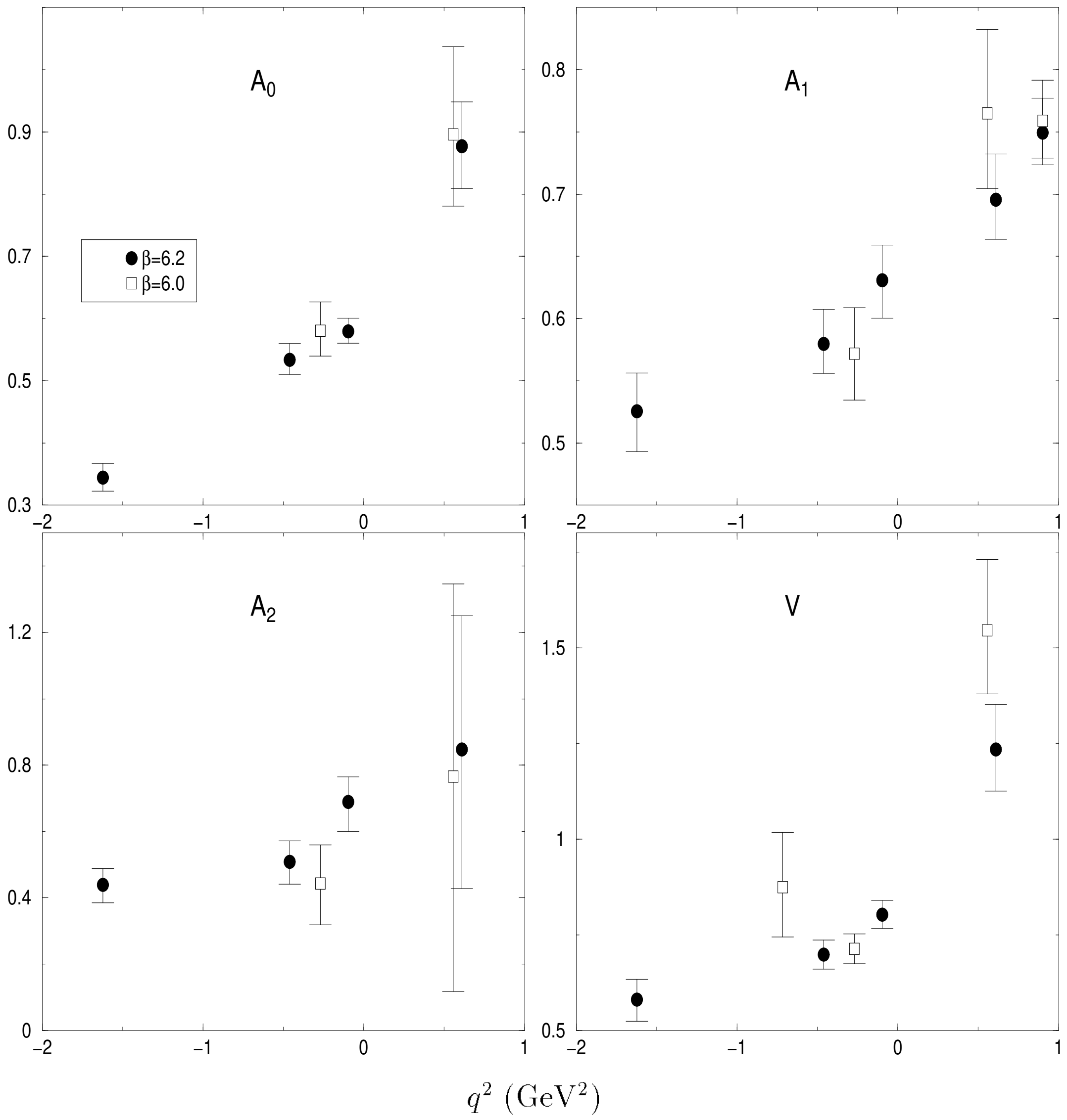

Figure 6.3: Comparison of $\beta = 6.0$ and $\beta = 6.2$ form factors for the decay $D_s^+ \to \phi \ell^+ \nu$.

limit. However this cannot be done reliably with just two β values. Also, the $\beta = 6.0$ results have such large errors it is unlikely that a meaningful continuum extrapolation would be possible even with $\beta = 6.4$ results. To compare lattice with experiment the $\beta = 6.2$ data were treated as continuum results. The $\beta = 6.0$ data were only used as a consistency check.

6.4 Differential decay rate

The differential decay rate for the decay P $\to$ V is [37]

$$\frac{d\Gamma}{dq^2} = \frac{G_F^2|V_{\mathrm{qq'}}|^2}{192\pi^3 m_{\mathrm{V}}^3} q^2[\lambda(q^2)]^{\frac{1}{2}} \left(|H^0(q^2)|^2 + |H^+(q^2)|^2 + |H^-(q^2)|^2 \right) \tag{6.8}$$

where $V_{\mathrm{qq'}}$ is the appropriate CKM matrix element,

$$H^0(q^2) = \frac{1}{2m_{\mathrm{V}}\sqrt{q^2}} \left(\frac{4m_{\mathrm{P}}^2|\vec{k}|^2}{m_{\mathrm{P}}+m_{\mathrm{V}}} A_2(q^2) - \left(m_{\mathrm{P}}^2 - m_{\mathrm{V}}^2 - q^2\right)\left(m_{\mathrm{P}}+m_{\mathrm{V}}\right) A_1(q^2) \right) , \tag{6.9}$$

$$H^{\pm}(q^2) = \left(m_{\mathrm{P}}+m_{\mathrm{V}}\right) A_1(q^2) \pm \frac{2m_{\mathrm{P}}|\vec{k}|^2}{m_{\mathrm{P}}+m_{\mathrm{V}}} V(q^2) \tag{6.10}$$

and

$$\lambda(q^2) = (m_{\mathrm{P}}^2 + m_{\mathrm{V}}^2 - q^2)^2 - 4m_{\mathrm{P}}^2 m_{\mathrm{V}}^2 \quad . \tag{6.11}$$

In the above $\vec{k}$ is the spatial part of k in the P rest frame. In explicitly Lorentz invariant form,

$$|\vec{k}| = \frac{[\lambda(q^2)]^{\frac{1}{2}}}{2m_{\mathrm{P}}} \quad . \tag{6.12}$$

This differential decay rate formula assumes that the lepton is massless, a good approximation for electrons and muons. It is integrated over the angles describing the orientations of the neutrino and lepton as these are not relevant here (although they are very relevant to experimental studies). The three polarisations of the V are summed over. The term in (6.8) proportional to $|H^0|^2$ is due to longitudinally polarised V's, the term proportional to $|H^+|^2 + |H^-|^2$ is due to transversely polarised V's. The kinematically allowed range of q^2 is $0 \le q^2 \le q^2_{max}$ where $q^2_{max} = (m_{\mathrm{P}} - m_{\mathrm{V}})^2$.

6.5 Pole fits

The most accurate experimental results for semileptonic decays are total decay rates. To calculate the total decay rate from the lattice results the form factors need to be parametrised by some model over the kinematically allowed range of q^2. For the form factor A_1 this is an interpolation in q^2 because its value is calculated at q^2_{max} with the $0 \to 0$ channel. The form factors A_2 and V are not known at q^2_{max}, so a small extrapolation is needed to parametrise them up to q^2_{max}. However A_2 and V are kinematically suppressed by factors of $|\vec{k}|^2$ at high q^2 so this extrapolation does not make the prediction for decay rate unreliable.

The nearest-pole-dominance approximation [38, 39] predicts the following q^2 dependence of the form factors:

$$F(q^2) = \frac{F(0)}{1 - q^2/m_F^2} \; , \tag{6.13}$$

where F is A_0, A_1, A_2 or V. The pole mass, m_F, is predicted to be the mass of a meson composed of the heavy and active quarks with definite spin J and parity P. Using the notation J^P, m_F is the mass of the 1^+ meson for A_1, A_2, the 0^- meson for A_0 and the 1^- meson for V. The values of the form factors at $q^2 = 0$ are not predicted by nearest-pole dominance.

To compare lattice with experiment the form factors should be fitted with enough free parameters to avoid strong model dependence and give a good fit to the data. Approximations, such as nearest-pole dominance, can then be tested from first principles. The form factors were fitted to the single pole ansatz (6.13), with $F(0)$ and m_F as free parameters. The constraint on the axial form factors at $q^2 = 0$ (equation 5.6) was enforced in the fits, reducing the number of free parameters by 1. The data for A_2 is very noisy at high q^2, so the pole mass associated with A_2 is poorly constrained. The same pole mass was used for A_1 and A_2 in the fits. This does not introduce much model dependence into the prediction for the decay rate because, as stated earlier, the contribution from A_2 is kinematically suppressed at high q^2.

In all cases the fit ansätze described above gave a good fit to the data. The fit parameters are listed in table C.5 with the lattice spacing determined from r_0. To test for scale dependence the fit parameters were recalculated using m_ρ to set the scale. These results are listed in table C.6. In all cases the error on $F(0)$ due to scale dependence is smaller than the statistical error. This is not surprising because $F(0)$ is dimensionless. The fitted pole masses in physical units are listed in table C.7. The typical scale dependence of a generic quantity with mass dimension is that its value in physical units varies as much as the difference determinations of the lattice spacing. The scale dependence of m_F is less than this. However the scale dependence of m_F is generally bigger than the statistical error.

The lattice pole masses are compared with the nearest-pole-dominance prediction in table C.7. For all the decays considered the lattice results agree within errors with the nearest-pole-dominance predictions for m_V and m_{A_1}. The lattice result for m_{A_0} is lower than expected for $D \to \phi$ and $D \to K^*$.

6.6 Comparison with experiment

In the following subsections the lattice data are compared with experimental results. Total decay rates are obtained by numerically integrating differential decay rates, which are calculated using the fit parameters in tables C.5 and C.6. The experimental results in the following subsections are all from the Particle Data Group (PDG) [4].

6.6.1 $D_s^+ \to \phi\ell^+\nu$

The ϕ is a flavour singlet. It was assumed to be pure $s\bar{s}$ for the light-quark extrapolation. Experiments show that this is a good approximation [4]. Disconnected diagrams where the s and $\bar{s}$ annihilate and are created from the vacuum contribute to the decay $D_s^+ \to \phi\ell^+\nu$. The connected diagram and the simplest disconnected diagram for $D_s^+ \to \phi\ell^+\nu$ are shown in figure 6.4. The OZI rule predicts that the connected diagram dominates the decay rate $D_s^+ \to \phi\ell^+\nu$. This is a phenomenological rule based on observing a large number of decay modes, and has not been derived from QCD. Disconnected diagrams were ignored for the calculation of decay rate here.

Using the PDG value $|V_{cs}| = 0.974 \pm 0.001$ the lattice prediction for total decay rate is $5.0 \pm 0.3 \times 10^{10}$ s^{-1}. The errors are statistical only. The scale dependence of the result gives a systematic error which is much smaller than the statistical error. There is also a systematic error due to the two types of fit

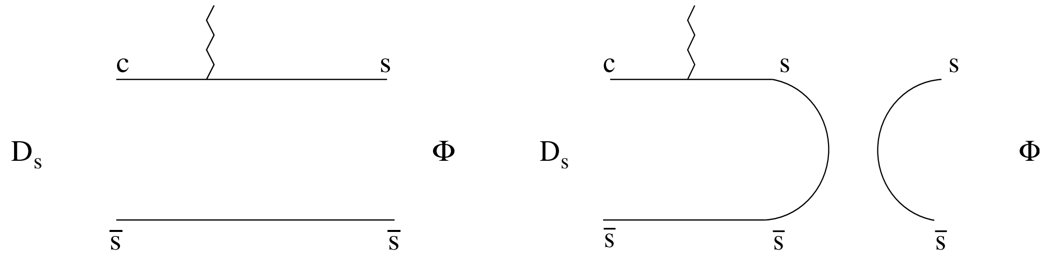

Figure 6.4: The connected (left) and a disconnected (right) diagram which contribute to the decay $D_s^+ \to \phi \ell^+ \nu$.

to the vector two-point correlators giving slightly different results for $Z_{\rm V}$. The result shown used the method 1 fit to obtain $Z_{\rm V}$. Using the method 2 fit gives form factors which are 4% higher, and a total decay rate which is 8% higher, i.e. $5.4 \pm 0.3 \times 10^{10}$ s^{-1}. The lattice decay rate is in reasonable agreement with the experimental world average of $4.0 \pm 0.5 \times 10^{10}$ s^{-1}. The agreement between the lattice and experimental decay rate can be thought of as an example of the OZI rule holding.

Form factor ratios at $q^2 = 0$ have been measured for this decay and for $D^+ \to \bar{K}^{*0} \ell^+ \nu$. These ratios are determined without making assumptions about the total decay rate and $|V_{cs}|$ [40]. Experimental determinations of the absolute values of the form factors are strongly model dependent. The lattice and experimental form factor ratios are

$$
\begin{array}{rcllll}
V(0)/A_1(0) & = & 1.92 \pm 0.32 & \text{(experiment)} & 1.36^{+5}_{-5} & \text{(this work)} \\
A_2(0)/A_1(0) & = & 1.60 \pm 0.24 & \text{(experiment)} & 0.99^{+6}_{-7} & \text{(this work)}
\end{array}
$$

The lattice determination of $V(0)$, $A_2(0)$ and $A_1(0)$ are correlated. As a result the fractional errors on the form factors ratios are quite small. The scale dependence of the ratios is insignificant. The meson overlap factor, $Z_{\rm V}$, cancels in the form factor ratio, so its uncertainty is not a source of systematic error. There is significant disagreement between the lattice form factor ratios and experiment.

6.6.2 $D^+ \to \bar{K}^{*0}\ell^+\nu$

The experimental results for this decay are the most accurate of all the decays considered in this work. The K^* is a flavour nonsinglet so the lattice prediction does not rely on the OZI rule. The lattice prediction for decay rate is $5.5 \pm 0.5 \times 10^{10}$ s^{-1}, which is in reasonable agreement with the experimental world average $4.5 \pm 0.4 \times 10^{10}$ s^{-1}. As for $D_s^+ \to \phi\ell^+\nu$, the decay rate obtained is 8% higher if method 2 fits are used for the two-point correlators. The lattice and experimental form factor ratios are

$$\begin{aligned} V(0)/A_1(0) &= 1.82 \pm 0.09 \quad \text{(experiment)} \quad 1.23^{+7}_{-7} \quad \text{(this work)} \\ A_2(0)/A_1(0) &= 0.78 \pm 0.07 \quad \text{(experiment)} \quad 1.03^{+7}_{-9} \quad \text{(this work)} \end{aligned}$$

There is significant disagreement between the lattice and experimental form factor ratios, especially for $V(0)/A_1(0)$.

The experimentally measured ratio $A_2(0)/A_1(0)$ is very different for $D^+ \to \bar{K}^{*0}\ell^+\nu$ and $D_s^+ \to \phi\ell^+\nu$. This is surprising because the two decays are related by $SU(3)$ flavour symmetry. The lattice results do not predict strong breaking of $SU(3)$ flavour symmetry for this ratio.

6.6.3 $D^+ \to \rho^0\ell^+\nu$

The form factors for $D \to \rho$ can be applied to the decays $D^+ \to \rho^0\ell^+\nu$ and $D^0 \to \rho^-\ell^+\nu$. However only $D^+ \to \rho^0\ell^+\nu$ has been observed experimentally. In the standard quark model its wave function is $(u\bar{u} - d\bar{d})/\sqrt{2}$. Unlike the ϕ disconnected diagrams do not contribute to the decay $D_s^+ \to \phi\ell^+\nu$ because any disconnected diagram involving a d quark is exactly cancelled by a disconnected diagram involving a u quark. The decay rate formula (6.8) is for the decay $D^0 \to \rho^-\ell^+\nu$. Isospin symmetry gives

$$\Gamma(D^+ \to \rho^0\ell^+\nu) = \frac{1}{2}\Gamma(D^0 \to \rho^-\ell^+\nu) \ . \tag{6.14}$$

The lattice prediction for total decay rate is $\Gamma(D^+ \to \rho^0\ell^+\nu) = 0.19 \pm 0.02 \times 10^{10}$ s^{-1}. This is in good agreement with the experimental result $\Gamma(D^+ \to$

$\rho^0 e^+\nu_e) = 0.21 \pm 0.08 \times 10^{10}$ s^{-1}. As mentioned in the previous two sections, the lattice decay rate is 8% higher if method 2 fits are used for the two-point correlators. The total decay rate has also been measured for the case where the lepton is a muon. The experimental result is $\Gamma(D^+ \to \rho^0\mu^+\nu_\mu) = 0.26 \pm 0.07 \times 10^{10}$ s^{-1}. The two measured decays cannot be directly compared because the phase space available for the final state is smaller in the muon case. The phase space effect has been estimated for the decay $D^+ \to \bar{K}^{*0}\ell^+\nu$ in [41]. In terms of decay rates the phase space effect is estimated to give

$$\frac{\Gamma(D^+ \to \bar{K}^{*0}\mu^+\nu_\mu)}{\Gamma(D^+ \to \bar{K}^{*0}e^+\nu_e)} = 0.9 \quad . \tag{6.15}$$

This result uses a model for the q^2 dependence of the form factors. Although the two decay rates in (6.15) are strongly model dependent, much of the model dependence cancels in the ratio. $SU(3)$ flavour symmetry suggests that the phase space factor will be similar for the decay $D^+ \to \rho^0\ell^+\nu$. Therefore the decay rates for $D^+ \to \rho^0 e^+\nu_e$ and $D^+ \to \rho^0\mu^+\nu_\mu$ disagree at about one standard deviation.

The form factors for $D^+ \to \rho^0\ell^+\nu$ have not been measured.

6.7 Comparison with other theoretical work

The form factors presented in this chapter have been calculated in several other works. The UKQCD collaboration calculated the form factors using quenched, $\beta = 6.2$ improved QCD in [42]. This work uses fully nonperturbative $\mathcal{O}(a)$ improvement, whereas the earlier UKQCD calculation used perturbative improvement. The leading discretisation errors of the earlier UKQCD calculation are $\mathcal{O}(\alpha_s a)$, the leading errors for this work are $\mathcal{O}(a^2)$. The results in [42] are compared with results from this work in table 6.1. The axial form factors from both calculations are in good agreement, although those calculated in this work are all slightly lower. There is some disagreement in the value of $V(0)$.

The form factors for P $\to$ V decays have also been calculated using quark models and sum rules. Theoretical results for $A_1(0)$, $A_2(0)$ and $V(0)$ for the decays $D \to \rho$ and $D \to K^*$ are listed in [43]. The axial form factors calculated

	$D \to K^*$		$D \to \rho^\pm$	
	UKQCD [42]	This work	UKQCD [42]	This work
$A_0(0)$	0.75^{+5}_{-11}	0.64^{+3}_{-3}	0.63^{+6}_{-9}	0.59^{+3}_{-3}
$A_1(0)$	0.70^{+7}_{-10}	0.65^{+2}_{-3}	0.63^{+6}_{-9}	0.60^{+3}_{-3}
$A_2(0)$	0.66^{+10}_{-15}	0.67^{+7}_{-7}	0.51^{+10}_{-15}	0.61^{+6}_{-7}
$V(0)$	1.01^{+30}_{-13}	0.80^{+5}_{-5}	0.95^{+29}_{-14}	0.71^{+5}_{-6}
Γ	$6.0^{+0.8}_{-1.6}$	5.5^{+5}_{-5}	0.43 ± 0.11	0.40 ± 0.04

Table 6.1: Comparison of some parameters related to the semileptonic decays $D \to K^*$ and $D \to \rho$. The decay rates are in units of 10^{10} s^{-1}. Errors for this work are statistical only.

in this work are within the spread of other theoretical results. The value of $V(0)$ calculated in this work is lower than all the other calculations in [43].

Chapter 7

The semileptonic decay $B \to \rho$

This chapter describes how the lattice form factors were extrapolated from simulation heavy quark masses of around charm to the mass of the b quark. The reliability of the extrapolation is tested. The form factors are compared with the experimental results of the CLEO collaboration and with other theoretical work.

7.1 Heavy quark scaling of the form factors

Heavy quark effective theory (HQET) is an approximation to QCD which can be applied to processes involving a heavy quark. The approximation requires that light quark degrees of freedom have four-momenta which are negligible compared with the mass of the heavy quark, m_H.

For the semileptonic decay considered in this work, HQET predicts how the form factors depend on m_H. The prediction is exact in the limit of infinite m_H. For finite m_H there are corrections suppressed by powers of Λ_{QCD}/m_H. In the infinite m_H limit, the form factor F obeys the scaling law [44]

$$F \ \alpha_s(m_H)^{2/\beta_0} \ m_H^N = \text{constant} \ , \tag{7.1}$$

where $N = -\frac{1}{2}$ for $F = V,\ A_0,\ A_2$ and $N = \frac{1}{2}$ for $F = A_1$. The strong coupling α_s appears because of the anomalous scaling of the flavour-changing current. β_0

is the first coefficient of the QCD β function. For a general number of flavours (n_f)

$$\beta_0 = 11 - \frac{2}{3} n_f \ . \tag{7.2}$$

In the quenched approximation there are no sea quarks so $\beta_0 = 11$.

In HQET m_H is taken to infinity with the heavy quark four-velocity held fixed. Therefore the scaling laws (7.1) are at fixed ω where

$$\omega = v.v' = \frac{m_{\rm P}^2 + m_{\rm V}^2 - q^2}{2 m_{\rm P} m_{\rm V}} \ . \tag{7.3}$$

Here v and v' are the four-velocities of the heavy-light pseudoscalar and the light vector respectively. The scaling laws (7.1) are derived by assuming that all the light quarks have energy which is negligible in the rest frame of the heavy quark. The light quark in the heavy-light meson always satisfies this. However the light quarks in the light vector meson violate this condition when q^2 is small. Therefore the scaling laws (7.1) are most reliable when q^2 is close to q^2_{max}, or equivalently ω is close to 1.

7.2 Extrapolation of the form factors to m_b

The form factors were first extrapolated in light quark mass as described in section 6.1. Then the heavy quark mass dependence was extrapolated from the simulation masses to m_b. The function used for the extrapolation is motivated by the heavy quark scaling laws described in the previous section.

It is convenient to extrapolate in terms of the pseudoscalar meson mass, which is a function of heavy quark mass. HQET predicts that [45]

$$m_{\rm P} = m_H + \bar{\Lambda} \ , \tag{7.4}$$

where $\bar{\Lambda}$ is independent of m_H. At finite m_H (7.4) is modified by terms suppressed by powers of Λ_{QCD}/m_H.

The ansatz used to extrapolate the form factors was

$$F \ \Theta(m_{\rm P}) \ m_{\rm P}^N = x_0 + \frac{x_1}{m_{\rm P}} + \frac{x_2}{m_{\rm P}^2} \ , \tag{7.5}$$

where the x_i are free parameters and the value of N is given below (7.1). The function Θ is

$$\Theta \;=\; \left(\frac{\log(m_{\mathrm{P}}/\Lambda_{QCD})}{\log(m_B/\Lambda_{QCD})}\right)^{\frac{2}{11}} \;, \tag{7.6}$$

which is chosen to be 1 at the B meson mass (m_B) for convenience. In the leading logarithm approximation for α_s,

$$\Theta(m_P) = \left(\frac{\alpha_s(m_P)}{\alpha_s(m_B)}\right)^{\frac{2}{11}} \;. \tag{7.7}$$

In the heavy-quark limit the ansatz (7.5) reduces to the correct scaling law. This is shown by rewriting it in terms of heavy quark mass. Substituting the m_H dependence of m_P (7.4) into (7.5) and expanding gives

$$F\ \alpha_s(m_H)^{2/\beta_0}\ m_H^N = x'_0 + \frac{x'_1}{m_H} + \frac{x'_2}{m_H^2} + \text{suppressed terms}\ . \tag{7.8}$$

This includes finite m_H corrections to m_{P}. The suppressed terms are mainly $\mathcal{O}(1/m_H^3)$. There are also suppressed terms from expanding Θ which are not inverse powers of m_H. The most significant of these is

$$\frac{2x_0\bar{\Lambda}}{11 m_H \log(m_H/\Lambda_{QCD})}\ . \tag{7.9}$$

Ignoring the suppressed terms, x_1 and x_2 in (7.5) allow for the leading and sub-leading corrections to the HQET scaling law.

7.2.1 Extrapolation of $|\vec{p}| = 0$ channels

The heavy quark scaling laws are for form factors at constant ω. Therefore the extrapolation ansatz (7.5) must be applied to form factors at constant ω for it to have the correct heavy-quark limit. For channels with $|\vec{p}| = 0$, ω is independent of m_{P}, so the results of these channels can be extrapolated immediately after the light-quark extrapolation. The function Θ depends on the QCD parameter Λ_{QCD}. This was set to be $\Lambda_{QCD} = 0.2$ GeV [4]. The result of the extrapolation is very weakly dependent on the value of Λ_{QCD} used, so the uncertainty in this value is an insignificant source of error. Two example extrapolations are shown in figure 7.1. The results are extrapolated to the point where the pseudoscalar mass is

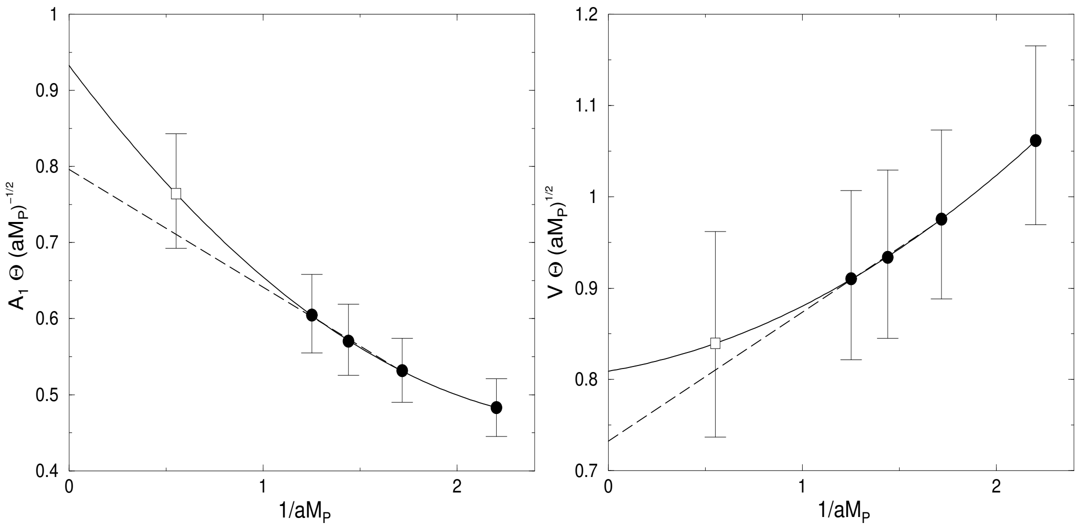

Figure 7.1: Examples of the extrapolation in heavy quark mass for channel $0 \to 1$. Quadratic (solid line) and linear (dashed line) extrapolations are shown. The open square is the result of the quadratic extrapolation to m_B.

equal to the experimental B meson mass. The lattice spacing is used to convert the B meson mass to lattice units, which introduces some scale dependence.

Extrapolations using (7.5) are referred to as quadratic, because the right-hand side is quadratic in $1/m_{\mathrm{P}}$. To test for systematic errors the heavy-quark extrapolation was also done using a linear extrapolation, i.e. (7.5) with x_2 fixed to 0. In general the linear extrapolation gives a bad fit to the four data points (see figure 7.1), so the linear extrapolation was done using only the three heaviest mass points. The linear and quadratic extrapolations are compared in figure 7.1. Both types of extrapolation have the correct HQET limit and agree with the data. Therefore the difference between the two extrapolations gives an indication of systematic errors.

7.2.2 Extrapolation of $|\vec{p}| \neq 0$ channels

Channels with $|\vec{p}| \neq 0$ are more difficult to extrapolate because ω is a function of heavy quark mass. The four different values of ω and q^2 for an example $|\vec{p}| \neq 0$

channel are listed in table 7.1. The final column of the table is explained later in this section.

κ_H	ω	a^2q^2	Δa^2q^2
0.1200	1.48	0.08204	-0.0196
0.1233	1.50	-0.00021	-0.0086
0.1266	1.54	-0.0662	0.0048
0.1299	1.62	-0.1140	0.0233

Table 7.1: Dependence of ω on heavy quark mass for channel $1 \to 1 \perp$, light quarks extrapolated to up/down.

The form factors for $|\vec{p}| \neq 0$ channels can be extrapolated using (7.5), ignoring the variation in ω. However such an extrapolation does not satisfy the HQET scaling law and will have additional systematic errors. Instead the form factors with different κ_H were interpolated in q^2 to constant ω, then extrapolated. A possible interpolation procedure is to use the pole fits described in section 6.5. However this procedure does not take advantage of the correlations in the data. Form factors from the same channel but with different κ_H are highly correlated. Therefore when the extrapolation ansatz (7.5) is fitted to the $|\vec{p}| = 0$ channels the parameters x_1 and x_2 have small statistical errors. Form factors from different channels are only slightly correlated. Therefore form factors with different κ_H interpolated with a basic pole fit are only slightly correlated, and the resulting extrapolated form factor has large statistical errors.

The interpolation procedure used was designed to retain as much as possible of the correlations in the data. For each channel $\tilde{\omega}$ was chosen, where $\tilde{\omega}$ lies within the range of the four different ω. The form factors can be obtained at $\tilde{\omega}$ with a small shift in q^2. The form factors were shifted in q^2 using a simple pole ansatz. The fit was constrained to pass through the channel being shifted, i.e. a one parameter fit. This fit was used to obtain the form factor at constant $\tilde{\omega}$ for each of the $|\vec{p}| \neq 0$ channels. $\tilde{\omega}$ was chosen to minimise the shifts in q^2 in a least squares sense. That is, the function

$$\sum_{\text{all } 4\ m_{\rm P}} \left(\Delta q^2(\tilde{\omega}, m_{\rm P})\right)^2 \tag{7.10}$$

was minimised with respect to $\tilde{\omega}$. Here Δq^2 is the shift in q^2. The Δq^2 for the example channel, with $\tilde{\omega}$ obtained in this way are listed in table 7.1. The Δq^2 are generally small, so that most of the correlations between data at constant channel is retained. The lowest q^2 determination of the form factors is for channel $1 \to 1_{||}$. Then a negative shift in q^2 is a small extrapolation of the data. For this channel only, $\tilde{\omega}$ was chosen to be $\omega(\kappa_H = 0.1200)$, so that all the Δq^2 are positive. Two example $|\vec{p}| \neq 0$ extrapolations are shown in figure 7.2.

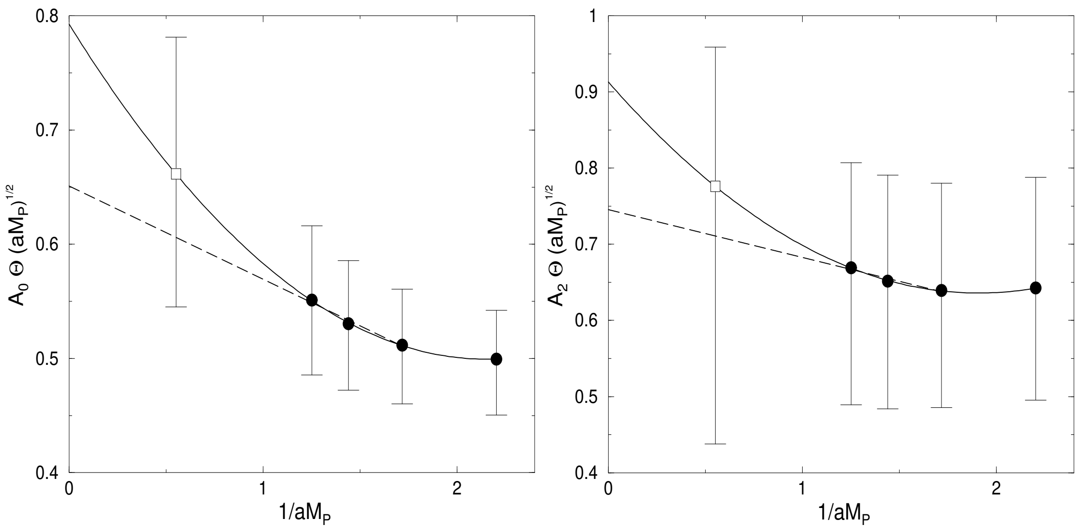

Figure 7.2: Examples of the extrapolation in heavy quark mass for $|\vec{p}| \neq 0$ channels. Quadratic (solid line) and linear (dashed line) extrapolations are shown. The right graph is channel $1 \to 1_{||}$ the left is $1 \to 1 \perp$. The open square is the result of the quadratic extrapolation to m_B.

7.2.3 Results

The extrapolation starts with form factors in the range negative q^2 to q^2_{max}. After the extrapolation the form factors are all at high q^2. For HQET to be reliable q^2 should be close to q^2_{max}. This is violated by some channels at the simulation m_H but is satisfied after the extrapolation. The $B \to \rho$ form factors obtained are shown in figure 7.3. The difference between the linear and quadratic extrapolation is always less than the statistical error and, in many cases, is small in comparison

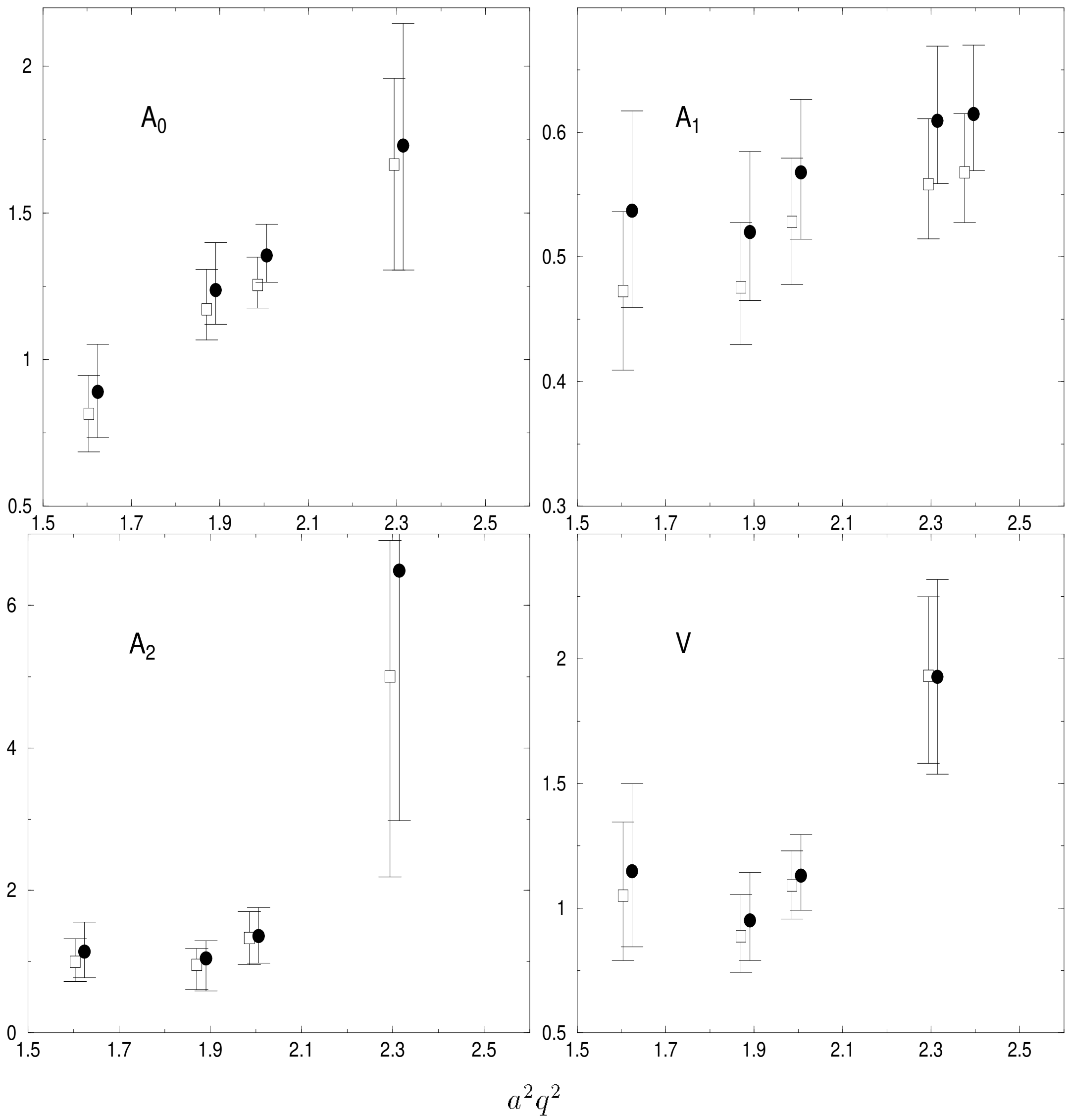

Figure 7.3: $B \to \rho$ form factors. The results from the quadratic extrapolation (filled circles) and linear extrapolation (open squares) are both shown. The linearly extrapolated data is slightly offset in q^2.

with the statistical error.

The form factors shown in figure 7.3 were calculated using r_0 to set the scale. To test for scale dependence the calculation was repeated using m_ρ to set the scale. The results change in two ways; the value of a form factor from a particular channel changes, and also the q^2 associated with a channel changes. As an example figure 7.4 shows A_1 with the scale set by the two different quantities. The scale dependence is smaller than the statistical errors, but not small enough to be ignored.

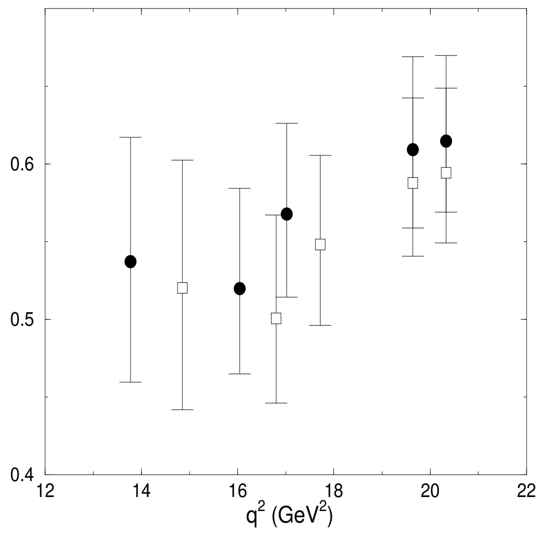

Figure 7.4: The form factor A_1 calculated using r_0 to set the scale (closed circles) and m_ρ to set the scale (open squares).

7.3 Comparison of $\beta = 6.0$ and $\beta = 6.2$

The $\beta = 6.0$ form factors were calculated for only a few channels and have large errors, so they cannot be interpolated to constant ω. Therefore only the $0 \to 0$ and $0 \to 1$ channels were extrapolated to m_b. The comparison between the two β is most interesting for $0 \to 0$, because then $q^2 = q^2_{max}$ and is independent of β. The two heavy-quark extrapolations at different β can be directly compared. Note that to compare the two extrapolations in lattice units the ratio of the lattice spacings is needed. Only A_1 can be determined from the $0 \to 0$ channel.

The two extrapolations of A_1 from the $0 \to 0$ channel are compared in figure 7.5. The form factors have been interpolated in light quark mass to strange for the comparison, because then the statistical errors are smallest. The fitted parameters used in the extrapolation are listed in table 7.2. The agreement between the two extrapolations is quite spectacular. There are several instances in this work where correlations between data points mean that spectacular agreement is not surprising. However, the $\beta = 6.0$ and $\beta = 6.2$ form factors are calculated using different gauge configurations and are completely uncorrelated. Therefore, given the size of the statistical errors on the x_i, the spectacular agreement between the two extrapolations is surprising.

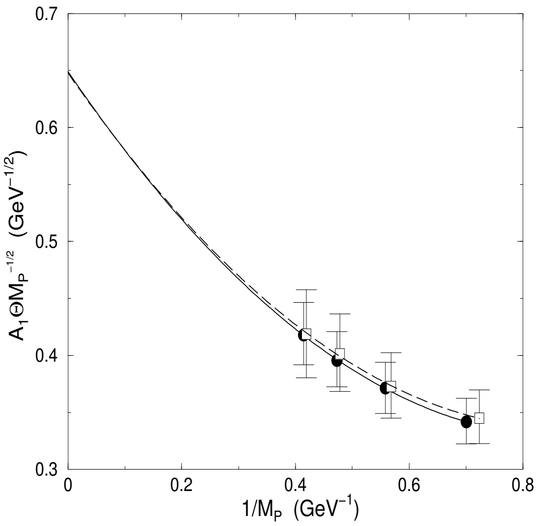

Figure 7.5: Comparison of the heavy-quark extrapolations for channel $0 \to 0$ at $\beta = 6.2$ (filled circles) and $\beta = 6.0$ (open squares).

	x_0	x_1	x_2
$\beta = 6.2$	1.11^{+7}_{-6}	-0.43^{+5}_{-5}	0.084^{+13}_{-12}
$\beta = 6.0$	1.05^{+9}_{-10}	-0.42^{+9}_{-9}	0.08^{+2}_{-2}

Table 7.2: The parameters used in the extrapolations shown in figure 7.5. The ansatz is (7.5). All the parameters are made dimensionless by multiplying by the appropriate power of the $\beta = 6.2$ lattice spacing.

The form factors at different β have different discretisation errors. The discretisation errors in this simulation are expected to be small at the charm scale. However there is a risk that the heavy-quark extrapolation amplifies the discretisation errors, giving a large systematic error on the $B \to \rho$ form factors. The comparison in figure 7.5 is good evidence that discretisation errors are under control after the extrapolation.

For channel $0 \to 1$ q^2 is a function of β, so a direct comparison cannot be made between extrapolations at different β. The extrapolated $\beta = 6.0$ form factors for channel $0 \to 1$ were compared with the $\beta = 6.2$ form factors and found to be in agreement. However the extrapolated $\beta = 6.0$ results have very large errors and do not give much information.

7.4 Comparison with other theoretical work

There have been several other theoretical calculations of the $B \to \rho$ form factors. They have been calculated with light cone sum rules (LCSR [14]), quark models ([46] and [15]) and with lattice QCD (UKQCD95 [47, 48]). The previous lattice calculation of the form factors is very similar to this work. The calculation used $\beta = 6.2$, quenched improved lattice QCD. However the calculation was improved perturbatively, and the passive quark mass was not extrapolated from strange to up/down.

In figure 7.6 the results of UKQCD95, LCSR and this work are compared. The LCSR approach can be applied in the range $0 \leq q^2 \leq 17\mathrm{GeV}^2$. The three calculations are in reasonable agreement for A_0 and V. For A_1 and A_2 the results of this work are significantly higher than UKQCD95 and LCSR.

The UKQCD95 calculation is very similar to this work, so it is surprising that the two calculations give different results for A_1 and A_2. The UKQCD95 calculation assumed that the form factors are independent of passive quark mass. The simulation used a passive quark mass of about strange and did not extrapolate; the form factors were actually extrapolated to the decay $B_s \to K^*$, although q^2 was calculated as if extrapolated to $B \to \rho$. To test if this assumption of UKQCD95 is reliable, it was used to calculate A_1 in this work. Figure (7.7) compares the A_1 for $B \to \rho$ calculated with, and without, the assumption of UKQCD95. Figure (7.7) shows that the assumption has a small effect on the form factor and does not explain the disagreement between UKQCD95 and this

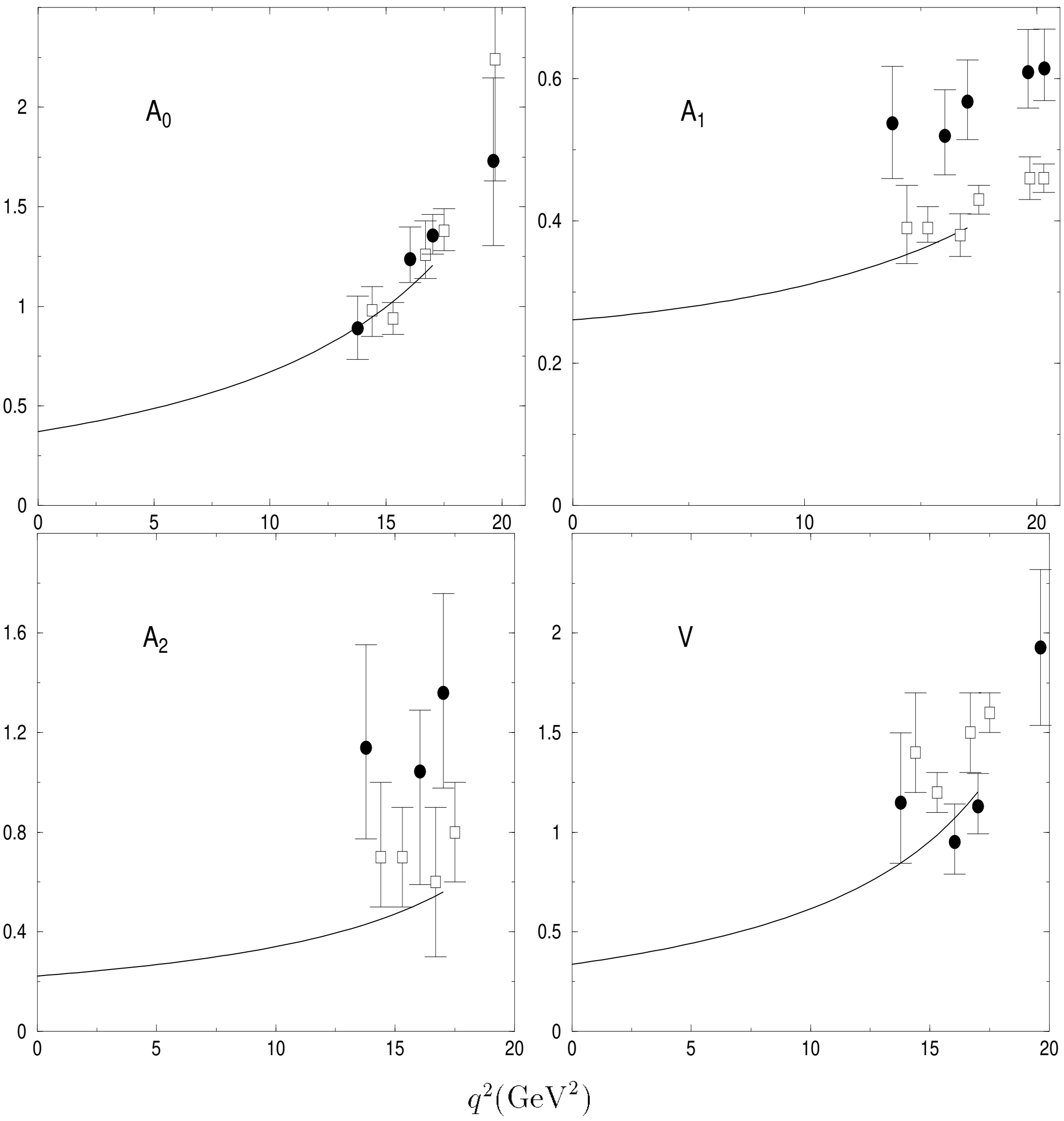

Figure 7.6: Comparison of three theoretical calculations of the $B \to \rho$ form factors; this work (closed circles) UKQCD95 (open squares) and LCSR (lines).

work.

The UKQCD95 calculation implemented improvement perturbatively. This reduced the leading discretisation error to $\mathcal{O}(\alpha_s a)$. This calculation uses non-perturbative improvement, and has leading discretisation errors of $\mathcal{O}(a^2)$. The different results of the two calculations is probably due to the different discretisation errors.

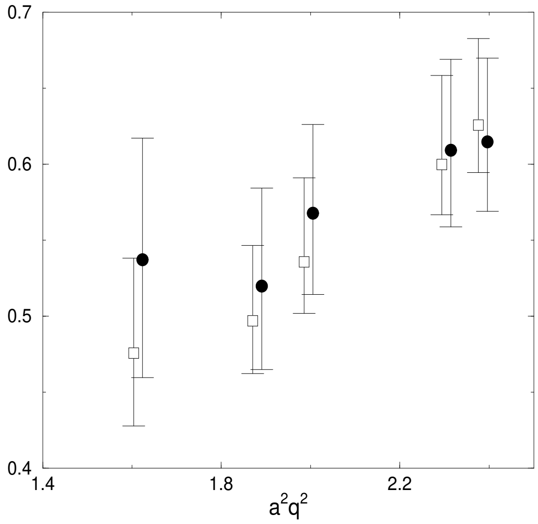

Figure 7.7: The form factor A_1 for $B \to \rho$, using the full extrapolation (closed circles) and omitting the passive quark extrapolation (open squares). The open squares are slightly offset in q^2.

7.5 Comparison with experiment

The CLEO collaboration are the only experimental group to observe the decay $B^0 \to \rho^- \ell^+ \nu$. They measured the total decay rate and also the partial rate ($\Delta\Gamma$) in three bins of q^2 [13]. The partial rate is $d\Gamma/dq^2$ integrated over part of the kinematically allowed range of q^2. The $\Delta\Gamma$ measured by the CLEO collaboration are shown in figure 7.8.

The measurement of total decay rate is $\Gamma = 17^{+4}_{-5} \times 10^7\ \mathrm{s}^{-1}$. This has smaller errors than the measurements of $\Delta\Gamma$ so, in principle, this is the best measurement to compare with theory. However the lattice results give the form factors for $q^2 \gtrsim 14\ \mathrm{GeV}^2$. To compare the lattice results with Γ the form factors need to be extrapolated in q^2 to cover the whole kinematically allowed range. This extrapolation is strongly model dependent and, as a result, the lattice prediction for Γ has a large systematic error. A safer procedure, used here, is to compare the lattice results with $\Delta\Gamma$ at high q^2.

The lattice results were used to calculate $d\Gamma/dq^2$ for each channel, using (6.8).

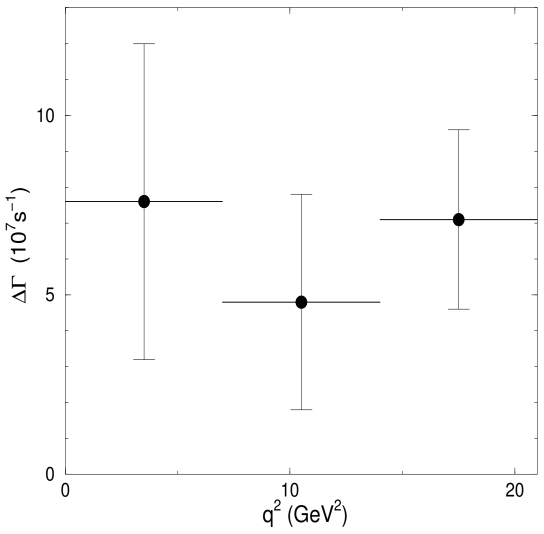

Figure 7.8: The partial decay rates for $B^0 \to \rho^- \ell^+ \nu$, measured by the CLEO collaboration. The errors are statistical, systematic and theoretical, combined in quadrature.

This was then interpolated in q^2 and integrated to obtain $\Delta\Gamma$. The interpolation used the method of [47] and is motivated by the following discussion. The q^2 dependence of $d\Gamma/dq^2$ can be factored into the product of two functions; the q^2 dependence of the volume of phase space and the q^2 dependence of the matrix element. The phase space factor is $q^2[\lambda(q^2)]^{\frac{1}{2}}$, which changes rapidly at high q^2 and is 0 at $q^2 = q^2_{max}$. The rest of the q^2 dependence of $d\Gamma/dq^2$ is due to

$$|M|^2 \equiv |H^0|^2 + |H^+|^2 + |H^-|^2 \ , \tag{7.11}$$

which depends on the form factors A_1, A_2 and V. The lattice determination of $|M|^2$ is shown in figure 7.9. In the range of q^2 for which the form factors have been determined the largest contribution to $|M|^2$ is from the form factor A_1. The contribution from A_1 becomes increasingly dominant as q^2 tends to q^2_{max}. At q^2_{max} $|M|^2$ is proportional to $(A_1)^2$. This is fortunate, because A_1 is the best determined of the three form factors.

Figure 7.9 shows that $|M|^2$ varies slowly with q^2 over the range for which it has been measured. This is because the form factors vary slowly over this range. The q^2 dependence of $|M|^2$ can be accurately approximated by a first-order Taylor

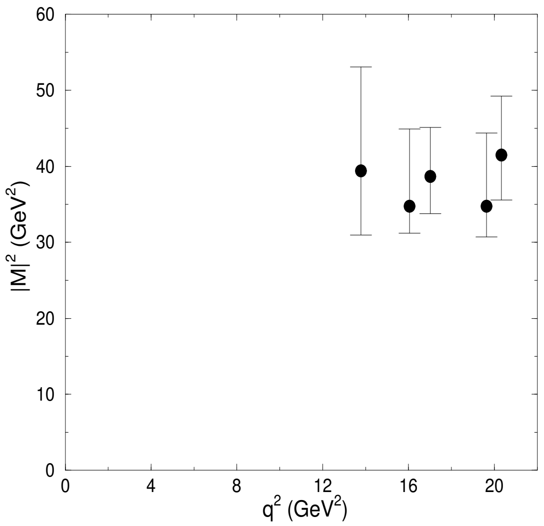

Figure 7.9: The q^2 dependence of the $B^0 \to \rho^- \ell^+ \nu$ matrix element, calculated using the lattice form factors. The extrapolation was quadratic and r_0 was used to set the scale.

expansion, i.e.

$$|M|^2 = \sigma_0 + \sigma_1 (q^2 - q^2_{max}) \ . \tag{7.12}$$

This ansatz was used to fit the lattice results, with the σ_i as free parameters. This ansatz is not expected to be reliable over the whole kinematically allowed range of q^2, but the numerical results show that it is accurate in the range 14 GeV^2 $<$ $q^2 < q^2_{max}$. In terms of the σ_i the differential decay rate is

$$\frac{d\Gamma}{dq^2}(B \to \rho \ell \nu_\ell) = \frac{|V_{ub}|^2 G_F^2 q^2 [\lambda(q^2)]^{\frac{1}{2}}}{192\pi^3 m_B^3} \Big(\sigma_0 + \sigma_1 (q^2 - q^2_{max}) \Big) \ . \tag{7.13}$$

The highest q^2 bin in which the CLEO collaboration measured $\Delta\Gamma$ is $14 < q^2 < 21$ GeV^2 (this is called $\Delta\Gamma_{>14}$ from here on). The lattice σ_i were compared with this measurement. The differential decay rate (7.13) was numerically integrated in the range $14 < q^2 < q^2_{max}$. This gives a result of the form

$$\Delta\Gamma_{>14} = |V_{ub}|^2 \times [\text{Lattice factor}] \ . \tag{7.14}$$

The comparison between lattice and experiment was made in two equivalent ways. $\Delta\Gamma_{>14}$ was calculated using the PDG's best value of $|V_{ub}| = 3.5 \times 10^{-3}$. The error on $|V_{ub}|$ was not included in the lattice prediction for $\Delta\Gamma_{>14}$, so that it is clear whether or not the lattice result and the CLEO measurement favour $|V_{ub}| = 3.5 \times 10^{-3}$. For the alternative comparison the lattice factor of (7.14) was used to obtain $|V_{ub}|$ from the CLEO measurement. The results for the σ_i, and the comparison with $\Delta\Gamma_{>14}$ are shown in table 7.3. For comparison, results of UKQCD95, the CLEO measurement and the PDG $|V_{ub}|$ are also shown. To investigate systematic errors the form factors were obtained in four slightly different ways. Two different extrapolations were used (linear, quadratic) and two different quantities were used to set the scale (m_ρ, r_0).

	σ_0 (GeV^2)	σ_1	$\Delta\Gamma_{>14}$ (10^7 s^{-1})	$\lvert V_{ub}\rvert \times 10^3$
Quadratic, r_0	38^{+8}_{-5}	$-0.3^{+1.9}_{-1.5}$	$8.7^{+1.9}_{-1.2}$	3.2 ± 0.6
Linear, r_0	33^{+7}_{-4}	$-0.5^{+1.4}_{-1.2}$	$7.6^{+1.5}_{-0.9}$	3.4 ± 0.7
Quadratic, m_ρ	36^{+8}_{-5}	$-0.6^{+2.2}_{-1.8}$	$8.1^{+1.8}_{-1.1}$	3.3 ± 0.7
Linear, m_ρ	30^{+6}_{-4}	$-0.9^{+1.6}_{-1.4}$	$6.9^{+1.4}_{-0.9}$	3.6 ± 0.7
UKQCD95	21^{+3}_{-3}	$-1.7^{+0.8}_{-1.3}$	$6.1^{+0.8}_{-0.6}$	3.8 ± 0.7
CLEO	-	-	7.1 ± 2.4	-
PDG	-	-	-	3.5 ± 1.5

Table 7.3: The high q^2 behavior of $d\Gamma/dq^2(B^0 \to \rho^- \ell^+ \nu\ )$. The lattice results of this study and of UKQCD95 are listed. For comparison the experimental result of the CLEO collaboration and the PDG value for $|V_{ub}|$ are also shown. Lattice errors are statistical only. The error on the PDG result is a 90% confidence interval, the other errors are 68% confidence intervals.

The lattice results and $|V_{ub}| = 3.5 \times 10^{-3}$ agree within errors with the CLEO measurement. This comparison uses only the lattice statistical errors. The systematic errors on the lattice results are much harder to estimate. The dominant sources of systematic error are discretisation effects, errors due to the heavy-quark extrapolation and quenching effects. Comparing the $\beta = 6.0$ and $\beta = 6.2$ lattice results for charm meson decays and for the $0 \to 0$ extrapolation suggest that discretisation errors are small, probably about 10% for the form factors. The heavy-quark extrapolation truncates the finite m_H corrections to the heavy-quark scaling laws. The effect of this truncation is tested by comparing the linear and quadratic extrapolations. A conservative assessment of this comparison suggests an error of 15% on the form factors. The scale dependence is small enough to ignore. The error due to using the quenched approximation cannot be assessed from the lattice results alone. The decay rates for charm mesons are in good agreement with experiment. Quenched calculations of the heavy-light semileptonic decays $B \to D, D^*$ [49] and $D \to K$ [36] are also in good agreement with experiment. This suggests that quenching effects are not too large. Precision calculations of the quenched light hadron spectrum find a disagreement of 10% between the lattice results and experiment [19, 20]. Therefore the quenching error for the form factors is estimated to be 10%. This error estimate should be regarded as an educated guess.

The four determinations of $\Delta\Gamma_{>14}$ in table 7.3 are all equally valid, so the best estimate of $\Delta\Gamma_{>14}$ is their average. This gives

$$\Delta\Gamma_{>14} = 7.8^{+1.7}_{-1.1} \pm 3.2 \times 10^{7}\ \mathrm{s}^{-1}\ , \tag{7.15}$$

where the errors are lattice statistical and systematic. The statistical error is taken to be the largest statistical error of the results in table 7.3. The systematic error is the three estimated systematic errors combined in quadrature. Note that a 10% error on the form factors gives a 10% error on $|V_{ub}|$, but a 20% error on $\Delta\Gamma$. Averaging the four determinations of $|V_{ub}|$ gives

$$3.4^{+0.4}_{-0.2} \pm 0.7 \pm 0.6 \times 10^{-3}\ , \tag{7.16}$$

where the errors are statistical, systematic and experimental. Adding the three sources of error in quadrature gives $|V_{ub}| = 3.4 \pm 1.0 \times 10^{-3}$, which is in agreement with the PDG.

Chapter 8

Conclusions

This thesis describes the results of a lattice QCD calculation of the form factors for the semileptonic decay of a heavy-light pseudoscalar meson to a light-light vector meson. The calculation used two values of the coupling to investigate discretisation errors. The results obtained using the finer of the two lattice spacings ($\beta = 6.2$) were compared with experimental results.

Form factors were calculated for the decays of charmed mesons. The decay rates for these decays depend on $|V_{cs}|$ and $|V_{cd}|$, which have been accurately determined by other methods. Therefore charmed meson decays are a good test of the reliability of the lattice results. The relevant decays are $D_s \to \phi$, $D \to K^*$ and $D \to \rho$. The decay $D_s \to \phi$ receives a contribution from disconnected diagrams, which was ignored. The lattice predictions for decay rate are compared with the experimental results in table 8.1. There is reasonable agreement between the lattice and experimental results.

	$D_s \to \phi$	$D \to K^*$	$D \to \rho$
Experiment Γ (10^{10} s^{-1})	4.0 ± 0.5	4.5 ± 0.4	0.21 ± 0.08
Lattice Γ (10^{10} s^{-1})	5.0 ± 0.3	5.5 ± 0.5	0.19 ± 0.02

Table 8.1: Comparison of lattice and experimental total decay rates. Lattice errors are statistical only.

Two form factor ratios have been measured for the decays $D_s \to \phi$ and $D \to K^*$, rather accurately in the latter case. The lattice and experimental ratios are compared in table 8.2. There is significant disagreement between lattice and experiment.

	$D_s \to \phi$		$D \to K^*$	
	$A_2(0)/A_1(0)$	$V(0)/A_1(0)$	$A_2(0)/A_1(0)$	$V(0)/A_1(0)$
Experiment	1.60 ± 0.24	1.92 ± 0.32	1.82 ± 0.09	0.78 ± 0.07
Lattice	0.99^{+6}_{-7}	1.36^{+5}_{-5}	1.03^{+7}_{-9}	1.23^{+7}_{-9}

Table 8.2: Comparison of lattice and experimental form factor ratios. Lattice errors are statistical only.

Form factors for the decay $B \to \rho$ were calculated. These were obtained by extrapolating simulation results in heavy quark mass. The lattice results were interpolated in q^2 to obtain a prediction for

$$\text{differential decay rate}/|V_{ub}|^2 \tag{8.1}$$

in the range 14 GeV$^2 < q^2 < q^2_{max}$. The partial decay rate in this range has been measured experimentally by the CLEO collaboration. Using the lattice and experimental results gives

$$|V_{ub}| = 3.4^{+0.4}_{-0.2} \pm 0.7 \pm 0.6 \times 10^{-3} , \tag{8.2}$$

where the errors are statistical, systematic and experimental. This is competitive with the Particle Data Group which quote $|V_{ub}| = 3.5 \pm 1.5 \times 10^{-3}$. Note that the PDG error is a 90% confidence interval, (8.2) is a 68% confidence interval.

This study used two values of β. The form factors at the different lattice spacings are in agreement, which gives confidence that discretisation errors are small. To reduce discretisation errors to the level where they are insignificant a continuum extrapolation should be used.

The heavy-quark extrapolation used to obtain $B \to \rho$ form factors causes a large systematic error. The form factors can, in principle, be calculated with a static heavy quark. If this is implemented then the heavy-quark extrapolation would become an interpolation which is a much more stable procedure.

The most difficult source of systematic error to eliminate is the quenched approximation. Ultimately the form factors should be calculated in full QCD, without the quenched approximation. The next generation of high performance computers will be powerful enough to do this calculation. However, initial unquenched calculations are likely to be on coarse lattices with low statistics. Therefore precision quenched form factor calculations are likely to be important in the short term.

Appendix A

Results for mesons

This appendix contains the results of fits to two-point correlation functions. Most fits used the single exponential ansatz,

$$C = A(e^{-aEt} + e^{-aE(T-t)}) \ .$$

In many cases the $|\vec{p}| \neq 0$ fits were done with aE determined by the dispersion relation, i.e. a one parameter fit. For fits using the dispersion relation the parameter A is given the superscrip ^{DR}. Table A.12 contains the results of two exponential fits. The two exponential ansatz and the notation are explained in section 4.5.

Table A.1: Heavy-light pseudoscalar mesons $|\vec{p}|^2 = 0$, $\beta = 6.2$.

κ_{heavy}	κ_{light}	A	am
0.12000	0.13460	54.0^{+10}_{-9}	0.8405^{+13}_{-10}
	0.13510	50.9^{+11}_{-11}	0.8231^{+17}_{-13}
	0.13530	50.0^{+12}_{-12}	0.8165^{+19}_{-14}
0.12330	0.13460	58.8^{+10}_{-10}	0.7387^{+12}_{-9}
	0.13510	55.5^{+11}_{-11}	0.7205^{+15}_{-11}
	0.13530	54.5^{+12}_{-13}	0.7136^{+18}_{-13}
0.12660	0.13460	64.3^{+11}_{-11}	0.6284^{+11}_{-8}
	0.13510	61.0^{+12}_{-13}	0.6091^{+14}_{-11}
	0.13530	60.0^{+13}_{-15}	0.6017^{+16}_{-12}
0.12990	0.13460	70.4^{+11}_{-14}	0.5051^{+10}_{-8}
	0.13510	67.3^{+13}_{-16}	0.4840^{+13}_{-11}
	0.13530	66.5^{+13}_{-19}	0.4758^{+14}_{-12}

Table A.2: Heavy-light pseudoscalar mesons $|\vec{p}|^2 = 1$, $\beta = 6.2$.

κ_{heavy}	κ_{light}	A	aE	A^{DR}
0.12000	0.13460	39.5^{+8}_{-8}	0.8789^{+16}_{-13}	40.2^{+7}_{-8}
	0.13510	36.7^{+10}_{-9}	0.863^{+2}_{-2}	37.3^{+8}_{-8}
	0.13530	35.8^{+11}_{-10}	0.856^{+2}_{-2}	36.3^{+8}_{-9}
0.12330	0.13460	43.3^{+9}_{-9}	0.7831^{+16}_{-12}	43.6^{+7}_{-8}
	0.13510	40.3^{+10}_{-10}	0.7663^{+20}_{-14}	40.4^{+8}_{-9}
	0.13530	39.3^{+11}_{-11}	0.760^{+2}_{-2}	39.3^{+8}_{-10}
0.12660	0.13460	47.3^{+10}_{-10}	0.6808^{+17}_{-12}	47.3^{+8}_{-9}
	0.13510	44.1^{+11}_{-11}	0.6635^{+20}_{-14}	43.8^{+7}_{-10}
	0.13530	43.0^{+12}_{-12}	0.657^{+2}_{-2}	42.6^{+8}_{-11}
0.12990	0.13460	51.0^{+11}_{-11}	0.5697^{+19}_{-13}	50.5^{+8}_{-10}
	0.13510	47.6^{+13}_{-12}	0.5516^{+22}_{-15}	46.9^{+8}_{-11}
	0.13530	46.5^{+14}_{-13}	0.545^{+2}_{-2}	45.6^{+8}_{-12}

Table A.3: Heavy-light pseudoscalar mesons $|\vec{p}|^2 = 2,\ \beta = 6.2$.

κ_{heavy}	κ_{light}	A	aE	A^{DR}
0.12000	0.13460	29.7^{+10}_{-10}	0.921^{+3}_{-2}	28.8^{+5}_{-6}
	0.13510	27.8^{+12}_{-12}	0.908^{+4}_{-3}	26.1^{+6}_{-6}
	0.13530	27.4^{+14}_{-14}	0.903^{+4}_{-4}	25.2^{+6}_{-7}
0.12330	0.13460	33.0^{+12}_{-12}	0.831^{+3}_{-3}	31.3^{+6}_{-6}
	0.13510	31.1^{+14}_{-15}	0.818^{+4}_{-3}	28.3^{+6}_{-7}
	0.13530	31^{+2}_{-2}	0.814^{+4}_{-4}	27.3^{+6}_{-8}
0.12660	0.13460	36.7^{+15}_{-15}	0.736^{+3}_{-3}	34.0^{+6}_{-7}
	0.13510	35^{+2}_{-2}	0.724^{+4}_{-4}	30.7^{+6}_{-8}
	0.13530	35^{+2}_{-2}	0.720^{+5}_{-5}	29.5^{+6}_{-9}
0.12990	0.13460	40^{+2}_{-2}	0.636^{+4}_{-4}	36.2^{+7}_{-9}
	0.13510	40^{+3}_{-3}	0.625^{+6}_{-5}	32.7^{+7}_{-9}
	0.13530	40^{+3}_{-3}	0.622^{+7}_{-6}	31.5^{+7}_{-10}

Table A.4: Light-light vector mesons $|\vec{p}|^2 = 0,\ \beta = 6.2$. The results of single exponential fits are shown and also, for comparison, the same parameters determined from double exponential fits. The results from double exponential fits have the superscript ^{2E}

κ_F	κ_L	A	am	A^{2E}	am^{2E}
0.13460	0.13460	0.0088^{+4}_{-4}	0.380^{+4}_{-3}	0.0090^{+4}_{-5}	0.382^{+4}_{-4}
	0.13510	0.0084^{+5}_{-5}	0.361^{+5}_{-5}	0.0086^{+5}_{-6}	0.364^{+6}_{-6}
	0.13530	0.0083^{+6}_{-6}	0.354^{+7}_{-5}	0.0084^{+6}_{-7}	0.357^{+7}_{-7}
0.13510	0.13460	0.0083^{+5}_{-5}	0.359^{+5}_{-4}	0.0085^{+5}_{-6}	0.362^{+6}_{-6}
	0.13510	0.0079^{+7}_{-6}	0.341^{+8}_{-6}	0.0082^{+7}_{-9}	0.344^{+8}_{-9}
	0.13530	0.0078^{+9}_{-7}	0.334^{+9}_{-8}	0.0080^{+8}_{-11}	0.338^{+9}_{-11}
0.13530	0.13460	0.0081^{+6}_{-5}	0.351^{+6}_{-5}	0.0083^{+7}_{-8}	0.354^{+7}_{-7}
	0.13510	0.0076^{+8}_{-6}	0.331^{+9}_{-7}	0.0078^{+9}_{-11}	0.335^{+10}_{-12}
	0.13530	0.0074^{+10}_{-7}	0.324^{+12}_{-9}	0.0076^{+11}_{-14}	0.328^{+12}_{-15}

Table A.5: Light-light vector mesons $|\vec{p}|^2 = 1,\ \beta = 6.2$.

κ_F	κ_L	method 1: A^{DR}	method 2: A^{DR}
0.13460	0.13460	0.0053^{+2}_{-2}	0.0049^{+2}_{-2}
	0.13510	0.0049^{+3}_{-3}	0.0046^{+3}_{-3}
	0.13530	0.0047^{+4}_{-3}	0.0044^{+4}_{-3}
0.13510	0.13460	0.0050^{+3}_{-3}	0.0046^{+3}_{-3}
	0.13510	0.0047^{+4}_{-3}	0.0043^{+4}_{-3}
	0.13530	0.0046^{+5}_{-4}	0.0042^{+5}_{-4}
0.13530	0.13460	0.0049^{+3}_{-3}	0.0045^{+3}_{-3}
	0.13510	0.0045^{+4}_{-3}	0.0041^{+5}_{-4}
	0.13530	0.0044^{+6}_{-4}	0.0041^{+6}_{-4}

Table A.6: Light-light vector mesons $|\vec{p}|^2 = 2,\ \beta = 6.2$.

κ_F	κ_L	method 1: A^{DR}	method 2: A^{DR}
0.13460	0.13460	0.0033^{+2}_{-2}	0.0030^{+2}_{-2}
	0.13510	0.0030^{+2}_{-2}	0.0027^{+2}_{-2}
	0.13530	0.0030^{+3}_{-3}	0.0026^{+2}_{-2}
0.13510	0.13460	0.0032^{+2}_{-3}	0.0028^{+2}_{-2}
	0.13510	0.0030^{+3}_{-3}	0.0025^{+2}_{-2}
	0.13530	0.0030^{+4}_{-3}	0.0024^{+3}_{-2}
0.13530	0.13460	0.0032^{+3}_{-3}	0.0027^{+2}_{-2}
	0.13510	0.0029^{+3}_{-3}	0.0024^{+3}_{-2}
	0.13530	0.0029^{+4}_{-4}	0.0023^{+3}_{-3}

Table A.7: Heavy-light pseudoscalar mesons $|\vec{p}|^2 = 0,\ \beta = 6.0$.

κ_{heavy}	κ_{light}	A	am
0.11230	0.13344	22.7^{+4}_{-5}	1.145^{+2}_{-2}
	0.13417	21.8^{+5}_{-7}	1.120^{+2}_{-2}
	0.13455	21.7^{+7}_{-9}	1.109^{+3}_{-3}
0.11730	0.13344	26.4^{+4}_{-6}	1.0058^{+15}_{-13}
	0.13417	25.4^{+6}_{-7}	0.980^{+2}_{-2}
	0.13455	25.4^{+8}_{-9}	0.968^{+3}_{-3}
0.12230	0.13344	30.3^{+5}_{-6}	0.8506^{+13}_{-11}
	0.13417	29.2^{+6}_{-7}	0.824^{+2}_{-2}
	0.13455	29.2^{+7}_{-9}	0.811^{+2}_{-2}
0.12730	0.13344	35.3^{+5}_{-7}	0.6748^{+13}_{-10}
	0.13417	34.5^{+6}_{-8}	0.6450^{+15}_{-12}
	0.13455	34.6^{+8}_{-9}	0.630^{+2}_{-2}

Table A.8: Heavy-light pseudoscalar mesons $|\vec{p}|^2 = 1,\ \beta = 6.0$.

κ_{heavy}	κ_{light}	A	aE
0.11230	0.13344	14.4^{+4}_{-4}	1.199^{+3}_{-2}
	0.13417	13.7^{+6}_{-6}	1.176^{+4}_{-3}
	0.13455	13.8^{+9}_{-8}	1.167^{+6}_{-5}
0.11730	0.13344	16.7^{+4}_{-5}	1.069^{+3}_{-2}
	0.13417	15.8^{+6}_{-6}	1.046^{+4}_{-3}
	0.13455	15.8^{+9}_{-9}	1.035^{+5}_{-4}
0.12230	0.13344	19.5^{+5}_{-6}	0.929^{+3}_{-2}
	0.13417	18.5^{+7}_{-7}	0.905^{+4}_{-3}
	0.13455	18.5^{+11}_{-10}	0.894^{+5}_{-4}
0.12730	0.13344	22.7^{+7}_{-8}	0.776^{+3}_{-2}
	0.13417	21.9^{+11}_{-10}	0.752^{+4}_{-3}
	0.13455	22.0^{+15}_{-13}	0.740^{+6}_{-5}

Table A.9: Heavy-light pseudoscalar mesons $|\vec{p}|^2 = 2,\ \beta = 6.0$.

κ_{heavy}	κ_{light}	A	aE
0.11230	0.13344	9.0^{+6}_{-6}	1.253^{+6}_{-5}
	0.13417	8.6^{+9}_{-7}	1.235^{+9}_{-7}
	0.13455	9.1^{+13}_{-11}	1.232^{+12}_{-11}
0.11730	0.13344	10.5^{+8}_{-7}	1.130^{+7}_{-5}
	0.13417	10.2^{+12}_{-9}	1.113^{+10}_{-8}
	0.13455	11.0^{+18}_{-15}	1.111^{+14}_{-12}
0.12230	0.13344	12.4^{+12}_{-10}	1.001^{+8}_{-7}
	0.13417	12.5^{+18}_{-14}	0.986^{+13}_{-10}
	0.13455	14^{+3}_{-2}	0.986^{+19}_{-15}
0.12730	0.13344	15^{+2}_{-2}	0.865^{+12}_{-11}
	0.13417	16^{+4}_{-3}	0.86^{+2}_{-2}
	0.13455	19^{+8}_{-5}	0.86^{+3}_{-3}

Table A.10: Light-light vector mesons $|\vec{p}|^2 = 0,\ \beta = 6.0$.

κ_F	κ_L	A	am
0.13344	0.13344	0.0329^{+13}_{-11}	0.538^{+5}_{-3}
	0.13417	0.0319^{+14}_{-13}	0.511^{+6}_{-4}
	0.13455	0.032^{+2}_{-2}	0.499^{+7}_{-6}
0.13417	0.13344	0.0319^{+15}_{-13}	0.510^{+6}_{-4}
	0.13417	0.0307^{+18}_{-15}	0.482^{+8}_{-5}
	0.13455	0.030^{+2}_{-2}	0.470^{+9}_{-8}
0.13455	0.13344	0.032^{+2}_{-2}	0.496^{+7}_{-5}
	0.13417	0.030^{+2}_{-2}	0.467^{+9}_{-7}
	0.13455	0.030^{+3}_{-2}	0.455^{+11}_{-10}

Table A.11: Light-light vector mesons $|\vec{p}|^2 = 1,\ \beta = 6.0$.

κ_F	κ_L	method 1: A^{DR}	method 2: A^{DR}
0.13344	0.13344	0.0169^{+6}_{-6}	0.0161^{+7}_{-6}
	0.13417	0.0166^{+8}_{-7}	0.0150^{+7}_{-6}
	0.13455	0.0166^{+8}_{-8}	0.0146^{+8}_{-7}
0.13417	0.13344	0.0157^{+7}_{-7}	0.0155^{+8}_{-7}
	0.13417	0.0154^{+8}_{-8}	0.0143^{+8}_{-7}
	0.13455	0.0155^{+9}_{-10}	0.0140^{+10}_{-9}
0.13455	0.13344	0.0153^{+8}_{-8}	0.0152^{+9}_{-8}
	0.13417	0.0152^{+9}_{-10}	0.0140^{+10}_{-9}
	0.13455	0.0154^{+10}_{-12}	0.0138^{+12}_{-11}

Table A.12: Double exponential fits to light light vector mesons $|\vec{p}|^2 = 0,\ \beta = 6.2$.

κ_F	κ_L	Z^0_F	Z^0_L	am_0	Z^1_F	Z^1_L	am_1
0.13460	0.13460	0.083^{+2}_{-3}	0.042^{+2}_{-2}	0.382^{+4}_{-4}	0.062^{+14}_{-12}	0.11^{+3}_{-2}	0.71^{+7}_{-5}
	0.13510	0.079^{+3}_{-3}	0.039^{+2}_{-2}	0.364^{+6}_{-6}	0.07^{+2}_{-2}	0.11^{+4}_{-2}	0.71^{+9}_{-7}
	0.13530	0.078^{+3}_{-4}	0.038^{+3}_{-3}	0.357^{+7}_{-7}	0.07^{+2}_{-2}	0.11^{+6}_{-3}	0.71^{+11}_{-8}
0.13510	0.13460	0.079^{+3}_{-3}	0.039^{+2}_{-2}	0.362^{+6}_{-6}	0.07^{+2}_{-2}	0.11^{+4}_{-2}	0.70^{+9}_{-6}
	0.13510	0.075^{+4}_{-5}	0.037^{+3}_{-3}	0.344^{+8}_{-9}	0.08^{+3}_{-2}	0.11^{+7}_{-3}	0.70^{+13}_{-9}
	0.13530	0.074^{+5}_{-6}	0.036^{+3}_{-4}	0.338^{+9}_{-11}	0.08^{+3}_{-2}	0.11^{+9}_{-3}	0.70^{+16}_{-10}
0.13530	0.13460	0.077^{+4}_{-4}	0.037^{+3}_{-3}	0.354^{+7}_{-7}	0.07^{+2}_{-2}	0.10^{+4}_{-2}	0.68^{+10}_{-7}
	0.13510	0.072^{+5}_{-6}	0.035^{+4}_{-4}	0.335^{+10}_{-12}	0.08^{+3}_{-2}	0.10^{+7}_{-2}	0.67^{+15}_{-9}
	0.13530	0.071^{+6}_{-9}	0.034^{+5}_{-5}	0.328^{+12}_{-15}	0.08^{+3}_{-2}	0.10^{+10}_{-3}	0.66^{+19}_{-10}

Appendix B

Results for form factors

This appendix lists the form factors obtained from fits to the lattice three-point correlation functions. Every channel that was fitted is listed, including channels regarded as unreliable.

Table B.1: Form factors, channel $0 \to 0$, $\beta = 6.2$.

κ_H	κ_P	κ_A	q^2a^2	A_1	A_2	A	V
2000	3460	3460	0.212^{+3}_{-3}	0.77^{+2}_{-2}	-	-	-
		3510	0.232^{+4}_{-5}	0.74^{+3}_{-2}	-	-	-
		3530	0.240^{+5}_{-6}	0.73^{+3}_{-3}	-	-	-
	3510	3460	0.213^{+4}_{-5}	0.77^{+3}_{-3}	-	-	-
		3510	0.233^{+6}_{-7}	0.74^{+3}_{-3}	-	-	-
		3530	0.242^{+7}_{-9}	0.72^{+4}_{-3}	-	-	-
2330	3460	3460	0.129^{+3}_{-3}	0.77^{+2}_{-2}	-	-	-
		3510	0.144^{+3}_{-4}	0.74^{+3}_{-2}	-	-	-
		3530	0.151^{+4}_{-5}	0.73^{+3}_{-2}	-	-	-
	3510	3460	0.129^{+3}_{-4}	0.77^{+3}_{-3}	-	-	-
		3510	0.144^{+5}_{-6}	0.74^{+3}_{-3}	-	-	-
		3530	0.152^{+6}_{-7}	0.72^{+3}_{-3}	-	-	-
2660	3460	3460	0.062^{+2}_{-2}	0.77^{+2}_{-2}	-	-	-
		3510	0.072^{+2}_{-3}	0.74^{+3}_{-2}	-	-	-
		3530	0.077^{+3}_{-3}	0.73^{+3}_{-2}	-	-	-
	3510	3460	0.062^{+2}_{-3}	0.77^{+3}_{-3}	-	-	-
		3510	0.072^{+3}_{-4}	0.74^{+3}_{-3}	-	-	-
		3530	0.077^{+4}_{-5}	0.73^{+3}_{-3}	-	-	-
2990	3460	3460	0.0158^{+9}_{-9}	0.78^{+2}_{-2}	-	-	-
		3510	0.0213^{+13}_{-15}	0.75^{+2}_{-2}	-	-	-
		3530	0.024^{+2}_{-2}	0.74^{+3}_{-2}	-	-	-
	3510	3460	0.0151^{+12}_{-13}	0.78^{+3}_{-3}	-	-	-
		3510	0.021^{+2}_{-2}	0.75^{+3}_{-3}	-	-	-
		3530	0.023^{+2}_{-3}	0.74^{+3}_{-3}	-	-	-

Table B.2: Form factors, channel $0 \to 1$, $\beta = 6.2$.

κ_H	κ_P	κ_A	q^2a^2	A_1	A_2	A	V
2000	3460	3460	0.075^{+2}_{-2}	0.63^{+2}_{-2}	0.75^{+8}_{-9}	0.12^{+2}_{-2}	0.87^{+3}_{-3}
		3510	0.088^{+3}_{-3}	0.60^{+3}_{-3}	0.71^{+8}_{-10}	0.14^{+2}_{-2}	0.85^{+4}_{-4}
		3530	0.094^{+3}_{-4}	0.60^{+3}_{-3}	0.71^{+10}_{-10}	0.15^{+2}_{-2}	0.84^{+4}_{-4}
	3510	3460	0.074^{+3}_{-3}	0.65^{+3}_{-3}	0.80^{+9}_{-11}	0.12^{+2}_{-2}	0.86^{+4}_{-4}
		3510	0.086^{+4}_{-5}	0.63^{+3}_{-3}	0.78^{+11}_{-12}	0.16^{+2}_{-3}	0.83^{+5}_{-4}
		3530	0.092^{+5}_{-6}	0.63^{+4}_{-4}	0.79^{+12}_{-13}	0.17^{+3}_{-3}	0.82^{+6}_{-5}
2330	3460	3460	0.008^{+2}_{-2}	0.63^{+2}_{-2}	0.70^{+7}_{-8}	0.014^{+3}_{-4}	0.85^{+3}_{-3}
		3510	0.018^{+2}_{-2}	0.60^{+3}_{-3}	0.66^{+7}_{-8}	0.031^{+6}_{-6}	0.82^{+4}_{-3}
		3530	0.022^{+2}_{-3}	0.60^{+3}_{-3}	0.65^{+9}_{-9}	0.040^{+7}_{-8}	0.81^{+4}_{-4}
	3510	3460	0.007^{+2}_{-2}	0.65^{+3}_{-3}	0.74^{+8}_{-10}	0.013^{+4}_{-5}	0.83^{+4}_{-4}
		3510	0.016^{+3}_{-3}	0.63^{+3}_{-3}	0.72^{+9}_{-10}	0.032^{+8}_{-9}	0.80^{+4}_{-4}
		3530	0.021^{+4}_{-4}	0.63^{+4}_{-4}	0.73^{+11}_{-11}	0.043^{+10}_{-12}	0.79^{+5}_{-5}
2660	3460	3460	-0.0406^{+10}_{-10}	0.63^{+2}_{-2}	0.64^{+6}_{-7}	-0.079^{+11}_{-9}	0.83^{+3}_{-3}
		3510	-0.0348^{+13}_{-15}	0.60^{+2}_{-3}	0.60^{+6}_{-7}	-0.070^{+10}_{-9}	0.80^{+3}_{-3}
		3530	-0.032^{+2}_{-2}	0.60^{+3}_{-3}	0.60^{+7}_{-8}	-0.066^{+9}_{-10}	0.79^{+4}_{-4}
	3510	3460	-0.0419^{+13}_{-13}	0.65^{+3}_{-3}	0.68^{+7}_{-8}	-0.089^{+14}_{-13}	0.81^{+4}_{-4}
		3510	-0.036^{+2}_{-2}	0.63^{+3}_{-3}	0.66^{+8}_{-9}	-0.082^{+14}_{-13}	0.77^{+4}_{-4}
		3530	-0.033^{+2}_{-3}	0.63^{+4}_{-4}	0.66^{+9}_{-10}	-0.079^{+13}_{-15}	0.76^{+5}_{-4}
2990	3460	3460	-0.0666^{+3}_{-3}	0.63^{+2}_{-3}	0.58^{+4}_{-5}	-0.16^{+2}_{-2}	0.83^{+3}_{-3}
		3510	-0.0649^{+4}_{-5}	0.61^{+2}_{-3}	0.54^{+5}_{-5}	-0.16^{+2}_{-2}	0.79^{+3}_{-3}
		3530	-0.0640^{+6}_{-7}	0.60^{+3}_{-3}	0.53^{+6}_{-6}	-0.16^{+2}_{-2}	0.77^{+4}_{-3}
	3510	3460	-0.0671^{+3}_{-3}	0.65^{+3}_{-3}	0.62^{+5}_{-6}	-0.18^{+3}_{-2}	0.80^{+4}_{-4}
		3510	-0.0656^{+5}_{-6}	0.64^{+3}_{-3}	0.59^{+6}_{-7}	-0.18^{+3}_{-2}	0.76^{+4}_{-4}
		3530	-0.0647^{+7}_{-8}	0.63^{+3}_{-4}	0.59^{+7}_{-7}	-0.19^{+3}_{-3}	0.73^{+4}_{-4}

Table B.3: Form factors, channel $0 \to 2$, $\beta = 6.2$.

κ_H	κ_P	κ_A	q^2a^2	A_1	A_2	A	V
2000	3460	3460	-0.041^{+2}_{-2}	0.36^{+3}_{-2}	0.25^{+5}_{-5}	-0.016^{+4}_{-4}	0.87^{+3}_{-3}
		3510	-0.032^{+2}_{-2}	0.34^{+3}_{-2}	0.23^{+5}_{-5}	-0.013^{+3}_{-4}	0.85^{+4}_{-4}
		3530	-0.028^{+2}_{-3}	0.33^{+3}_{-3}	0.23^{+6}_{-6}	-0.012^{+3}_{-4}	0.84^{+4}_{-4}
	3510	3460	-0.043^{+2}_{-2}	0.36^{+3}_{-3}	0.25^{+7}_{-6}	-0.019^{+6}_{-6}	0.86^{+4}_{-4}
		3510	-0.035^{+3}_{-3}	0.33^{+4}_{-3}	0.23^{+7}_{-7}	-0.016^{+6}_{-6}	0.83^{+5}_{-4}
		3530	-0.030^{+3}_{-4}	0.32^{+4}_{-3}	0.23^{+8}_{-8}	-0.015^{+6}_{-5}	0.82^{+6}_{-5}
2330	3460	3460	-0.0937^{+11}_{-11}	0.36^{+3}_{-2}	0.25^{+4}_{-4}	-0.043^{+9}_{-9}	0.85^{+3}_{-3}
		3510	-0.0875^{+14}_{-16}	0.34^{+3}_{-2}	0.23^{+5}_{-5}	-0.042^{+10}_{-10}	0.82^{+4}_{-3}
		3530	-0.085^{+2}_{-2}	0.33^{+3}_{-3}	0.23^{+5}_{-5}	-0.043^{+11}_{-11}	0.81^{+4}_{-4}
	3510	3460	-0.0957^{+14}_{-14}	0.36^{+3}_{-3}	0.25^{+6}_{-6}	-0.047^{+14}_{-14}	0.83^{+4}_{-4}
		3510	-0.090^{+2}_{-2}	0.33^{+4}_{-3}	0.22^{+7}_{-6}	-0.047^{+15}_{-15}	0.80^{+4}_{-4}
		3530	-0.087^{+2}_{-3}	0.33^{+4}_{-3}	0.22^{+7}_{-7}	-0.05^{+2}_{-2}	0.79^{+5}_{-5}
2660	3460	3460	-0.1275^{+5}_{-5}	0.37^{+2}_{-2}	0.26^{+4}_{-4}	-0.070^{+13}_{-14}	0.83^{+3}_{-3}
		3510	-0.1244^{+7}_{-8}	0.35^{+3}_{-2}	0.23^{+4}_{-4}	-0.07^{+2}_{-2}	0.80^{+3}_{-3}
		3530	-0.1230^{+8}_{-10}	0.34^{+3}_{-2}	0.23^{+5}_{-5}	-0.08^{+2}_{-2}	0.79^{+4}_{-4}
	3510	3460	-0.1286^{+6}_{-6}	0.36^{+3}_{-3}	0.25^{+5}_{-5}	-0.07^{+2}_{-2}	0.81^{+4}_{-4}
		3510	-0.1258^{+9}_{-10}	0.34^{+4}_{-3}	0.22^{+6}_{-5}	-0.08^{+2}_{-2}	0.77^{+4}_{-4}
		3530	-0.1244^{+11}_{-13}	0.33^{+4}_{-3}	0.22^{+6}_{-6}	-0.08^{+2}_{-3}	0.76^{+5}_{-4}
2990	3460	3460	-0.13645^{+14}_{-12}	0.37^{+2}_{-2}	0.28^{+4}_{-3}	-0.10^{+2}_{-2}	0.83^{+3}_{-3}
		3510	-0.13696^{+9}_{-6}	0.35^{+3}_{-2}	0.25^{+4}_{-4}	-0.11^{+2}_{-2}	0.79^{+3}_{-3}
		3530	-0.13706^{+6}_{-2}	0.35^{+3}_{-2}	0.24^{+4}_{-4}	-0.11^{+2}_{-2}	0.77^{+4}_{-3}
	3510	3460	-0.1360^{+3}_{-2}	0.37^{+3}_{-3}	0.27^{+5}_{-4}	-0.10^{+2}_{-3}	0.80^{+4}_{-4}
		3510	-0.13671^{+22}_{-14}	0.35^{+4}_{-3}	0.24^{+5}_{-4}	-0.11^{+3}_{-3}	0.76^{+4}_{-4}
		3530	-0.13692^{+19}_{-10}	0.34^{+4}_{-3}	0.23^{+5}_{-5}	-0.12^{+3}_{-3}	0.73^{+4}_{-4}

Table B.4: Form factors, channel $1 \to 0$, $\beta = 6.2$.

κ_H	κ_P	κ_A	q^2a^2	A_1	A_2	A	V
2000	3460	3460	0.182^{+4}_{-4}	0.72^{+3}_{-3}	1.2^{+5}_{-5}	0.6^{+2}_{-3}	0.87^{+3}_{-3}
		3510	0.203^{+5}_{-5}	0.70^{+3}_{-3}	1.4^{+6}_{-6}	0.8^{+3}_{-4}	0.85^{+4}_{-4}
		3530	0.212^{+6}_{-6}	0.69^{+4}_{-3}	1.6^{+7}_{-7}	1.0^{+4}_{-4}	0.84^{+4}_{-4}
	3510	3460	0.184^{+5}_{-5}	0.72^{+4}_{-3}	1.2^{+7}_{-7}	0.6^{+4}_{-4}	0.86^{+4}_{-4}
		3510	0.205^{+7}_{-8}	0.70^{+4}_{-4}	1.5^{+8}_{-8}	1.0^{+5}_{-5}	0.83^{+5}_{-4}
		3530	0.215^{+8}_{-9}	0.69^{+5}_{-4}	1.8^{+10}_{-9}	1.2^{+6}_{-6}	0.82^{+6}_{-5}
2330	3460	3460	0.095^{+3}_{-3}	0.71^{+3}_{-3}	0.9^{+3}_{-4}	0.27^{+10}_{-12}	0.85^{+3}_{-3}
		3510	0.112^{+4}_{-4}	0.69^{+3}_{-3}	1.0^{+4}_{-4}	0.4^{+2}_{-2}	0.82^{+4}_{-3}
		3530	0.119^{+4}_{-5}	0.68^{+4}_{-3}	1.1^{+5}_{-5}	0.5^{+2}_{-2}	0.81^{+4}_{-4}
	3510	3460	0.096^{+4}_{-4}	0.72^{+4}_{-3}	0.8^{+5}_{-5}	0.3^{+2}_{-2}	0.83^{+4}_{-4}
		3510	0.113^{+5}_{-6}	0.69^{+4}_{-4}	1.0^{+6}_{-6}	0.4^{+2}_{-2}	0.80^{+4}_{-4}
		3530	0.121^{+6}_{-8}	0.68^{+5}_{-4}	1.2^{+6}_{-7}	0.6^{+3}_{-3}	0.79^{+5}_{-5}
2660	3460	3460	0.022^{+2}_{-2}	0.71^{+3}_{-3}	0.6^{+2}_{-2}	0.06^{+2}_{-2}	0.83^{+3}_{-3}
		3510	0.035^{+3}_{-3}	0.68^{+3}_{-3}	0.7^{+2}_{-3}	0.11^{+4}_{-5}	0.80^{+3}_{-3}
		3530	0.040^{+3}_{-4}	0.67^{+3}_{-3}	0.7^{+3}_{-3}	0.15^{+5}_{-6}	0.79^{+4}_{-4}
	3510	3460	0.023^{+3}_{-3}	0.71^{+4}_{-3}	0.6^{+3}_{-3}	0.06^{+3}_{-3}	0.81^{+4}_{-4}
		3510	0.035^{+4}_{-5}	0.68^{+4}_{-4}	0.7^{+4}_{-4}	0.12^{+6}_{-6}	0.77^{+4}_{-4}
		3530	0.042^{+5}_{-6}	0.67^{+5}_{-4}	0.8^{+4}_{-4}	0.17^{+8}_{-8}	0.76^{+5}_{-4}
2990	3460	3460	-0.0327^{+13}_{-14}	0.69^{+3}_{-2}	0.43^{+10}_{-11}	-0.09^{+2}_{-2}	0.83^{+3}_{-3}
		3510	-0.025^{+2}_{-2}	0.67^{+3}_{-3}	0.43^{+13}_{-14}	-0.08^{+2}_{-2}	0.79^{+3}_{-3}
		3530	-0.021^{+2}_{-3}	0.66^{+3}_{-3}	0.5^{+2}_{-2}	-0.07^{+2}_{-2}	0.77^{+4}_{-3}
	3510	3460	-0.033^{+2}_{-2}	0.69^{+4}_{-3}	0.39^{+15}_{-15}	-0.09^{+3}_{-3}	0.80^{+4}_{-4}
		3510	-0.025^{+3}_{-3}	0.67^{+4}_{-4}	0.4^{+2}_{-2}	-0.08^{+3}_{-3}	0.76^{+4}_{-4}
		3530	-0.020^{+3}_{-4}	0.66^{+5}_{-4}	0.4^{+2}_{-2}	-0.07^{+3}_{-3}	0.73^{+4}_{-4}

Table B.5: Form factors, channel $1 \to 1 \parallel$, $\beta = 6.2$.

κ_H	κ_P	κ_A	q^2a^2	A_1	A_2	A	V
2000	3460	3460	0.176^{+2}_{-2}	0.70^{+7}_{-7}	1.8^{+11}_{-11}	0.8^{+6}_{-6}	0.87^{+3}_{-3}
		3510	0.190^{+3}_{-4}	0.65^{+8}_{-8}	1.3^{+11}_{-10}	0.7^{+7}_{-6}	0.85^{+4}_{-4}
		3530	0.196^{+4}_{-4}	0.62^{+9}_{-8}	1.1^{+12}_{-11}	0.6^{+7}_{-6}	0.84^{+4}_{-4}
	3510	3460	0.174^{+3}_{-3}	0.68^{+10}_{-10}	1.6^{+15}_{-14}	0.8^{+8}_{-8}	0.86^{+4}_{-4}
		3510	0.188^{+4}_{-5}	0.62^{+12}_{-11}	1.0^{+14}_{-13}	0.6^{+9}_{-8}	0.83^{+5}_{-4}
		3530	0.195^{+5}_{-6}	0.59^{+13}_{-11}	0.7^{+15}_{-13}	0.4^{+10}_{-8}	0.82^{+6}_{-5}
2330	3460	3460	0.104^{+2}_{-2}	0.71^{+7}_{-7}	1.7^{+12}_{-12}	0.6^{+5}_{-5}	0.85^{+3}_{-3}
		3510	0.115^{+2}_{-3}	0.65^{+8}_{-8}	1.2^{+12}_{-11}	0.5^{+6}_{-5}	0.82^{+4}_{-3}
		3530	0.120^{+3}_{-3}	0.63^{+9}_{-8}	1.0^{+13}_{-11}	0.4^{+6}_{-5}	0.81^{+4}_{-4}
	3510	3460	0.103^{+2}_{-3}	0.68^{+10}_{-10}	1.4^{+16}_{-15}	0.5^{+7}_{-6}	0.83^{+4}_{-4}
		3510	0.114^{+3}_{-4}	0.61^{+12}_{-11}	0.8^{+15}_{-14}	0.3^{+7}_{-7}	0.80^{+4}_{-4}
		3530	0.119^{+4}_{-5}	0.59^{+13}_{-11}	0.5^{+16}_{-14}	0.2^{+8}_{-7}	0.79^{+5}_{-5}
2660	3460	3460	0.0482^{+13}_{-13}	0.71^{+7}_{-7}	1.7^{+15}_{-14}	0.3^{+4}_{-4}	0.83^{+3}_{-3}
		3510	0.056^{+2}_{-2}	0.66^{+8}_{-8}	1.1^{+15}_{-13}	0.3^{+5}_{-4}	0.80^{+3}_{-3}
		3530	0.059^{+2}_{-2}	0.63^{+9}_{-8}	0.8^{+15}_{-14}	0.2^{+5}_{-4}	0.79^{+4}_{-4}
	3510	3460	0.047^{+2}_{-2}	0.68^{+10}_{-10}	$1.^{+2}_{-2}$	0.2^{+6}_{-5}	0.81^{+4}_{-4}
		3510	0.054^{+2}_{-3}	0.62^{+12}_{-11}	$0.^{+2}_{-2}$	0.1^{+6}_{-5}	0.77^{+4}_{-4}
		3530	0.058^{+3}_{-3}	0.59^{+13}_{-12}	$0.^{+2}_{-2}$	0.0^{+7}_{-6}	0.76^{+5}_{-4}
2990	3460	3460	0.0116^{+6}_{-7}	0.72^{+8}_{-7}	$2.^{+3}_{-2}$	0.1^{+4}_{-3}	0.83^{+3}_{-3}
		3510	0.0155^{+9}_{-10}	0.67^{+9}_{-8}	$1.^{+2}_{-2}$	0.1^{+4}_{-4}	0.79^{+3}_{-3}
		3530	0.0173^{+11}_{-13}	0.64^{+10}_{-9}	$1.^{+2}_{-2}$	0.1^{+4}_{-4}	0.77^{+4}_{-3}
	3510	3460	0.0109^{+8}_{-9}	0.68^{+11}_{-10}	$1.^{+3}_{-3}$	0.0^{+5}_{-5}	0.80^{+4}_{-4}
		3510	0.0146^{+12}_{-14}	0.62^{+13}_{-12}	$0.^{+3}_{-3}$	-0.1^{+5}_{-5}	0.76^{+4}_{-4}
		3530	0.0165^{+15}_{-18}	0.59^{+15}_{-13}	$0.^{+3}_{-3}$	-0.1^{+6}_{-5}	0.73^{+4}_{-4}

Table B.6: Form factors, channel $1 \to 1 \perp$, $\beta = 6.2$.

κ_H	κ_P	κ_A	q^2a^2	A_1	A_2	A	V
2000	3460	3460	0.039^{+2}_{-2}	0.60^{+2}_{-2}	0.60^{+7}_{-6}	0.046^{+7}_{-7}	0.87^{+3}_{-3}
		3510	0.053^{+3}_{-4}	0.58^{+2}_{-2}	0.57^{+7}_{-7}	0.064^{+10}_{-10}	0.85^{+4}_{-4}
		3530	0.059^{+4}_{-4}	0.57^{+2}_{-2}	0.56^{+7}_{-8}	0.073^{+11}_{-12}	0.84^{+4}_{-4}
	3510	3460	0.037^{+3}_{-3}	0.61^{+3}_{-2}	0.63^{+9}_{-9}	0.048^{+10}_{-9}	0.86^{+4}_{-4}
		3510	0.051^{+4}_{-5}	0.59^{+3}_{-3}	0.59^{+9}_{-10}	0.067^{+15}_{-14}	0.83^{+5}_{-4}
		3530	0.058^{+5}_{-6}	0.58^{+3}_{-3}	0.58^{+10}_{-10}	0.08^{+2}_{-2}	0.82^{+6}_{-5}
2330	3460	3460	-0.033^{+2}_{-2}	0.58^{+2}_{-2}	0.55^{+6}_{-6}	-0.042^{+5}_{-5}	0.85^{+3}_{-3}
		3510	-0.022^{+2}_{-3}	0.56^{+2}_{-2}	0.52^{+6}_{-6}	-0.029^{+4}_{-5}	0.82^{+4}_{-3}
		3530	-0.017^{+3}_{-3}	0.56^{+2}_{-2}	0.51^{+6}_{-6}	-0.023^{+4}_{-5}	0.81^{+4}_{-4}
	3510	3460	-0.034^{+2}_{-3}	0.60^{+3}_{-2}	0.56^{+7}_{-7}	-0.047^{+7}_{-8}	0.83^{+4}_{-4}
		3510	-0.024^{+3}_{-4}	0.58^{+3}_{-3}	0.53^{+8}_{-8}	-0.033^{+7}_{-7}	0.80^{+4}_{-4}
		3530	-0.018^{+4}_{-5}	0.57^{+3}_{-3}	0.52^{+8}_{-9}	-0.026^{+6}_{-7}	0.79^{+5}_{-5}
2660	3460	3460	-0.0889^{+13}_{-13}	0.57^{+2}_{-2}	0.48^{+5}_{-5}	-0.125^{+13}_{-13}	0.83^{+3}_{-3}
		3510	-0.081^{+2}_{-2}	0.55^{+2}_{-2}	0.46^{+5}_{-5}	-0.118^{+13}_{-13}	0.80^{+3}_{-3}
		3530	-0.078^{+2}_{-2}	0.55^{+2}_{-2}	0.45^{+5}_{-5}	-0.116^{+13}_{-14}	0.79^{+4}_{-4}
	3510	3460	-0.090^{+2}_{-2}	0.59^{+3}_{-2}	0.49^{+6}_{-6}	-0.13^{+2}_{-2}	0.81^{+4}_{-4}
		3510	-0.083^{+2}_{-3}	0.57^{+3}_{-2}	0.46^{+6}_{-7}	-0.13^{+2}_{-2}	0.77^{+4}_{-4}
		3530	-0.079^{+3}_{-3}	0.57^{+3}_{-3}	0.46^{+7}_{-7}	-0.12^{+2}_{-2}	0.76^{+5}_{-4}
2990	3460	3460	-0.1255^{+6}_{-7}	0.55^{+2}_{-2}	0.41^{+4}_{-4}	-0.20^{+2}_{-2}	0.83^{+3}_{-3}
		3510	-0.1216^{+9}_{-10}	0.54^{+2}_{-2}	0.39^{+4}_{-4}	-0.20^{+2}_{-2}	0.79^{+3}_{-3}
		3530	-0.1198^{+11}_{-13}	0.53^{+2}_{-2}	0.38^{+4}_{-4}	-0.20^{+2}_{-2}	0.77^{+4}_{-3}
	3510	3460	-0.1262^{+8}_{-9}	0.58^{+3}_{-2}	0.41^{+5}_{-5}	-0.22^{+2}_{-3}	0.80^{+4}_{-4}
		3510	-0.1225^{+12}_{-14}	0.56^{+3}_{-2}	0.39^{+5}_{-5}	-0.22^{+3}_{-3}	0.76^{+4}_{-4}
		3530	-0.1206^{+15}_{-18}	0.56^{+3}_{-2}	0.39^{+5}_{-6}	-0.22^{+3}_{-3}	0.73^{+4}_{-4}

Table B.7: Form factors, channel $1 \to 1_{\downarrow\uparrow}$, $\beta = 6.2$.

κ_H	κ_P	κ_A	q^2a^2	A_1	A_2	A	V
2000	3460	3460	-0.098^{+2}_{-2}	0.54^{+3}_{-3}	0.54^{+6}_{-6}	-0.102^{+11}_{-11}	0.87^{+3}_{-3}
		3510	-0.084^{+3}_{-4}	0.52^{+3}_{-3}	0.52^{+6}_{-6}	-0.090^{+10}_{-10}	0.85^{+4}_{-4}
		3530	-0.078^{+4}_{-4}	0.51^{+3}_{-3}	0.51^{+6}_{-6}	-0.084^{+10}_{-9}	0.84^{+4}_{-4}
	3510	3460	-0.100^{+3}_{-3}	0.58^{+4}_{-4}	0.58^{+7}_{-7}	-0.115^{+15}_{-14}	0.86^{+4}_{-4}
		3510	-0.086^{+4}_{-5}	0.55^{+4}_{-4}	0.56^{+8}_{-8}	-0.100^{+14}_{-13}	0.83^{+5}_{-4}
		3530	-0.079^{+5}_{-6}	0.54^{+4}_{-4}	0.55^{+8}_{-9}	-0.094^{+14}_{-13}	0.82^{+6}_{-5}
2330	3460	3460	-0.170^{+2}_{-2}	0.52^{+3}_{-3}	0.46^{+5}_{-5}	-0.18^{+2}_{-2}	0.85^{+3}_{-3}
		3510	-0.159^{+2}_{-3}	0.50^{+3}_{-3}	0.45^{+5}_{-5}	-0.17^{+2}_{-2}	0.82^{+4}_{-3}
		3530	-0.154^{+3}_{-3}	0.49^{+3}_{-3}	0.44^{+5}_{-5}	-0.17^{+2}_{-2}	0.81^{+4}_{-4}
	3510	3460	-0.171^{+2}_{-3}	0.56^{+3}_{-3}	0.50^{+6}_{-6}	-0.20^{+2}_{-2}	0.83^{+4}_{-4}
		3510	-0.161^{+3}_{-4}	0.53^{+3}_{-4}	0.48^{+6}_{-7}	-0.19^{+2}_{-2}	0.80^{+4}_{-4}
		3530	-0.155^{+4}_{-5}	0.52^{+4}_{-4}	0.47^{+6}_{-7}	-0.18^{+2}_{-2}	0.79^{+5}_{-5}
2660	3460	3460	-0.2259^{+13}_{-13}	0.50^{+2}_{-3}	0.39^{+3}_{-4}	-0.24^{+2}_{-2}	0.83^{+3}_{-3}
		3510	-0.218^{+2}_{-2}	0.48^{+2}_{-3}	0.38^{+4}_{-4}	-0.24^{+2}_{-2}	0.80^{+3}_{-3}
		3530	-0.215^{+2}_{-2}	0.48^{+3}_{-3}	0.37^{+4}_{-4}	-0.24^{+2}_{-2}	0.79^{+4}_{-4}
	3510	3460	-0.227^{+2}_{-2}	0.55^{+3}_{-4}	0.41^{+5}_{-5}	-0.27^{+3}_{-3}	0.81^{+4}_{-4}
		3510	-0.220^{+2}_{-3}	0.52^{+3}_{-4}	0.40^{+5}_{-5}	-0.26^{+3}_{-3}	0.77^{+4}_{-4}
		3530	-0.216^{+3}_{-3}	0.51^{+4}_{-4}	0.39^{+5}_{-6}	-0.26^{+3}_{-3}	0.76^{+5}_{-4}
2990	3460	3460	-0.2625^{+6}_{-7}	0.49^{+2}_{-3}	0.31^{+3}_{-3}	-0.29^{+3}_{-2}	0.83^{+3}_{-3}
		3510	-0.2587^{+9}_{-10}	0.47^{+2}_{-3}	0.31^{+3}_{-3}	-0.30^{+3}_{-2}	0.79^{+3}_{-3}
		3530	-0.2569^{+11}_{-13}	0.46^{+3}_{-3}	0.30^{+3}_{-3}	-0.30^{+3}_{-3}	0.77^{+4}_{-3}
	3510	3460	-0.2633^{+8}_{-9}	0.53^{+3}_{-3}	0.33^{+4}_{-4}	-0.33^{+3}_{-3}	0.80^{+4}_{-4}
		3510	-0.2596^{+12}_{-14}	0.51^{+3}_{-4}	0.32^{+4}_{-4}	-0.33^{+4}_{-3}	0.76^{+4}_{-4}
		3530	-0.2577^{+15}_{-18}	0.51^{+3}_{-4}	0.32^{+4}_{-5}	-0.33^{+4}_{-3}	0.73^{+4}_{-4}

Table B.8: Form factors, channel $1 \to 2 \perp$, $\beta = 6.2$.

κ_H	κ_P	κ_A	q^2a^2	A_1	A_2	A	V
2000	3460	3460	-0.083^{+2}_{-2}	0.29^{+3}_{-3}	0.14^{+6}_{-6}	-0.012^{+9}_{-9}	0.87^{+3}_{-3}
		3510	-0.073^{+2}_{-3}	0.27^{+3}_{-3}	0.12^{+6}_{-6}	-0.012^{+9}_{-9}	0.85^{+4}_{-4}
		3530	-0.068^{+3}_{-3}	0.27^{+4}_{-3}	0.11^{+7}_{-6}	-0.013^{+9}_{-9}	0.84^{+4}_{-4}
	3510	3460	-0.086^{+2}_{-2}	0.28^{+5}_{-4}	0.11^{+8}_{-8}	-0.008^{+14}_{-14}	0.86^{+4}_{-4}
		3510	-0.076^{+3}_{-4}	0.27^{+5}_{-5}	0.10^{+9}_{-9}	-0.010^{+14}_{-14}	0.83^{+5}_{-4}
		3530	-0.071^{+4}_{-4}	0.26^{+5}_{-5}	0.10^{+10}_{-10}	-0.012^{+14}_{-14}	0.82^{+6}_{-5}
2330	3460	3460	-0.1414^{+13}_{-13}	0.29^{+3}_{-3}	0.15^{+5}_{-5}	-0.03^{+2}_{-2}	0.85^{+3}_{-3}
		3510	-0.134^{+2}_{-2}	0.27^{+3}_{-3}	0.12^{+5}_{-5}	-0.03^{+2}_{-2}	0.82^{+4}_{-3}
		3530	-0.131^{+2}_{-2}	0.26^{+3}_{-3}	0.12^{+6}_{-6}	-0.03^{+2}_{-2}	0.81^{+4}_{-4}
	3510	3460	-0.143^{+2}_{-2}	0.28^{+4}_{-4}	0.12^{+7}_{-7}	-0.02^{+2}_{-2}	0.83^{+4}_{-4}
		3510	-0.136^{+2}_{-3}	0.26^{+5}_{-4}	0.10^{+7}_{-8}	-0.02^{+2}_{-2}	0.80^{+4}_{-4}
		3530	-0.133^{+3}_{-3}	0.26^{+5}_{-5}	0.11^{+8}_{-8}	-0.03^{+3}_{-3}	0.79^{+5}_{-5}
2660	3460	3460	-0.1830^{+8}_{-8}	0.28^{+3}_{-3}	0.15^{+4}_{-4}	-0.05^{+2}_{-2}	0.83^{+3}_{-3}
		3510	-0.1785^{+10}_{-12}	0.27^{+3}_{-3}	0.13^{+5}_{-5}	-0.05^{+2}_{-2}	0.80^{+3}_{-3}
		3530	-0.1764^{+12}_{-14}	0.26^{+3}_{-3}	0.13^{+5}_{-5}	-0.05^{+2}_{-2}	0.79^{+4}_{-4}
	3510	3460	-0.1844^{+10}_{-10}	0.28^{+4}_{-4}	0.13^{+6}_{-6}	-0.04^{+3}_{-3}	0.81^{+4}_{-4}
		3510	-0.1801^{+14}_{-16}	0.26^{+4}_{-4}	0.11^{+6}_{-7}	-0.04^{+3}_{-3}	0.77^{+4}_{-4}
		3530	-0.178^{+2}_{-2}	0.26^{+5}_{-4}	0.11^{+7}_{-7}	-0.05^{+4}_{-4}	0.76^{+5}_{-4}
2990	3460	3460	-0.2041^{+2}_{-2}	0.27^{+3}_{-3}	0.16^{+4}_{-3}	-0.07^{+2}_{-3}	0.83^{+3}_{-3}
		3510	-0.2028^{+3}_{-4}	0.26^{+3}_{-3}	0.14^{+4}_{-4}	-0.08^{+3}_{-3}	0.79^{+3}_{-3}
		3530	-0.2021^{+4}_{-5}	0.26^{+3}_{-3}	0.13^{+4}_{-4}	-0.09^{+3}_{-3}	0.77^{+4}_{-3}
	3510	3460	-0.2045^{+2}_{-2}	0.27^{+4}_{-4}	0.14^{+5}_{-5}	-0.06^{+4}_{-4}	0.80^{+4}_{-4}
		3510	-0.2034^{+4}_{-5}	0.26^{+4}_{-4}	0.12^{+6}_{-5}	-0.07^{+4}_{-4}	0.76^{+4}_{-4}
		3530	-0.2027^{+5}_{-6}	0.26^{+5}_{-4}	0.12^{+6}_{-6}	-0.08^{+5}_{-4}	0.73^{+4}_{-4}

Table B.9: Form factors, channel $1 \to 2 \parallel$, $\beta = 6.2$.

κ_H	κ_P	κ_A	q^2a^2	A_1	A_2	A	V
2000	3460	3460	0.054^{+2}_{-2}	0.45^{+4}_{-4}	0.35^{+11}_{-13}	0.036^{+14}_{-15}	-
		3510	0.064^{+2}_{-3}	0.43^{+4}_{-4}	0.30^{+12}_{-14}	0.05^{+2}_{-2}	-
		3530	0.069^{+3}_{-3}	0.42^{+4}_{-4}	0.29^{+13}_{-15}	0.05^{+2}_{-2}	-
	3510	3460	0.052^{+2}_{-2}	0.44^{+6}_{-6}	0.3^{+2}_{-2}	0.04^{+2}_{-2}	-
		3510	0.061^{+3}_{-4}	0.41^{+6}_{-6}	0.3^{+2}_{-2}	0.05^{+3}_{-3}	-
		3530	0.066^{+4}_{-4}	0.40^{+6}_{-6}	0.2^{+2}_{-2}	0.06^{+3}_{-3}	-
2330	3460	3460	-0.0043^{+13}_{-13}	0.46^{+4}_{-4}	0.35^{+10}_{-12}	-0.003^{+2}_{-2}	-
		3510	0.003^{+2}_{-2}	0.44^{+4}_{-4}	0.30^{+11}_{-13}	0.003^{+2}_{-2}	-
		3530	0.006^{+2}_{-2}	0.43^{+4}_{-4}	0.29^{+12}_{-14}	0.005^{+3}_{-3}	-
	3510	3460	-0.006^{+2}_{-2}	0.45^{+5}_{-5}	0.31^{+15}_{-16}	-0.005^{+3}_{-3}	-
		3510	0.001^{+2}_{-3}	0.42^{+6}_{-6}	0.3^{+2}_{-2}	0.001^{+2}_{-2}	-
		3530	0.004^{+3}_{-3}	0.41^{+6}_{-6}	0.2^{+2}_{-2}	0.004^{+4}_{-4}	-
2660	3460	3460	-0.0459^{+8}_{-8}	0.47^{+4}_{-4}	0.36^{+10}_{-10}	-0.04^{+2}_{-2}	-
		3510	-0.0414^{+10}_{-12}	0.45^{+4}_{-4}	0.30^{+11}_{-12}	-0.04^{+2}_{-2}	-
		3530	-0.0393^{+12}_{-14}	0.44^{+5}_{-4}	0.29^{+11}_{-13}	-0.04^{+2}_{-2}	-
	3510	3460	-0.0473^{+10}_{-10}	0.46^{+5}_{-5}	0.31^{+13}_{-14}	-0.05^{+2}_{-2}	-
		3510	-0.0430^{+14}_{-16}	0.43^{+6}_{-5}	0.24^{+14}_{-15}	-0.04^{+2}_{-2}	-
		3530	-0.041^{+2}_{-2}	0.42^{+6}_{-6}	0.2^{+2}_{-2}	-0.04^{+2}_{-2}	-
2990	3460	3460	-0.0670^{+2}_{-2}	0.47^{+3}_{-3}	0.36^{+9}_{-10}	-0.08^{+3}_{-3}	-
		3510	-0.0657^{+3}_{-4}	0.45^{+4}_{-4}	0.29^{+10}_{-11}	-0.08^{+3}_{-3}	-
		3530	-0.0650^{+4}_{-5}	0.44^{+4}_{-4}	0.28^{+11}_{-11}	-0.09^{+3}_{-4}	-
	3510	3460	-0.0674^{+2}_{-2}	0.46^{+5}_{-5}	0.31^{+12}_{-13}	-0.08^{+4}_{-4}	-
		3510	-0.0663^{+4}_{-5}	0.44^{+5}_{-5}	0.23^{+13}_{-14}	-0.08^{+4}_{-4}	-
		3530	-0.0656^{+5}_{-6}	0.43^{+6}_{-6}	0.22^{+14}_{-15}	-0.09^{+5}_{-5}	-

Table B.10: Form factors, channel $0 \to 0$, $\beta = 6.0$.

κ_H	κ_P	κ_A	q^2a^2	A_1	A_2	A	V
1230	3344	3344	0.368^{+4}_{-6}	0.78^{+3}_{-2}	-	-	-
		3417	0.403^{+5}_{-7}	0.75^{+3}_{-3}	-	-	-
		3455	0.421^{+7}_{-9}	0.74^{+3}_{-3}	-	-	-
	3417	3344	0.371^{+5}_{-7}	0.77^{+3}_{-3}	-	-	-
		3417	0.408^{+7}_{-9}	0.74^{+4}_{-4}	-	-	-
		3455	0.427^{+10}_{-12}	0.73^{+4}_{-4}	-	-	-
1730	3344	3344	0.219^{+3}_{-4}	0.78^{+2}_{-2}	-	-	-
		3417	0.246^{+4}_{-6}	0.76^{+3}_{-2}	-	-	-
		3455	0.260^{+6}_{-7}	0.75^{+3}_{-3}	-	-	-
	3417	3344	0.220^{+4}_{-5}	0.78^{+3}_{-3}	-	-	-
		3417	0.249^{+6}_{-7}	0.75^{+4}_{-4}	-	-	-
		3455	0.264^{+8}_{-9}	0.74^{+4}_{-4}	-	-	-
2230	3344	3344	0.098^{+2}_{-3}	0.78^{+2}_{-2}	-	-	-
		3417	0.116^{+3}_{-4}	0.75^{+2}_{-2}	-	-	-
		3455	0.126^{+4}_{-5}	0.75^{+3}_{-3}	-	-	-
	3417	3344	0.098^{+3}_{-4}	0.78^{+3}_{-3}	-	-	-
		3417	0.117^{+4}_{-5}	0.75^{+3}_{-3}	-	-	-
		3455	0.127^{+5}_{-6}	0.75^{+4}_{-3}	-	-	-
2730	3344	3344	0.0187^{+9}_{-12}	0.78^{+2}_{-2}	-	-	-
		3417	0.0271^{+13}_{-18}	0.76^{+2}_{-2}	-	-	-
		3455	0.032^{+2}_{-2}	0.76^{+3}_{-2}	-	-	-
	3417	3344	0.0180^{+11}_{-15}	0.79^{+3}_{-2}	-	-	-
		3417	0.027^{+2}_{-2}	0.77^{+3}_{-3}	-	-	-
		3455	0.032^{+3}_{-3}	0.77^{+3}_{-3}	-	-	-

Table B.11: Form factors, channel $0 \to 1$, $\beta = 6.0$.

κ_H	κ_P	κ_A	q^2a^2	A_1	A_2	A	V
1230	3344	3344	0.075^{+3}_{-4}	0.59^{+3}_{-3}	0.50^{+10}_{-12}	0.036^{+10}_{-13}	0.78^{+4}_{-4}
		3417	0.097^{+3}_{-5}	0.56^{+3}_{-3}	0.45^{+11}_{-13}	0.046^{+15}_{-17}	0.75^{+4}_{-4}
		3455	0.108^{+4}_{-6}	0.55^{+3}_{-3}	0.42^{+13}_{-14}	0.05^{+2}_{-2}	0.74^{+4}_{-4}
	3417	3344	0.072^{+3}_{-5}	0.59^{+4}_{-4}	0.47^{+15}_{-17}	0.04^{+2}_{-2}	0.76^{+5}_{-5}
		3417	0.095^{+5}_{-6}	0.55^{+4}_{-5}	0.4^{+2}_{-2}	0.05^{+2}_{-2}	0.74^{+5}_{-5}
		3455	0.106^{+6}_{-7}	0.53^{+5}_{-5}	0.4^{+2}_{-2}	0.05^{+3}_{-3}	0.72^{+6}_{-6}
1730	3344	3344	-0.039^{+2}_{-3}	0.59^{+3}_{-3}	0.50^{+9}_{-10}	-0.024^{+7}_{-6}	0.77^{+3}_{-3}
		3417	-0.023^{+2}_{-3}	0.57^{+3}_{-3}	0.46^{+10}_{-11}	-0.014^{+4}_{-4}	0.74^{+3}_{-4}
		3455	-0.015^{+3}_{-4}	0.55^{+3}_{-3}	0.42^{+11}_{-12}	-0.009^{+4}_{-4}	0.72^{+4}_{-4}
	3417	3344	-0.041^{+2}_{-3}	0.60^{+4}_{-4}	0.50^{+12}_{-14}	-0.028^{+10}_{-10}	0.74^{+4}_{-4}
		3417	-0.025^{+3}_{-4}	0.57^{+4}_{-4}	0.44^{+14}_{-15}	-0.017^{+7}_{-7}	0.72^{+5}_{-5}
		3455	-0.017^{+4}_{-5}	0.55^{+5}_{-5}	0.4^{+2}_{-2}	-0.011^{+6}_{-5}	0.70^{+5}_{-5}
2230	3344	3344	-0.1202^{+9}_{-13}	0.59^{+2}_{-2}	0.48^{+7}_{-8}	-0.09^{+2}_{-2}	0.74^{+3}_{-3}
		3417	-0.1115^{+13}_{-19}	0.56^{+3}_{-3}	0.43^{+8}_{-9}	-0.09^{+2}_{-2}	0.72^{+3}_{-3}
		3455	-0.107^{+2}_{-2}	0.55^{+3}_{-3}	0.40^{+9}_{-9}	-0.08^{+2}_{-2}	0.70^{+3}_{-3}
	3417	3344	-0.1221^{+12}_{-16}	0.60^{+3}_{-4}	0.49^{+10}_{-11}	-0.11^{+3}_{-3}	0.72^{+4}_{-4}
		3417	-0.113^{+2}_{-2}	0.57^{+4}_{-4}	0.43^{+11}_{-12}	-0.10^{+3}_{-3}	0.69^{+4}_{-4}
		3455	-0.109^{+2}_{-3}	0.55^{+5}_{-4}	0.38^{+13}_{-13}	-0.09^{+3}_{-3}	0.67^{+4}_{-4}
2730	3344	3344	-0.15414^{+5}_{-5}	0.60^{+2}_{-2}	0.45^{+5}_{-6}	-0.17^{+3}_{-3}	0.75^{+3}_{-3}
		3417	-0.1533^{+2}_{-2}	0.57^{+3}_{-2}	0.40^{+6}_{-7}	-0.17^{+3}_{-3}	0.72^{+3}_{-3}
		3455	-0.1524^{+4}_{-4}	0.55^{+3}_{-3}	0.36^{+7}_{-7}	-0.17^{+4}_{-3}	0.70^{+3}_{-3}
	3417	3344	-0.154212	0.62^{+3}_{-3}	0.45^{+8}_{-8}	-0.20^{+4}_{-4}	0.72^{+3}_{-3}
		3417	-0.1537^{+2}_{-2}	0.59^{+4}_{-3}	0.39^{+9}_{-9}	-0.20^{+5}_{-4}	0.68^{+4}_{-3}
		3455	-0.1530^{+4}_{-4}	0.56^{+4}_{-4}	0.33^{+10}_{-10}	-0.20^{+5}_{-5}	0.66^{+4}_{-4}

Table B.12: Form factors, channel $1 \to 0$, $\beta = 6.0$.

κ_H	κ_P	κ_A	q^2a^2	A_1	A_2	A	V
1230	3344	3344	0.297^{+4}_{-6}	0.80^{+5}_{-4}	0.6^{+6}_{-6}	0.2^{+3}_{-3}	0.78^{+4}_{-4}
		3417	0.336^{+6}_{-8}	0.79^{+5}_{-5}	0.7^{+8}_{-8}	0.3^{+4}_{-4}	0.75^{+4}_{-4}
		3455	0.356^{+8}_{-10}	0.78^{+6}_{-6}	0.9^{+9}_{-11}	0.4^{+5}_{-5}	0.74^{+4}_{-4}
	3417	3344	0.303^{+6}_{-8}	0.81^{+6}_{-6}	0.7^{+10}_{-10}	0.2^{+4}_{-4}	0.76^{+5}_{-5}
		3417	0.343^{+8}_{-10}	0.79^{+8}_{-7}	0.8^{+12}_{-13}	0.3^{+6}_{-6}	0.74^{+5}_{-5}
		3455	0.365^{+11}_{-13}	0.79^{+9}_{-8}	0.8^{+14}_{-16}	0.4^{+8}_{-8}	0.72^{+6}_{-6}
1730	3344	3344	0.139^{+3}_{-5}	0.78^{+4}_{-4}	0.6^{+4}_{-4}	0.11^{+10}_{-10}	0.77^{+3}_{-3}
		3417	0.170^{+5}_{-6}	0.77^{+5}_{-5}	0.8^{+5}_{-6}	0.19^{+15}_{-17}	0.74^{+3}_{-4}
		3455	0.187^{+6}_{-8}	0.77^{+6}_{-6}	0.9^{+6}_{-7}	0.3^{+2}_{-2}	0.72^{+4}_{-4}
	3417	3344	0.143^{+5}_{-6}	0.79^{+6}_{-6}	0.7^{+6}_{-7}	0.1^{+2}_{-2}	0.74^{+4}_{-4}
		3417	0.176^{+6}_{-8}	0.77^{+8}_{-7}	0.8^{+8}_{-9}	0.2^{+2}_{-3}	0.72^{+5}_{-5}
		3455	0.193^{+9}_{-10}	0.78^{+9}_{-8}	0.9^{+9}_{-11}	0.3^{+3}_{-4}	0.70^{+5}_{-5}
2230	3344	3344	0.005^{+2}_{-4}	0.74^{+4}_{-4}	0.6^{+3}_{-3}	0.005^{+3}_{-5}	0.74^{+3}_{-3}
		3417	0.028^{+3}_{-5}	0.73^{+5}_{-5}	0.7^{+3}_{-3}	0.04^{+2}_{-2}	0.72^{+3}_{-3}
		3455	0.040^{+5}_{-6}	0.73^{+6}_{-6}	0.7^{+4}_{-5}	0.06^{+3}_{-4}	0.70^{+3}_{-3}
	3417	3344	0.007^{+3}_{-4}	0.75^{+6}_{-6}	0.7^{+3}_{-4}	0.008^{+6}_{-8}	0.72^{+4}_{-4}
		3417	0.031^{+5}_{-6}	0.73^{+7}_{-7}	0.7^{+5}_{-5}	0.05^{+3}_{-4}	0.69^{+4}_{-4}
		3455	0.045^{+7}_{-8}	0.74^{+9}_{-8}	0.8^{+6}_{-7}	0.08^{+5}_{-7}	0.67^{+4}_{-4}
2730	3344	3344	-0.095^{+2}_{-2}	0.69^{+4}_{-4}	0.46^{+13}_{-14}	-0.11^{+4}_{-4}	0.75^{+3}_{-3}
		3417	-0.081^{+2}_{-3}	0.68^{+5}_{-5}	0.5^{+2}_{-2}	-0.12^{+5}_{-5}	0.72^{+3}_{-3}
		3455	-0.073^{+3}_{-4}	0.69^{+6}_{-6}	0.5^{+2}_{-3}	-0.13^{+6}_{-5}	0.70^{+3}_{-3}
	3417	3344	-0.095^{+2}_{-3}	0.70^{+6}_{-6}	0.5^{+2}_{-2}	-0.13^{+7}_{-6}	0.72^{+3}_{-3}
		3417	-0.080^{+3}_{-4}	0.68^{+7}_{-7}	0.5^{+3}_{-3}	-0.14^{+7}_{-7}	0.68^{+4}_{-3}
		3455	-0.071^{+4}_{-5}	0.69^{+8}_{-8}	0.5^{+3}_{-4}	-0.15^{+9}_{-8}	0.66^{+4}_{-4}

Table B.13: Form factors, channel $1 \to 1 \perp$, $\beta = 6.0$.

κ_H	κ_P	κ_A	q^2a^2	A_1	A_2	A	V
1230	3344	3344	-0.013^{+3}_{-4}	-	-	-	0.78^{+4}_{-4}
		3417	0.012^{+4}_{-5}	-	-	-	0.75^{+4}_{-4}
		3455	0.025^{+5}_{-6}	-	-	-	0.74^{+4}_{-4}
	3417	3344	-0.014^{+4}_{-5}	-	-	-	0.76^{+5}_{-5}
		3417	0.012^{+5}_{-7}	-	-	-	0.74^{+5}_{-5}
		3455	0.025^{+7}_{-8}	-	-	-	0.72^{+6}_{-6}
1730	3344	3344	-0.137^{+2}_{-3}	-	-	-	0.77^{+3}_{-3}
		3417	-0.118^{+3}_{-4}	-	-	-	0.74^{+3}_{-4}
		3455	-0.108^{+4}_{-5}	-	-	-	0.72^{+4}_{-4}
	3417	3344	-0.139^{+3}_{-4}	-	-	-	0.74^{+4}_{-4}
		3417	-0.120^{+4}_{-5}	-	-	-	0.72^{+5}_{-5}
		3455	-0.109^{+5}_{-6}	-	-	-	0.70^{+5}_{-5}
2230	3344	3344	-0.2352^{+14}_{-19}	-	-	-	0.74^{+3}_{-3}
		3417	-0.223^{+2}_{-3}	-	-	-	0.72^{+3}_{-3}
		3455	-0.216^{+3}_{-3}	-	-	-	0.70^{+3}_{-3}
	3417	3344	-0.237^{+2}_{-2}	-	-	-	0.72^{+4}_{-4}
		3417	-0.224^{+3}_{-3}	-	-	-	0.69^{+4}_{-4}
		3455	-0.217^{+3}_{-4}	-	-	-	0.67^{+4}_{-4}
2730	3344	3344	-0.2953^{+6}_{-8}	-	-	-	0.75^{+3}_{-3}
		3417	-0.2897^{+9}_{-12}	-	-	-	0.72^{+3}_{-3}
		3455	-0.2864^{+12}_{-16}	-	-	-	0.70^{+3}_{-3}
	3417	3344	-0.2962^{+7}_{-10}	-	-	-	0.72^{+3}_{-3}
		3417	-0.2906^{+11}_{-14}	-	-	-	0.68^{+4}_{-3}
		3455	-0.287^{+2}_{-2}	-	-	-	0.66^{+4}_{-4}

Appendix C

Phenomenological results

Table C.1: Form factors for the decay $D_s^+ \to \phi\ell^+\nu$. q^2 is in lattice units.

Channel	q^2	A_0	A_1	A_2	V
$0 \to 0$	0.106	-	0.75^{+3}_{-3}	-	-
$0 \to 1$	-0.012	0.58^{+2}_{-2}	0.63^{+3}_{-3}	0.69^{+8}_{-9}	0.80^{+4}_{-4}
$1 \to 0$	0.072	0.88^{+7}_{-7}	0.70^{+4}_{-3}	0.8^{+4}_{-4}	1.23^{+12}_{-11}
$1 \to 1 \perp$	-0.054	0.53^{+3}_{-2}	0.58^{+3}_{-2}	0.51^{+6}_{-7}	0.70^{+4}_{-4}
$1 \to 1_{\Downarrow\Uparrow}$	-0.191	0.34^{+2}_{-2}	0.53^{+3}_{-3}	0.44^{+5}_{-5}	0.58^{+5}_{-6}

Table C.2: Form factors for the decay $D^+ \to \bar{K}^{*0}\ell^+\nu$. q^2 is in lattice units.

Channel	q^2	A_0	A_1	A_2	V
$0 \to 0$	0.112	-	0.75^{+4}_{-4}	-	-
$0 \to 1$	-0.012	0.59^{+3}_{-3}	0.68^{+4}_{-5}	0.78^{+11}_{-13}	0.76^{+6}_{-6}
$1 \to 0$	0.081	0.90^{+12}_{-12}	0.70^{+5}_{-5}	0.9^{+6}_{-6}	1.2^{+2}_{-2}
$1 \to 1 \perp$	-0.053	0.56^{+4}_{-4}	0.61^{+4}_{-3}	0.53^{+10}_{-10}	0.63^{+6}_{-6}
$1 \to 1_{\Downarrow\Uparrow}$	-0.190	0.38^{+3}_{-4}	0.59^{+5}_{-5}	0.48^{+7}_{-8}	0.63^{+9}_{-8}

Table C.3: Form factors for the decay $D^+ \to \rho^0 \ell^+ \nu$. q^2 is in lattice units.

Channel	q^2	A_0	A_1	A_2	V
$0 \to 0$	0.142	-	0.70^{+5}_{-4}	-	-
$0 \to 1$	0.004	0.58^{+4}_{-3}	0.64^{+5}_{-5}	0.74^{+14}_{-15}	0.71^{+7}_{-7}
$1 \to 0$	0.115	0.90^{+14}_{-14}	0.66^{+7}_{-6}	1.1^{+8}_{-8}	1.2^{+2}_{-2}
$1 \to 1 \perp$	-0.034	0.56^{+5}_{-4}	0.58^{+5}_{-4}	0.48^{+11}_{-12}	0.59^{+6}_{-6}
$1 \to 1_{\parallel}$	-0.171	0.36^{+4}_{-4}	0.55^{+5}_{-6}	0.46^{+8}_{-9}	0.59^{+10}_{-10}

Table C.4: Form factors for the decay $B^0 \to \rho^- \ell^+ \nu$. q^2 is in lattice units, the quadratic heavy quark extrapolation was used.

Channel	q^2	A_0	A_1	A_2	V
$0 \to 0$	2.396	-	0.61^{+6}_{-5}	-	-
$0 \to 1$	2.006	1.36^{+11}_{-9}	0.57^{+6}_{-5}	1.4^{+4}_{-4}	1.13^{+16}_{-14}
$1 \to 0$	2.314	1.7^{+4}_{-4}	0.61^{+6}_{-5}	6^{+2}_{-4}	1.9^{+4}_{-4}
$1 \to 1 \perp$	1.891	1.24^{+16}_{-12}	0.52^{+6}_{-5}	1.0^{+2}_{-5}	1.0^{+2}_{-2}
$1 \to 1_{\parallel}$	1.624	0.9^{+2}_{-2}	0.54^{+8}_{-8}	1.1^{+4}_{-4}	1.1^{+4}_{-3}

Table C.5: Results from fitting the lattice form factors to the ansätze described in section 6.5. Pole masses are in lattice units. r_0 was used to set the scale, which gives $a^{-1} = 2.913$ GeV.

decay	$V(0)$	$A_0(0)$	$A_1(0)$	$A_2(0)$	M_V^2	$M_{A_0}^2$	$M_{A_1}^2$
$D_s^+ \to \phi \ell^+ \nu$	0.85^{+4}_{-3}	0.63^{+2}_{-2}	0.63^{+2}_{-2}	0.62^{+5}_{-5}	0.53^{+5}_{-4}	0.24^{+2}_{-2}	0.69^{+13}_{-10}
$D^+ \to \bar{K}^{*0} \ell^+ \nu$	0.80^{+5}_{-5}	0.64^{+3}_{-3}	0.65^{+2}_{-3}	0.67^{+7}_{-7}	0.58^{+14}_{-8}	0.28^{+5}_{-4}	0.9^{+4}_{-2}
$D^+ \to \rho^0 \ell^+ \nu$	0.71^{+5}_{-6}	0.59^{+3}_{-3}	0.60^{+3}_{-3}	0.61^{+6}_{-7}	0.57^{+14}_{-7}	0.31^{+5}_{-4}	1.0^{+6}_{-3}

Table C.6: Results from fitting the lattice form factors to the ansätze described in section 6.5. Pole masses are in lattice units. m_ρ was used to set the scale, which gives $a^{-1} = 2.54$ GeV.

decay	$V(0)$	$A_0(0)$	$A_1(0)$	$A_2(0)$	M_V^2	$M_{A_0}^2$	$M_{A_1}^2$
$D_s^+ \to \phi\ell^+\nu$	0.83^{+3}_{-3}	0.61^{+2}_{-2}	0.62^{+2}_{-2}	0.63^{+5}_{-5}	0.57^{+4}_{-3}	0.30^{+3}_{-2}	0.74^{+11}_{-9}
$D^+ \to \bar{K}^{*0}\ell^+\nu$	0.79^{+5}_{-5}	0.64^{+3}_{-3}	0.66^{+3}_{-3}	0.70^{+7}_{-7}	0.63^{17}_{-9}	0.37^{+9}_{-6}	1.1^{+7}_{-3}
$D^+ \to \rho^0\ell^+\nu$	0.67^{+6}_{-6}	0.59^{+4}_{-3}	0.60^{+3}_{-3}	0.61^{+8}_{-8}	0.60^{+16}_{-7}	0.38^{+7}_{-5}	1.4^{+12}_{-4}

Table C.7: The pole masses obtained from fitting the lattice data compared with the nearest-pole-dominance prediction of [38]. All masses are in GeV. Lattice pole masses are calculated with both r_0 and m_ρ used to set the scale. The nearest-pole-dominance predictions are meson masses; in all cases the experimental error on the meson mass is smaller than the accuracy quoted.

decay	mass	Lattice (r_0)	Lattice (m_ρ)	Pole dominance
	m_V	2.13^{+10}_{-9}	1.92^{+7}_{-6}	2.11
$D_s^+ \to \phi\ell^+\nu$	m_{A_1}	2.4^{+2}_{-2}	2.19^{+14}_{-14}	2.54
	m_{A_0}	1.44^{+7}_{-7}	1.40^{+6}_{-5}	1.97
	m_V	2.2^{+3}_{-2}	2.0^{+3}_{-1}	2.11
$D^+ \to \bar{K}^{*0}\ell^+\nu$	m_{A_1}	2.8^{+6}_{-4}	2.7^{+7}_{-4}	2.54
	m_{A_0}	1.55^{+13}_{-11}	1.53^{+17}_{-13}	1.97
	m_V	2.2^{+3}_{-1}	1.97^{+25}_{-11}	2.01
$D^+ \to \rho^0\ell^+\nu$	m_{A_1}	2.9^{+6}_{-3}	3.0^{+11}_{-5}	2.42
	m_{A_0}	1.62^{+13}_{-11}	1.56^{+14}_{-11}	1.87

Bibliography

[1] Y. Fukuda *et al.*, Phys. Rev. Lett. **81**, 1562 (1998).

[2] P. Ramond, *Journeys beyond the standard model* (Perseus Books, Reading, USA, 1999).

[3] P. Renton, *Electroweak Interactions* (Cambridge University Press, Cambridge, 1990).

[4] D.E. Groom *et al.*, Eur. Phys. J. C **15**, 1 (2000).

[5] I. J. R. Aitchison and A. J. G. Hey, *Gauge Theories in Particle Physics* (Hilger, Bristol, 1989).

[6] J. D. Richman and P. R. Burchat, Rev. Mod. Phys. **67**, 893 (1995).

[7] L. Wolfenstein, Phys. Rev. Lett. **51**, 1945 (1983).

[8] Z. Ligeti, $|V_{cb}|$ and $|V_{ub}|$ from B decays: Recent progress and limitations, hep-ph/9908432.

[9] M. Wise, Recent Progress in Heavy Quark Physics, hep-ph/0111167.

[10] C. W. Bauer, Z. Ligeti, and M. E. Luke, Phys. Rev. **D64**, 113004 (2001).

[11] A. K. Leibovich, $|V_{ub}|$ from semileptonic decay and $b \to s\gamma$, hep-ph/0011181.

[12] J. P. Alexander *et al.*, Phys. Rev. Lett. **77**, 5000 (1996).

[13] B. H. Behrens *et al.*, Phys. Rev. D **61**, 052001 (2000).

[14] P. Ball and V. M. Braun, Phys. Rev. **D58**, 094016 (1998).

[15] M. Beyer and D. Melikhov, Phys. Lett. **B436**, 344 (1998).

[16] I. Montvay and G. Münster, *Quantum Fields on a Lattice* (Cambridge University Press, Cambridge, 1994).

[17] H. J. Rothe, *Lattice gauge theories: An Introduction* (World Scientific, Singapore, 1992).

[18] K. G. Wilson, Phys. Rev. D **10**, 2445 (1974).

[19] UKQCD Collaboration, K.C. Bowler *et al.*, Phys. Rev. D **62**, 054506 (2000).

[20] CP-PACS Collaboration, S. Aoki *et al.*, Phys. Rev. Lett. **84**, 238 (2000).

[21] M. Lüscher, S. Sint, R. Sommer and P. Weisz, Nucl. Phys. B **478**, 365 (1996).

[22] K. Symanzik, Nucl. Phys. B **226**, 187 (1983).

[23] M. Lüscher, S. Sint, R. Sommer, P. Weisz and U. Wolff, Nucl. Phys. B **491**, 323 (1997).

[24] T. Bhattacharya, R. Gupta, W. Lee, S. Sharpe, Phys. Rev. D **63**, 074505 (2001).

[25] P. Lacock, A. McKerrell, C. Michael, I.M. Stopher and P.W. Stephenson, Phys. Rev. D **51**, 6403 (1995).

[26] UKQCD Collaboration, P. Boyle, A novel gauge invariant multi-state smearing technique, hep-lat/9903033.

[27] C. W. Bernard, A. X. El-Khadra and A. Soni, Phys. Rev. D **43**, 2140 .

[28] C. W. Bernard and A. Soni, Nucl. Phys. Proc. Suppl. **9**, 155 (1989).

[29] H. Hoeber, Ph.D. thesis, University of Edinburgh, 1994.

[30] W.H. Press *et al.*, *Numerical Recipies in C* (Cambridge University Press, Cambridge, 1988).

[31] C. Michael and A. McKerrell, Phys. Rev. D **51**, 3745 (1995).

[32] G. Lepage, in *From Actions to Answers*, edited by T. DeGrand and D. Toussaint (World Scientific, Singapore, 1990).

[33] S. Sint and P. Weisz, Nucl. Phys. B **502**, 251 (1997).

[34] G.M. de Divitiis and R. Petronzio, Phys. Lett. B **419**, 311 (1998).

[35] UKQCD Collaboration, C. M. Maynard, Nucl. Phys. Proc. Suppl. **83**, 322 (2000).

[36] A. Abada *et al.*, Heavy to light semileptonic decays of pseudoscalar mesons from lattice QCD, hep-lat/0011065.

[37] F. J. Gilman and R. L. Singleton, Phys. Rev. **D41**, 142 (1990).

[38] M. Bauer, B. Stech and M. Wirbel, Z. Phys. C **29**, 627 (1985).

[39] D. Fakirov and B. Stech, Nucl. Phys. **B133**, 315 (1978).

[40] E. M. Aitala *et al.*, Phys. Lett. **B440**, 435 (1998).

[41] J. G. Korner and G. A. Schuler, Z. Phys. **C46**, 93 (1990).

[42] UKQCD Collaboration, K. C. Bowler *et al.*, Phys. Rev. **D51**, 4905 (1995).

[43] D. Melikhov and B. Stech, Phys. Rev. **D62**, 014006 (2000).

[44] N. Isgur and M. B. Wise, Phys. Rev. **D42**, 2388 (1990).

[45] M. Neubert, Introduction to B physics, hep-ph/0001334.

[46] D. Scora and N. Isgur, Phys. Rev. **D52**, 2783 (1995).

[47] UKQCD Collaboration, J. M. Flynn *et al.*, Nucl. Phys. **B461**, 327 (1996).

[48] UKQCD Collaboration, J. M. Flynn and J. Nieves, Nucl. Phys. **B476**, 313 (1996).

[49] UKQCD Collaboration, G. N. Lacagnina, The Isgur-Wise function on the lattice, hep-lat/0109006.